On the changes in dynamic behavior produced by the hydraulic turbine runner damage

Ming Zhang

On the Changes in Dynamic Behavior produced by the Hydraulic Turbine Runner Damage

Doctoral Thesis

Presented to the Department of Fluid Mechanics of the

Universitat Politècnica de Catalunya (UPC) by

Ming Zhang

Under the supervision of

Dr. Eng. Carme Valero and Dr. Eng. David Valentín

Barcelona, July, 2019

CONTENTS

ACKNOWLEGEMENT

First of all, I would like to express my deepest gratitude to my thesis supervisor, Dr. Eng. Carme Valero and the co-director Dr. Eng. David Valentín for their time, support, advice and encouragement throughout all the work carried out during these years. This work could not be possible without their constant support. They really taught me a lot during the past four years, and a lot of troubles were caused by me to them.

Special thanks to Professor Dr. Eng. Eduard Egusquiza and Dr. Eng. Alfredo Guardo. In the beginning, I was a blank paper in this area. They recruited me here and gave me many freedoms to choose what I wanted to study. They also gave me many bits of helps and suggestions during the first two years of my study. I am so fortunate to meet them all.

Thanks to all my group members of CDIF, especially to Mònica Egusquiza and Alex Presas, for their kindly helps. Thanks to Dr. Eng. Xavier Escaler and other students in the department (Weiqiang Zhao, Linlin Geng, Jian Chen and Lingyan He) for their accompanies during these years. To get along with them are very happy. Thanks to Paloma Ferrer and David Castañer for their friendly helps when I live abroad.

I want to express my gratitude to my family members who support me and give me motivations and courage for so many years. I hope I can spend more time with them in the future. Special thanks should be given to the Chinese Scholarship Council (CSC), without whose financial support, it would be much more difficult for me to learn abroad.

Barcelona, July 2019
Ming Zhang

I

ABSTRACT

Hydropower plays a very important role in the world electricity generation nowadays. Hydropower is one type of renewable energy and is the only renewable energy source that can provide a wide range of power regulation with fast response, which is very important for the electricity grid stability. Hydraulic turbines are the key equipment of hydropower plants. The power concentration in hydraulic turbines is increasing very fast in the past years. As a consequence, heads and fluid velocities are higher, and the hydraulic excitation forces on the turbine runner increase. On the other hand, to improve the efficiency of hydraulic turbines, the thickness and weight of the runner have been decreased as much as possible, which also increases the stresses in the runner. Furthermore, the operation range of hydraulic turbines is widened in order to satisfy the end-users' demand of larger regulation capacity. This operation at extreme off-design conditions leads to even larger forces.

Due to these reasons, many fatigue failure cases have been reported in the literature. Some fatigue failure cases showed very large cracks, which also indicates the challenge of crack monitoring during operations. To monitor the cracks in hydraulic turbines, it is imperative to study the effect of a crack on the dynamic behavior of hydraulic turbines. The dynamic behavior of hydraulic turbines has been studied extensively during the past decade. However, most of these studies were focused on Francis turbines and pump turbines, and the dynamic behavior of other types of hydraulic turbines, e.g., Kaplan turbines, have still been studied limitedly. Moreover, all of these studies were conducted on runners without cracks, and the effect of a crack on the dynamic behavior of hydraulic turbines has still not been studied before.

In the present thesis, the effect of a crack on the dynamic behavior of Kaplan turbines and Francis turbines has been studied in detail. The research emphasis is laid on Kaplan turbines. This is divided into two steps. First, the dynamic behavior of an intact Kaplan turbine runner is studied. Then, based on the dynamic behavior of intact turbine runners, the effect of a crack on one blade is investigated. A systematic approach has been used for study. The research start from numerical models, and then, the numerical results are validated by experiments. The studies on the numerical models are conducted step by step from simplified blade models to single blade models and continuously to whole turbine models. The knowledge obtained on Kaplan turbines is also applied to a Francis turbine runner, whose dynamic behavior was previously studied

RESUMEN

La energía hidroeléctrica juega un papel muy importante en la generación de electricidad hoy en día. La energía hidroeléctrica es la única fuente de energía renovable que puede proporcionar gran regulacion de potencia con una respuesta rápida, que es precisamente lo que demanda la red eléctrica. El elemento más importante en plantas hidroeléctricas es la turbina hidráulica. La concentración de potencia en turbinas hidráulicas está aumentando muy rápido hoy en día. Como consecuencia, las presiones y velocidades son mayores, y por lo tanto las fuerzas de excitación aumentan. Por otro lado, para mejorar la eficiencia de las turbinas hidráulicas, así como para lograr mayores aceleraciones durante las variaciones de carga, el grosor / peso del rodete se disminuye tanto como es posible, lo que también aumenta es estrés que recibe el rodete. Además, el rango de operación de las turbinas hidráulicas se está viendo ampliado para satisfacer la demanda de los usuarios proporcionando una mayor capacidad de regulación. La operación de las turbinas en condiciones fuera de diseño conlleva todavía a mayores fuerzas y esfuerzos en el rodete.

Debido a estas razones, han habido muchos fallos por fatiga de componentes de turbinas hidráulicas en los últimos años. En algunos casos se encontraron grandes fisuras en la estructura, lo que indica que son difíciles de detectar con los actuales sistema de monitoreo de estas máquinas. Para controlar la aparición de fisuras en turbinas hidráulicas, es imprescindible estudiar el efecto de estas fisuras en el comportamiento dinámico de turbinas hidráulicas. El comportamiento dinámico de turbinas hidráulicas se ha estudiado en detenimiento durante la última década.. Sin embargo, la mayoría de estos estudios se centraron en turbinas Francis y bomba turbinas, mientras que el comportamiento dinámico de otros tipos de turbinas hidráulicas, como por ejemplo, las turbinas Kaplan, no ha sido estudiado todavía con detalle. Además, todos estos estudios se realizaron en rodetes sin fisuras, con lo que el efecto de una fisura en el comportamiento dinámico de turbinas hidraulicas todavía no se conoce.

En esta tesis se ha estudiado el efecto de una fisura en el comportamiento dinámico de turbinas Kaplan y Francis. El énfasis de la investigación está puesto sobre todo en turbinas Kaplan. Primero se ha estudiado el comportamiento dinámico de un rodete de turbina Kaplan intacto. Luego, basándose en el comportamiento dinámico de los rodetes intactos, se ha investigado el efecto de una fisura en una pala. Para realizar la investigación se ha realizado un estudio sistemático: las investigaciones parten de modelos numéricos, y luego los resultados se han validado con experimentos. Los estudios con los modelos numéricos se han llevado a cabo paso a paso, desde modelos de álabes simplificados hasta un modelo de un álabe de turbina Kaplan o del rodete entero. El conocimiento obtenido en las turbinas Kaplan también se ha aplicado a un rodete de turbina Francis, cuyo comportamiento dinámico se había estudiado previamente.

List of Figures

List of Tables

Nomenclature

Latin symbols

E the mechanical energy of flowing fluid

z the potential energy of flowing fluid

p the pressure of flowing fluid

ρ the density of flowing fluid

V the velocity of flowing fluid

g gravity acceleration

N_s specific speed of hydraulic turbines

Ω rotation speed of hydraulic turbines

Q flow rate of hydraulic turbines

H head of hydraulic turbines

M_s mass of the structure

C_s damping of the structure

K_s stiffness of the structure

t instant time

F_s force applied on the structure

x response of the structure

X response amplitude of the structure

ω vibration frequency

φ vibration phase

ξ damping ratio

ω_n natural frequency of the structure

ω_d damped natural frequency

ω_A frequency of the higher half power point

ω_B frequency of the lower half power point

X_p response of point p of the structure

F_q force applied at the point q of the structure

ϕ_{pq} vibration phase difference between point p and q

α_{pq} weighting factor between point p and q

F_f fluid force applied on the structure

M_a added mass

C_a added damping

K_a added stiffness

f_f natural frequency of the submerged structures

ξ_f damping ratio of the submerged structures

λ added mass factor

F_{fs} coupling fluid force

M_{fs} coupling fluid mass

K_{fs} coupling fluid stiffness

M_f equivalent fluid mass

C_f equivalent fluid damping

VII

K_f equivalent fluid stiffness

ϕ mode shape of one mode

$f_{damaged}$ natural frequency of the damaged mode

$f_{undamaged}$ natural frequency of the undamaged mode

$H(j\omega)$ transfer matrices

$f_{b,n}$ frequency of the rotor stator interaction

f_r the rotating speed of the runner

Z_b the number of rotating blades

n the order of harmonics

k excitation mode number

Z_v the number of guide vanes

m the order of harmonics from the rotating view

$U_{1\,max}$ maximum dimensionless modal displacement with damage

$U_{0\,max}$ maximum dimensionless modal displacement without damage

Abbreviations

DOF degree of freedom

EMA experimental modal analysis

EXP. experiment

SIM. simulation

FDR frequency decrease ratio

FRR frequency reduction ratio

FEM finite element method

FFT Fast Fourier Transform

FRF frequency response function

FSI fluid structure interaction

MDOF multiple degree-of-freedom

ND nodal diameter

NL nodal line

NMA numerical modal analysis

SDOF single degree-of-freedom

RSI rotor structure interaction

LF localization factor

CHAPTER 1. INTRODUCTION

The main purpose of this chapter is to explain the background and motivation of the topic of this thesis. First is shown why the topic of the thesis is important to be studied. Then, the state of the art in the effect of damage on the dynamic behavior of hydraulic turbines, the effect of damage in other types of turbines with similar geometries and the failure mechanism in Kaplan turbines and Francis turbines. The objectives and methodology are also introduced. Finally, the main characteristics of the turbines under analysis are introduced in this chapter.

1.1. Background and interest of the topic

Hydropower plays a very important role in electricity generation in the world now. In 2016, approximately 16.65% of the electricity was generated by hydro resources (Figure 1-1). Hydropower is one type of renewable energy (hydro, solar, wind, geothermal, tide, etc.). During the past decade, the renewable resources used for electricity production have increased drastically (Figure 1-2(a)), especially the wind and solar power (Figure1-2(b)), while hydropower electricity generation has remained almost constant during this period (Figure 1-2(a)). In contrast, fossil fuels and nuclear generating sources are less used every year due to their environmental impact (Figure 1-2(a)).
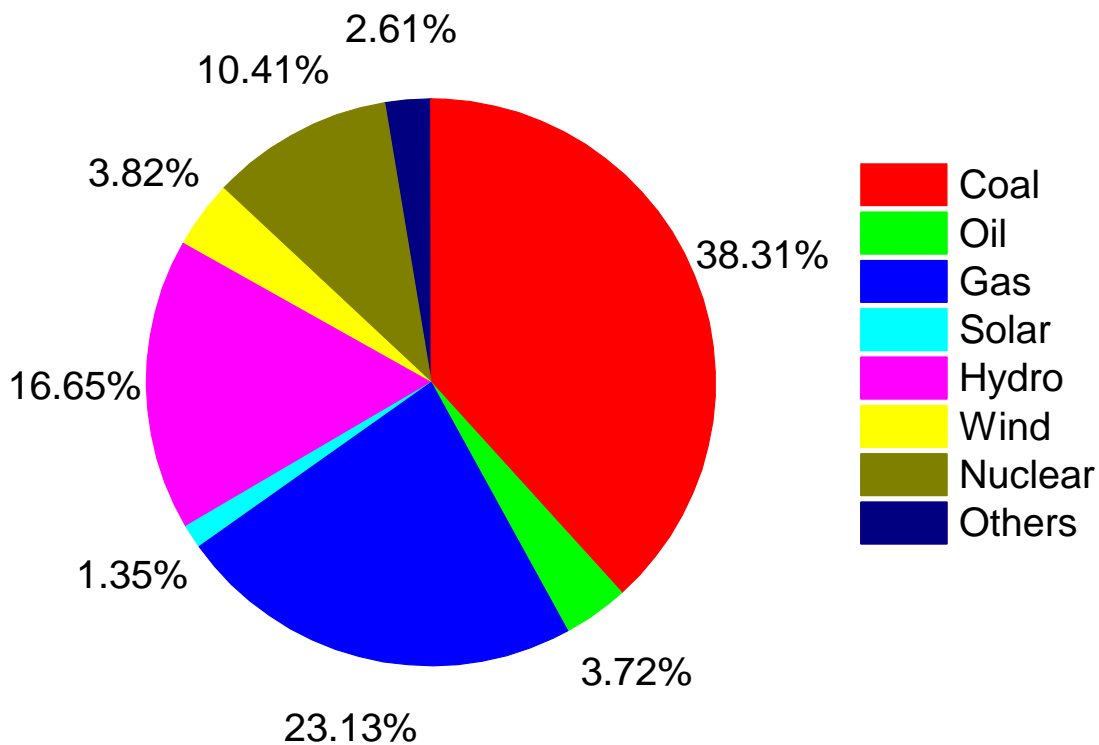
Figure 1-1. World electricity generation mix in 2016 [1].

However, some of these renewable energy sources are quite dependent on the weather conditions, especially the wind and solar power, which makes their generation capacities difficult to be stable. This fact leads to the requirements of more regulation, flexibility and fast response of other electricity generating sources in order to stabilize the power grid. Hydropower is the only energy source that can provide a wide range of power regulation (from 20 to 100% the maximum generating power) with fast response (startup and stop and load changes in less than one minute). Furthermore, it can store large amounts of energy by using Reversible Pump-Turbine when there is a surplus of electricity in the grid.

Hydraulic turbines are the key equipment of hydraulic power plants. According to the way of the energy conversion, the hydraulic machinery can be classified into two types: impulse turbine, e.g., Pelton turbines, and reaction turbine, e.g., Francis turbines and Kaplan turbines [2]. The

classification of hydraulic turbines will be introduced more detailly in Section 1.2. Under the abovementioned circumstances, hydraulic turbines are therefore increasingly working in off-design conditions, and they are subjected to transient events(start-stop, load variations and load rejections) much more times in one day than before [3, 4]. These transient events can induce high unsteady pressure pulsation to the runner, which can cause severer wear to the runner and greatly reduces its lifetime. Figure 1-3(a) shows an example of the dynamic stresses of a Francis turbine for different operating conditions. It is shown that for this machine, in the startup, low load and high load stages, the dynamic stresses are much higher than those at full power. This behavior is confirmed by analyzing the damage that the runner suffers at every operating condition in comparison with a startup (see Figure 1-3(b)).
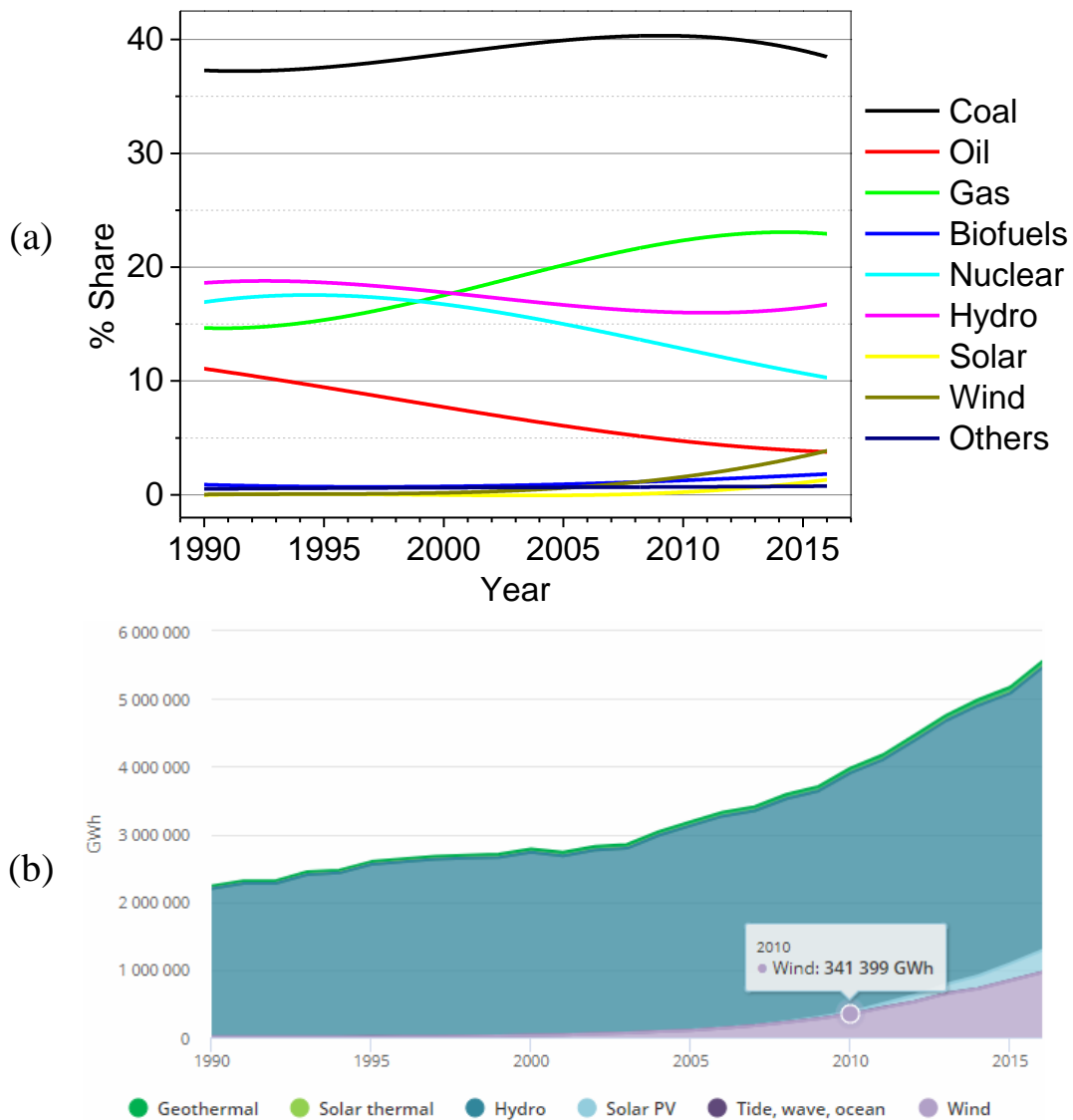
Figure 1-2. (a) World electricity production by source, 1990-2016. Data from International Energy Agency (IEA) [1]. (b) World wind and solar power generation trend from 1990 to 2016. Sources from International Energy Agency(IEA) statistics [1].

(a)   (b)
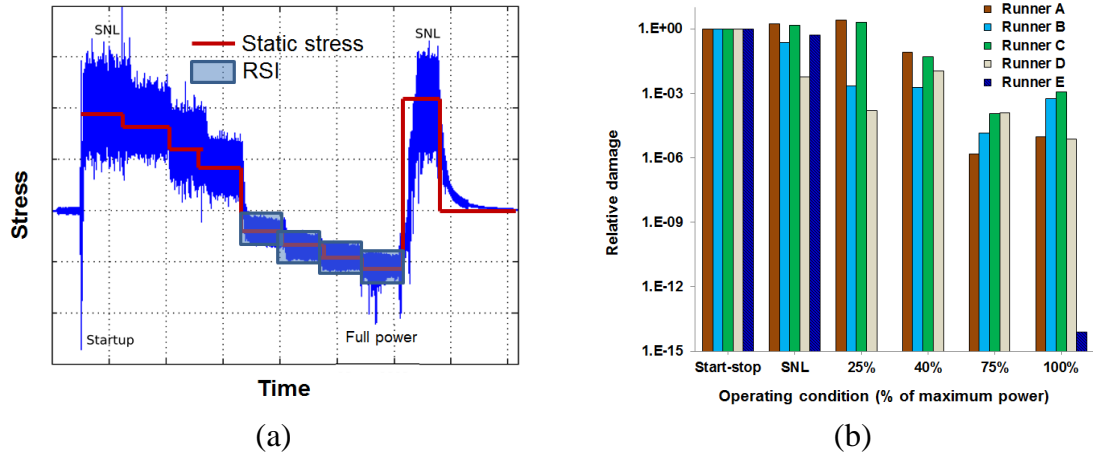
Figure 1-3. (a) Stress in a runner blade of a Francis turbine for different operating conditions. (b) Relative damage of a start-up and different operating conditions of Francis runners. SNL: speed-no-load. Source [5].

In addition, there is a constant trend to increase the power concentration in hydraulic turbines either for new power plants or during the upgrading of existing ones. As a consequence, heads and fluid velocities are higher, and the hydraulic excitation forces on the turbine runners increase. On the other hand, to improve the efficiencies of hydraulic turbines and to reduce the manufacture cost, the thickness and weight of the runner have been decreased as much as possible, which also increases the stresses in the runner [3].

Due to all these reasons, several fatigue failures of different types of turbines have been reported in the literature [4, 6-13]. Cracking is the most common type of fatigue problem. D Frunzăverde, et al., reported a severe Francis turbine failure case, in which a large crack originated from the welt joint between one blade and the crown, and made the whole blade fractured (Figure 1-4(a)) [13]. Egusquiza, et al. [10], reported a failure case in a pump-turbine, in which a part of the crown broke down due to the crack development under high hydraulic forces (Figure 1-4(b)).

(a)   (b)

Figure 1-4. (a) Broken Francis runner [13]. (b) Broken Pump-Turbine runner [10].

These severe failure cases also indicate the challenges of crack monitoring during operations. Egusquiza, et al. [14], have shown that the damage in Figure 1-3(b) is difficult to induce high vibrations to reach the vibration alarm of the monitoring system. To better monitor the crack failures, it is imperative to study the effect of a crack on the dynamic behavior of hydraulic turbines. Meanwhile, except for the above-mentioned common damage reasons, for each specific type of hydraulic turbines, there may be some special reasons for damage appearances.

In the present thesis, the effect of a crack on the dynamic behavior of Kaplan turbines and Francis turbines has been studied in detail. The research emphasis is laid on Kaplan turbines. This is divided into two steps. First, the dynamic behavior of an intact Kaplan turbine runner is studied. Then, based on the dynamic behavior of intact turbine runners, the effect of a crack on one blade is investigated. A systematic approach has been used for study. The researches start from numerical models, and then, the numerical results are validated by experiments. The studies on the numerical models are conducted step by step from simplified blade models to single blade models and continuously to whole turbine models. The knowledge obtained on Kaplan turbines is also applied to a Francis turbine runner, whose dynamic behavior was previously studied.

1.2. State of the art

The state of the art related to the topic of this study has been divided into three different sections. The first one is the state of the art of Kaplan turbines, the second in Francis turbines, and the last one is the effect of a crack on the dynamic behavior of other similar types of turbines, e.g., gas turbines and aero-engine turbines, to provide some useful references for hydraulic turbines.

1.2.1 Research on Kaplan turbines

1.2.1.1 Fundamental knowledge about hydraulic turbines

Hydraulic turbines may be classified in different ways. The most common classification is according to the energy conversion. According to the theory of hydromechanics, the mechanical energy of flowing fluid contains three components, which are the potential energy (z), the pressure energy (p/ρ) and the kinetic energy ($V^2/2g$). If the mechanical energy of the unit weight of fluid is defined as E, then [15]:

$$E = z + \frac{p}{\rho} + \frac{V^2}{2g} \qquad (1-1)$$

Different type of hydraulic turbine runner can convert different components of fluid mechanical energy. By this way, the hydraulic machinery can be classified into two types: impulse turbine and reaction turbine [2]. Impulse turbines only convert the fluid kinetic energy and they are operated in open air. Common impulse turbines are Pelton turbines and cross-flow (Banki) turbines. For reaction turbines, the fluid pressure energy and kinetic energy are converted within the turbine runner. Due to the characteristics of energy conversion, the reaction turbine must be fully submerged in water, which makes the working condition more complicated than impulse turbines. According to the way of geometrical features, reaction turbines can be classified into Francis turbines, Kaplan turbines and diagonal flow turbines.

The performance of hydraulic machinery largely depends on the design of turbine runner.

During the turbine selection and design, a parameter called specific speed is generally used as the main criteria. This parameter summarizes the three physical parameters of a hydraulic turbine: head, flow rate and rotating speed, as expressed by Equation (1-2) [16].

$$N_S = \frac{\Omega Q^{1/2}}{(gH)^{3/4}} \qquad (1-2)$$

where N_s is the specific speed, Ω is the rotating speed in radians per second, Q is the flow rate in cubic meters per second, H is the net head in meters, and g is the gravity acceleration. Consequently, with the given head and flow rate for a specific power plant, and the rotating speed required by the generator, the specific speed can be calculated and used as the starting point for the analytical design of the turbine. Figure 1-5 shows different turbine shapes selected according to different specific speed.
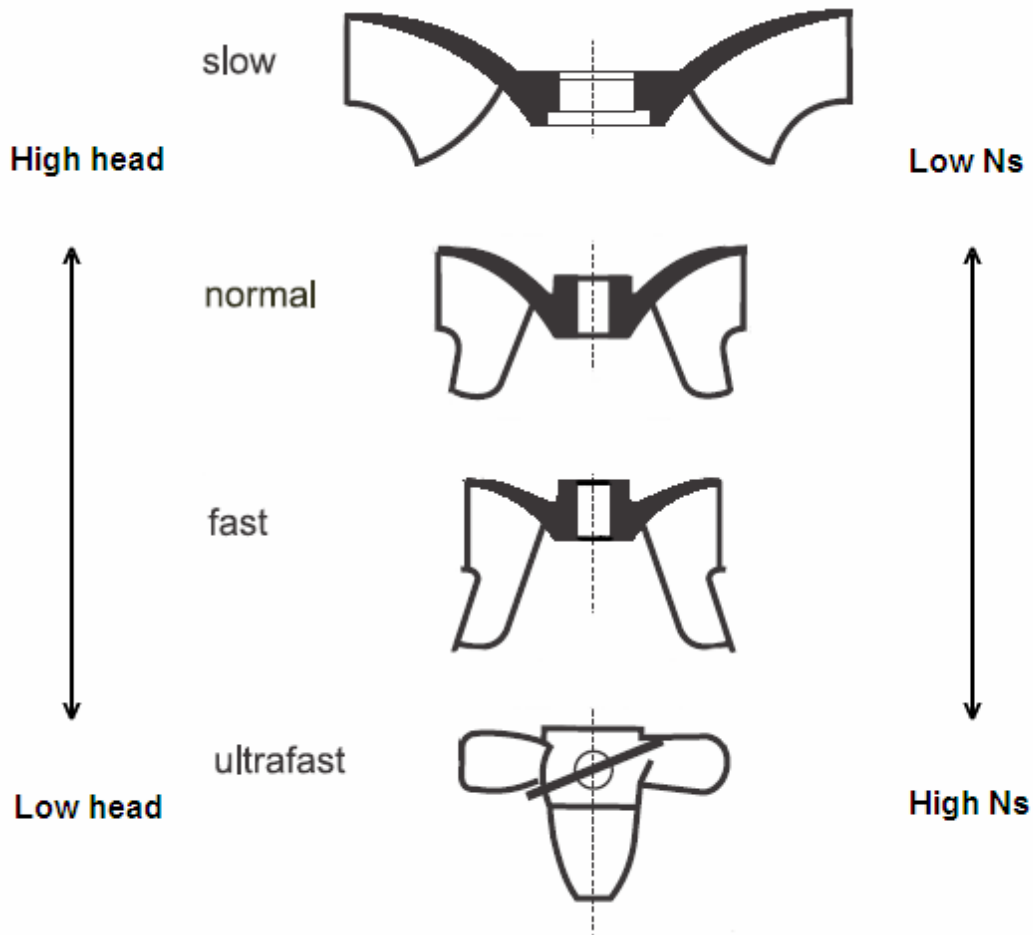
Figure 1-5. Comparison of turbine shape vs. specific speed [11].

1.2.1.2. Description of Kaplan turbines

The structure of a Kaplan turbine runner and the connected components is shown in Figure 1-6. A Kaplan runner is usually composed by a hub and some blades with the rods connected to the hub. Inside the hub, there is a control system that can adjust the angle of the blades through the

rotation of the rods. The water flows axially through the runner, and for this reason, the Kaplan turbine is also referred to as axial-flow turbine. The advantage of Kaplan turbine over radial-flow turbines is that it can adjust the angle of the blades when the water flow condition changes, which improves the efficiency of power production and keeps the turbine always under on-cam conditions. The flow rate of the water through the turbine can be controlled by varying the angle of the guide vanes; the pitch of the runner blades must then also be appropriately adjusted. Each setting of the guide vanes corresponds to one particular setting of the runner blades in order to obtain the highest efficiency.
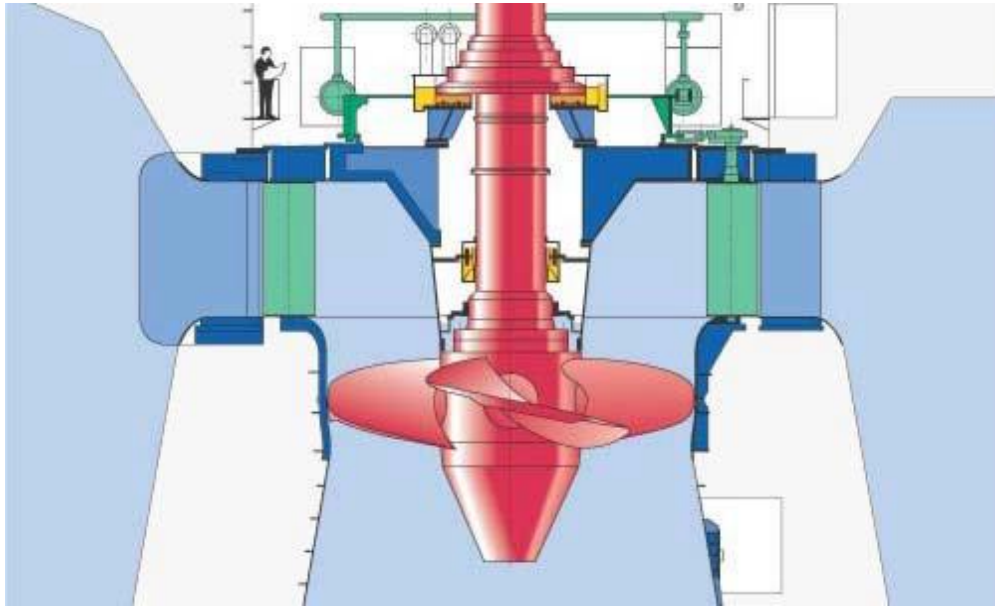
Figure 1-6. Structure of a Kaplan turbine [17].

The heads of Kaplan turbines are usually low, which may cover a range from 1 m to about 30 m. Under such conditions, a relatively larger flow rate compared with high head turbines is required for a given output. Therefore, Kaplan turbines are comparatively larger. Moreover, as having adjustable runner blades controlled by the control system, which is installed inside the runner hub, the construction of the Kaplan turbine becomes naturally more complicated.

1.2.1.3. Main types of damage in Kaplan turbines

Fatigue damage is one of the most common types of damage in Kaplan turbines. There are different stages of fatigue damage where defects may nucleate in an initially undamaged section and propagate stably until a catastrophic fracture [4]. Beach marks can usually be identified in the crack faces, which is an important sign of fatigue problems [9, 10]. Other types of damage in Kaplan turbines can be cavitation damage and silt erosion , etc.[18-20].

1.2.1.4. Research state of Kaplan turbines

Until now, the dynamic behavior of Kaplan turbine runners has been studied very limitedly. Although many research conclusions on Francis turbines or pump turbines can be applied to Kaplan turbines, its structural characteristics determine that there are many differences of its dynamic behavior from that of Francis turbines or pump turbines. The runner of a Kaplan turbine is an

assembly of blades, hub and control system, and the blades of Kaplan turbines are not firmly constrained like those of Francis turbines or pump turbines. Moreover, the blades of the runner are far away from the head cover and the only nearby surface is the chamber wall due to the narrow clearance in the tip of the blades. The effect of the surrounding water and boundary conditions are different from that of Francis turbines or pump turbines. Danilo, et al. [21], studied the modal behavior of an axial flow turbine numerically and experimentally, and the results showed that the blades' mode-shapes are not affected between each other due to the too rigid hub. Therefore, the modal behavior of the whole runner can be represented by the modal behavior of a single blade. However, for Kaplan turbines, the hub may be not as rigid as that of axial flow turbines, and the blades can probably affect each other's vibration. All these things are worth a comprehensive study and are still not available in the literature. The effect of a crack on its dynamic behavior has also not been studied before.

Kaplan turbines are subjected to both static and dynamic pressure loads. The static pressure load is proportional to the flow rate passing through the runner and the dynamic pressure load is commonly caused by the Rotor-Stator Interaction (RSI) [22], although it relatively small compared with the static pressure value due to the large distance between the guide vanes and blades in Kaplan turbines[23, 24]. Other dynamic phenomena such as vortex rope, tip vortex and Von Karman vortices [4, 24-26] can also cause dynamic pressure loads, but their appearances are less usual. Some studies [11, 23] have shown that the water pressure load can induce high-stress concentrations at the root area of the blade. Moreover, if the material has defects in this zone, the fatigue process can be greatly accelerated. Frunzaverde et al [11] reported a case where a large crack appeared at the leading-edge side root hole of the turbine blade due to high-stress concentrations. Because the runner is not a rigid body, the high hydraulic forces can be passed to the control system, and sometimes can break some other parts of the turbine. Yongyao et al [8] studied a case where the piston rod of the control system was broken also due to high hydraulic loads in the blade.

Some of these studies presented also cases of resonance, where the natural frequencies of the runner coincided with the dynamic pressure excitation frequencies, increasing drastically the blade vibration, and therefore causing severe damage on the blade. Transient events will often lead to high amplitude pressure fluctuations on different parts of the turbine including the rotating parts, which also affect severely the turbine residual-life. General transient events in hydro turbines can be load variation, no-load condition, startup and shutdown, load rejection, etc. [3].

Another case of fatigue damage in Kaplan turbines, but less common, is rubbing. Due to the small tip clearance (generally of about 0.05% the runner diameter), the blade tip may contact the stationary wall due to high radial forces, generally caused by the unbalances or fluid instabilities [27]. Rubbing in rotating machines is known to produce high impact forces and can lead to catastrophic failures in the worst-case scenario [28]. F. Thiery et al. [27] performed some theoretical analysis of blade tip-wall contacts. They introduced some parameters to study the problem, like the contact stiffness or damping. Results showed that, under rotation, if the contact frequency is near a natural frequency of the rotor, the vibration of the shaft could be amplified drastically, also increasing the strength of the contact. However, this study is only theoretical, and there are no failure cases of prototype Kaplan turbines due to rubbing available in the literature.

1.2.2. Research on Francis turbines

1.2.2.1. Description of Francis turbines
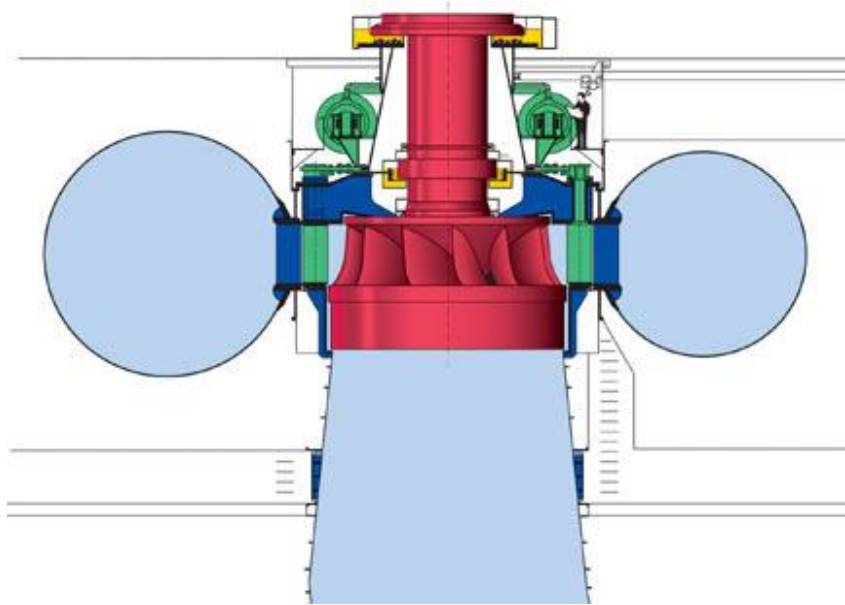
Figure 1-7. Structure of a Francis turbine [29].

Francis turbines are the most widely used type of hydraulic turbines due to their good performance in high and low water flow rates and heads as well as their low cost. The main structure of a Francis turbine runner and the connected components is shown in Figure 1-7. The runner consists of three parts: crown, band and blades. The blades are non-adjustable and firmly constrained by the crown and band. The flowing water first enters the spiral casing, which is an annular channel surrounding the runner, and then flows between the stay vanes, which give the water the optimum flow direction. Then, the water enters into the runner and produces the rotation in the runner. Water enters the runner radially and leaves axially. The guide vanes are adjustable, which on the one hand, can control the flow rate and load of the runner, and on the other hand, can ensure most energy of the water to be transferred to the runner without being consumed by the eddies and other undesirable flow phenomena.

In design and manufacture, Francis turbines are much more complex than Pelton turbines, requiring a specific design for each head/flow condition to obtain optimum efficiency. With large flexibility of designs in consideration of various parameters, a large head ranges from about 30 m up to 700 m can be covered. The most powerful Francis turbines, which are installed in the Three Gorges powerplant of China, have an output of up to 800 MW.

1.2.2.2. Main types of damage in Francis turbines

The main types of damage in Francis turbines are approximately the same with those of Kaplan turbines introduced in Chapter 1.2.1.3. The rotor stator interaction (RSI) is much stronger in Francis turbines than that in Kaplan turbines due to the closer distances between the guide vanes and blades. Because the blades are nonadjustable, the leading-edge cavitation and vortex rope is more likely to appear in Francis turbines [30]. Vortex rope will result in so called draft tube surge which propagates

9

into whole hydraulic system eventually leading to fatigue cracks of the blades or power swing phenomena of the electrical generator [4, 31].

1.2.2.3. Research state of Francis turbines

The dynamic behavior of intact Francis turbines has been extensively studied since the new century. These studies were conducted step by step and tried to understand the dynamic behavior of the real runners and the influence of all factors. Some of the investigations were conducted on pump-turbines, but many conclusions are general for Francis turbines. The investigations are based on reduced scale runners or prototype runners. A real Francis turbine runner is connected to the shaft at the crown top face, and the shaft is connected to the generator as well as supported by the bearings and thrust rings. The runner is surrounded by flowing water with close distances to the covers and case walls. All these factors may affect the dynamic behavior of the runner.

The first step is to research the dynamic behavior of the runner in air without any support. Most of them are based on reduced scale runner models [16, 32-34]. They discuss how the modal shapes of a Francis turbine runner or pump turbine runner are. The main modal shapes of this kind of structures are formed by the different number of nodal diameters. For Francis turbine runners, the maximum deformation is usually located in the band or the blades depending on the modal shapes and N_s of the runners.

Then, these reduced scale models were submerged into an infinite water domain [16, 32-34]. When a structure is submerged in water, its vibration is affected by the added mass, added damping and added stiffness effect. The added stiffness can nearly be neglected for hydraulic turbine runners. The added mass and added damping effect can be much more significant. The natural frequencies are mainly affected by the added mass effect, which may decrease the natural frequencies 20-40% compared with those in air depending on the modal shapes. The modal shapes with a higher number of nodal diameters have more affectation in the natural frequency value. Due to the added mass effect, the modal shapes in water can be slightly different from those in air.

The influence of the support of a prototype Pump turbine runner has been investigated thoroughly in [35] experimentally and numerically. In that research, the supports varied from without any support to fixed support at the crown face and continues to connect with the shaft and generator constrained by the bearings and thrust rings. Results showed that the natural frequencies of some modes, particular the first mode, can vary a lot depending on the supports.

The next is the influence of the boundary conditions of the water domain. In the beginning, the nearby surfaces were all treated as rigid walls. Tanaka [36] was one of the first authors who investigated this topic in pump turbines. He concluded that confining the runner with nearby rigid surfaces decreases the natural frequencies by about 50% of the natural frequency in air, which was more significant than in infinite water. These conclusions were also reached by Liang in its doctoral thesis for Francis turbine and pump turbine prototypes [37]. Mao and wang [38] also studied the influence of the clearances on the natural frequencies of a high-head Francis turbine, observing in this case, a reduction of 30-40% in the natural frequency compared with those in air depending on the modal shape. Valentín, et al. [39], investigated the effect of boundary conditions of a large

Francis turbine. They demonstrated that the radial gap has a big influence in the runner natural frequencies (about 40-50% of reduction against the natural frequency in air depending on the mode-shape) and lower in the shaft and generator natural frequencies.

In all of these works, the boundaries were always thought to be completely rigid. However, this is not always true for the real prototype runner. Head and lower covers that confine the runner are not completely rigid and have their own dynamic behavior, which may affect the dynamic behavior of the runner. Presas, et al. [40], observed in their investigation with a reduced scale pump turbine model that the nearby boundaries may not behave as completely rigid, which may affect the dynamic behavior of the runner. However, this phenomenon could not be investigated in detail. Petter, et al.[41], studied the housing effect on the modal behavior of a low specific speed Francis runner through installing the runner in air, in water and in the turbine house. They also found that some modes with high modal displacements on the disc became difficult to be distinguished probably due to the high damping. Valentín, et al. [42], experimentally studied the dynamic behavior of a vibrating disk submerged in a fluid-filled tank and confined with a nonrigid cover, and they found that when the natural frequencies of casing and disk are in the same frequency range, the dynamic behavior of the disk was affected especially when the distance between disk and cover was small. Huang, et al. [35], investigated numerically and experimentally the natural frequencies and modal shapes of the head cover of a pump turbine prototype, confirming that its dynamic behavior is complex and has to be considered when studying natural frequencies of prototype runners.

Other factors that may affect the dynamic behavior of the runner can be the surrounding water conditions. For real prototype runners, the surrounding water is flowing and sometimes cavitation may occur, which have been shown to be able to affect the dynamic behavior of submerged hydrofoils [43, 44]. Therefore, the best way to research the dynamic behavior of runners is to measure the dynamic behavior of runners in operation directly. Valentín, et al. [45], have demonstrated the feasibility of detecting natural frequencies of hydraulic turbines while in operation using strain gauges and several natural frequencies have been determined accurately in their experiment. However, all the studies above were conducted on intact runners and the effect of a crack on the dynamic behavior of runners has also not been studied before.

The fatigue failure mechanism in Francis turbines is approximately the same as that of Kaplan turbines. Most cracking failures in Francis turbines occurred at the zone of blade trailing edge near the crown [7, 13, 46, 47]. This is because, on the one hand, this zone is easy to have the highest stress concentration under the water pressure load, which has been demonstrated by many researchers[7, 13, 46-49], and on the other hand, this zone is the welding joint zone of the crown and blades, which makes it easy to have material defects and high residual stress [4, 13]. D Frunzăverde, et al. [13], showed that the large crack in that zone occurred due to both the high stress and material defects. Saeed, et al. [47], showed in their failure analysis that the cracks in that zone were due to the combination of the residual stresses, static stresses, and dynamic stresses.

1.2.3. Research on other types of turbines

Because there are not many studies on the effect of a crack on the dynamic behavior of hydraulic turbines, similar research on other types of turbines, e.g., aero-engine turbines and gas

turbines, may provide some useful references.

The effect of a crack on the dynamic behavior of aero-engine turbines or gas turbines has been studied extensively in the past. These turbines can be seen as bladed-disk structures or one-dimensionally periodic systems, which means they can be seen as assemblies with identical substructures in a one-dimensionally cyclic way. For bladed-disk structures with substructure mistuning, the well-known vibration localization will occur [51-57]. For a strongly localized mode, the frequency quickly deviates from the original tuned frequency, and the deformation localizes to the damaged substructure. The mistuning of substructures can be introduced by manufacturing tolerances or long-time wears. Cracking on the blades is also one type of mistuning and the vibration localization induced by it has been widely studied recently [58, 59].

According to the models used for the study, these researches usually can be divided into two categories. One is on simplified models, like the lumped parameter models[58, 60]. For each substructure of one bladed-disk structure, the disk part and the blade can be simplified into lumped masses (or beams) separately or into one lumped mass together, and then massless springs are used to consider the coupling effects between different substructures. Using lumped parameter models, it is easy to do theoretical analysis to get some general conclusions on one type of bladed-disk structures, but the accuracy with real turbines is usually poor. Another one is on high fidelity models and the non-linear effect caused by the crack faces in contact [61, 62]. Using high fidelity models is computational time consuming, but good accuracies with real turbines can be obtained.

Hydraulic turbines can also be seen as blade-disk structures or one-dimensionally cyclic systems. Therefore, a crack on the blade of one hydraulic turbine runner may induce vibration localization to it. However, each type of hydraulic turbines has its own structural characteristics. Therefore, crack induced vibration localizations in different types of hydraulic turbines ought to show different properties. Moreover, hydraulic turbine runners are surrounded by water and it may have large influences on the vibration localizations. Until now, there are still no studies on the vibration localization in submerged bladed-disk structures to the author's knowledge.

1.3 Research line

The main research line of the Fluid Mechanics Department and the Center for Industrial Diagnostics and Fluid Dynamic (CDIF) is based on the dynamic behavior of hydraulic turbines. Since 2005, several theses presented were related to the topic of the dynamic behavior of model or prototype turbines runners [35, 37, 63]. Most of them are focused on Francis turbines or pump turbines. However, there are still some types of turbine runners, e.g., Kaplan turbines, whose dynamic behavior has not been studied before. Moreover, the effect of the runner damage has not been investigated as well. Some uncommon damage cases in some specific types of hydraulic turbines have been seen during those research years. Therefore, it was decided to perform an investigation on the dynamic behavior of a Kaplan turbine runner firstly. Then, based on the dynamic behavior of intact runners, e.g., Francis runners and Kaplan runners, the effects of a crack on the runners is investigated.

1.4. Objectives

The main objective of this doctoral thesis is to evaluate the influence of a crack damage on the dynamic behavior of hydraulic turbines. To do so, two types of model or prototype hydraulic turbines, Francis turbine and Kaplan turbine, have been chosen for study. The objectives can be separated into two parts, the ones of Kaplan turbines and the ones of Francis turbines.

-Objectives of the research on Kaplan turbines:

• To study the dynamic behavior, i.e. natural frequencies and mode-shapes, of a prototype Kaplan turbine step by step from a plate to single blade and continuously to the whole runner.

• To study the changes on the modal behavior of a prototype Kaplan turbine due to a crack on one blade.

• To perform a failure investigation of the crack damage on a prototype Kaplan turbine blade to reveal the reason of the damage.

-Objectives of the research on Francis turbines:

• To numerically study the effect of a crack on the dynamic behavior of a Francis turbine runner model, applying the knowledge acquired with Kaplan turbines.

1.5. Methodology

The methodology of this thesis can be seen in Figure 1-8. The research topic can be divided into Kaplan turbines and Francis turbines. However, the research emphasis is laid on Kaplan turbines. This is divided into two steps. First, the dynamic behavior of an intact Kaplan turbine runner is studied. Then, based on the dynamic behavior of intact turbine runners, the effect of a crack on one blade is investigated. A systematic approach has been used for study. The researches start from numerical models, and then, the numerical results are validated by experiments. The studies on the numerical models are conducted step by step from simplified blade models to single blade models and continuously to whole turbine models. Then, the knowledge obtained on Kaplan turbines is applied to a Francis turbine runner, whose dynamic behavior was previously studied

Crack induced Dynamic Behavior Changes

Kaplan turbines

Numerical Models

Simplified blade

Single blade

Whole runner
(air, water)

Without
Crack

With
Crack

Analysis

Experimental Modal
Analysis

Validation

Francis turbines

Numerical Francis runner
model without crack

Available
Experimental Data

Validation

With Crack
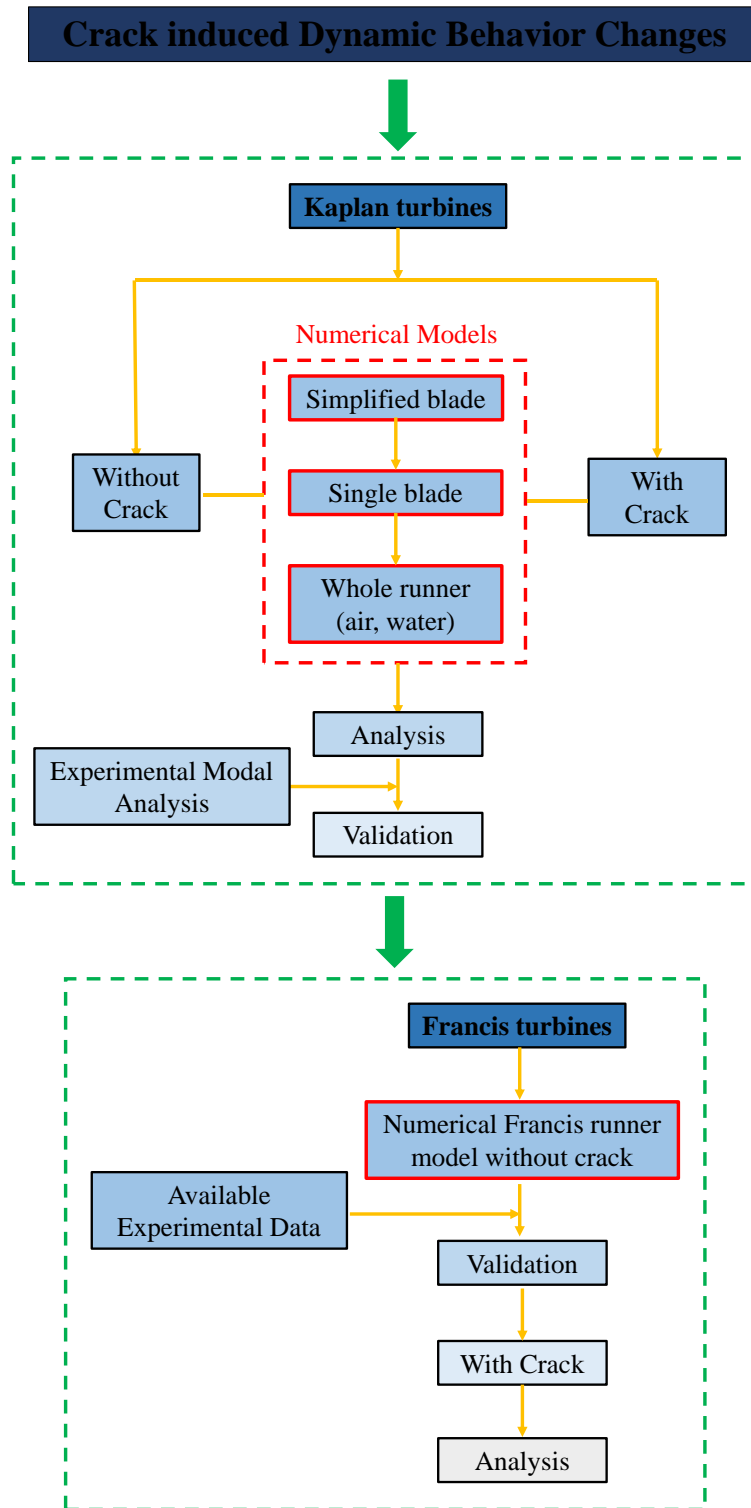
Analysis

Figure 1-8. The methodology of this thesis.

1.6. Main characteristics of the turbines under analysis

1.6.1. Prototype Kaplan turbine

The Kaplan turbine under analysis has a head of 34 m and a maximum power of 73 MW. It is a vertical machine supported by a thrust bearing in the lower side of the generator, and two radial

bearings, one in the turbine side and another in the generator side. The structure of the turbine is shown in Figure 1-9. The runner has 6 blades rotating at 125 rpm, and the distributor has 24 guide vanes. The tip clearance is of 0.09% the outlet diameter of the runner (D_{out}). Inside the hub, there is a control system to adjust the angle of the blades.
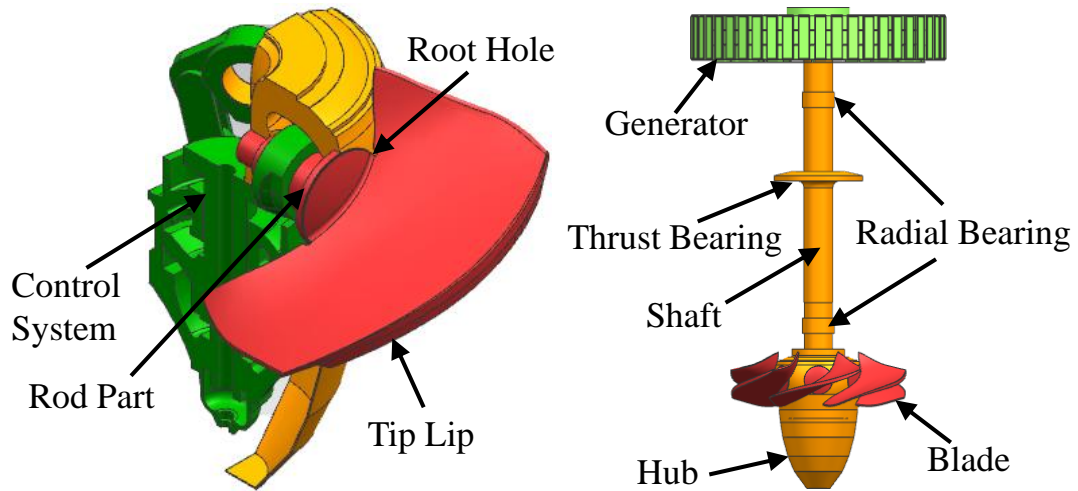
Figure 1-9. Structure of the prototype Kaplan turbine.
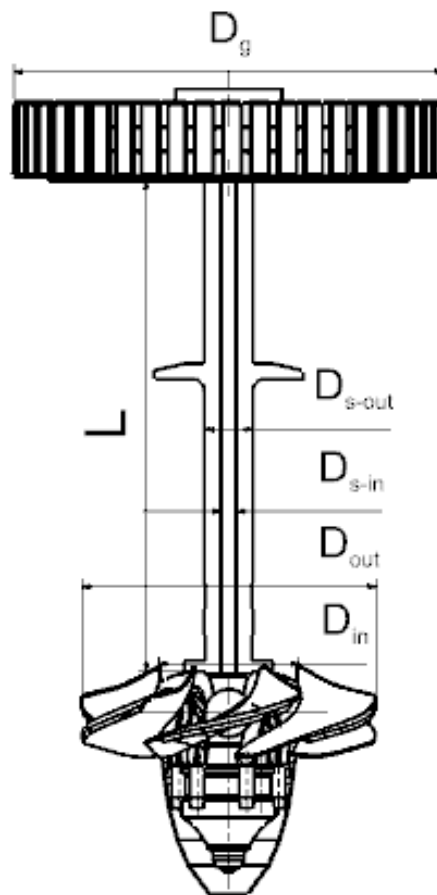
Figure 1-10. Main dimensions of the prototype Kaplan turbine.

The main dimensions of the turbine are shown in Figure 1-10. The relationship between the

inlet diameter (D_{in}) and the outer diameter (D_{out}) is about $D_{in}/D_{out} = 0.51$. The total length of the shaft L is about 1.68 times of the runner outer diameter D_{out}. It is a one-piece hollow structure with a central hole. The outside diameter of the shaft D_{s-out} is about 0.16 times D_{out}, and the diameter of the central hole D_{s-in} is 0.05 times D_{out}. The diameter of the generator D_g is about 1.4 times D_{out}, and it is formed by 48 poles that are supported by a spider type structure. Except for the generator, the other parts of the turbine are all made of stainless steel. However, the generator is formed by the poles and the spider structure, which are made from different types of materials and the total weight of the generator is 20300 Kg. The property of stainless steel is shown in Table 1-1. The material properties of the generator are all the same with those of the stainless steel apart from a modified density to make its total weight to be 20300 Kg.

Table 1-1. Properties of the Kaplan turbine material.

Properties	Young's modulus	Density	Poisson's ratio
Value	193 GPa	7750 kg/m^3	0.31

One inspection of the runner showed a large crack starting from the leading-edge side root hole of one of the blades (Figure 1-11). The total length of the crack is about 600mm long. The machine was then investigated to reveal the cause of this large crack.

(a)   (b)
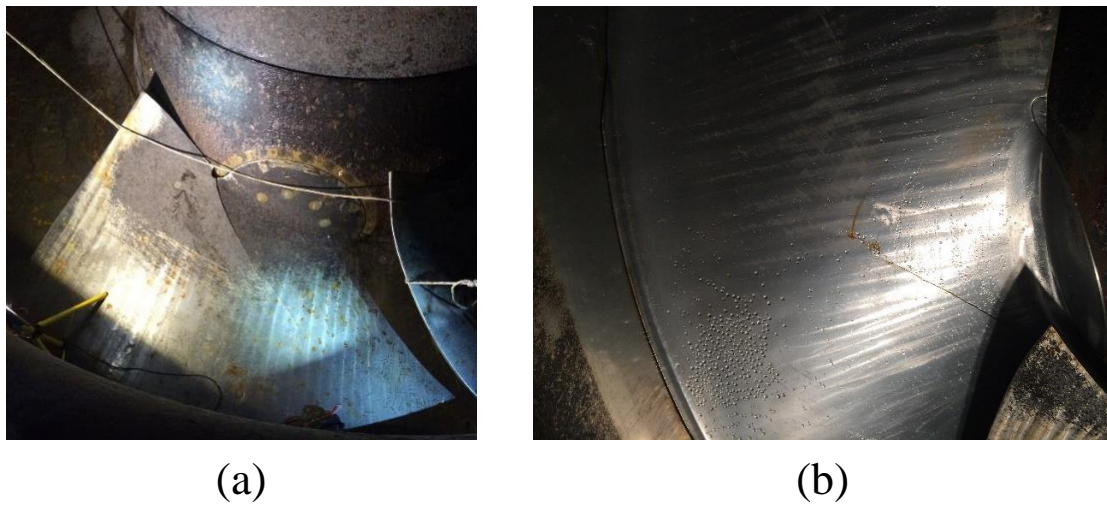
Figure 1-11. View of the blade with crack. (a) Pressure side. (b) Suction side.

1.7.2. Francis turbine runner model

The intact Francis runner model used in this thesis is a replica at a reduced scale of 1:10 of a Francis turbine runner with a dimensionless specific speed of 0.56. This model is the same as that used in [16, 32]. The model runner has 17 blades and a diameter of 409 mm. The shape of the runner with the main dimensions is shown in Figure 1-12. The material used is a bronze alloy whose properties are given by Table 1-2.

Table 1-2. Properties of the Francis runner model material.

Properties	Young's modulus	Density	Poisson's ratio
Value	110 GPa	8300 kg/m^3	0.34
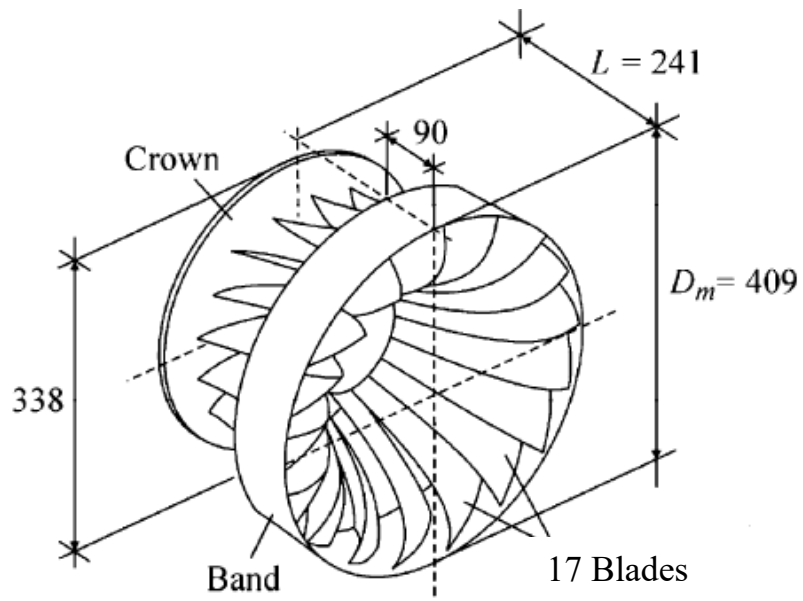
Figure 1-12. Francis runner model and its main dimensions in mm [16].

17

CHAPTER 2. Study on Numerical Models

The main purpose of this chapter is to numerically study the effect of a crack on the dynamic behavior of Kaplan turbines and Francis turbines. This chapter consists of three parts. The first part is a brief introduction to the theoretical knowledge that is possible to be used for analysis. The second part is a systematic study on the dynamic behavior of Kaplan turbines with and without a crack from simplified blade models to the whole runner. The third part is the effect of a crack on the dynamic behavior of a Francis runner model. The content of the third part has been published in the paper" Zhang M, Valentin D, Valero C, et al. Numerical study on the dynamic behavior of a Francis turbine runner model with a crack[J]. Energies, 2018, 11(7): 1630".

2.1. Theoretical background

2.1.1. System parameter determination

For a single degree-of-freedom (SDOF) system, the governing equation of the structural motion can be described by Eq. (2-1), and the solution of it can be expressed as in Equation (2-2).

$$M_s \ddot{x} + C_s \dot{x} + K_s x = F_s(t) \qquad (2-1)$$

$$\text{x} = \text{X} \sin(\omega t + \varphi) \qquad (2-2)$$

where M_s, C_s, K_s are the mass, damping and stiffness of the structure, x is the displacement at any given instant time, t, X is the maximum displacement, circular frequency $\omega = 2 \cdot \pi \cdot f$, f is frequency (Hz) and φ, the phase shift. The damping ratio ξ, the natural frequency ω_n, and the damped natural frequency ω_d are as following:

$$\xi = \frac{C_s}{2\sqrt{K_s M_s}} \qquad (2-3)$$

$$\omega_n = \sqrt{\frac{K_s}{M_s}} \qquad (2-4)$$

$$\omega_d = \omega_n\sqrt{1 - \xi^2} \qquad (2-5)$$

The frequency response function (FRF) of single dof system can be calculated as the relationship of the displacement and the applied force:

$$\frac{X}{F} = \frac{1/K_s}{\sqrt{\left[1 - \left(\frac{\omega}{\omega_n}\right)^2\right]^2 - \left[2\xi\left(\frac{\omega}{\omega_n}\right)\right]^2}} \qquad (2-6)$$

The damped natural frequency ω_d is found at maximum FRF amplitude and for low damping ratio it can be assumed that the maximum amplitude is reached when $\omega = \omega_n = \omega_d$. Under this assumption, the damping ratio can be obtained from the FRF using the half-band method [64]:

$$\xi = \frac{\omega_B - \omega_A}{2\omega_d} \qquad (2-7)$$

ω_A and ω_B are the frequencies whose amplitudes correspond to the half power of FRF that equals $(2\xi K)^{-1}$. Then, the stiffness K, mass M and damping C of the system can be calculated as:

$$K_s = \frac{1}{2\xi \left(\frac{X}{F}\right)_{\omega = \omega_d}} \qquad (2-8)$$

$$M_s = \frac{1 - \xi^2}{2\omega_d^2 \xi \left(\frac{X}{F}\right)_{\omega=\omega_d}} \tag{2-9}$$

$$C_s = \frac{\sqrt{1 - \xi^2}}{\omega_d \left(\frac{X}{F}\right)_{\omega=\omega_d}} \tag{2-10}$$

Now, let us consider a multiple dof system. The FRF at any point p due to a force at point q for an N dof system can be written as follows:

$$\frac{X_p}{F_q} = \sum_{i=1}^{N} \left(\frac{X_p}{F_q}\right)_i \sin\left(\omega t - \phi_{pq,i}\right) \tag{2-11}$$

where,

$$\left(\frac{X_p}{F_q}\right)_i = \frac{\alpha_{pq,i} \frac{1}{K_{s,i}}}{\sqrt{\left[1 - \left(\frac{\omega}{\omega_{n,i}}\right)^2\right]^2 - \left[2\xi_i \left(\frac{\omega}{\omega_{n,i}}\right)\right]^2}} \tag{2-12}$$

In Equations (2-11) and (2-12), the subscript i indicates the corresponding value at the ith natural frequency. It can be observed that the main difference with the response in a single dof system is the weighting value $\alpha_{pq,i}$. This value corresponds to the normalized modal shape of the corresponding on, i. Then, the value of $\alpha_{pq,i}$ goes from -1 to 1 and depends on the positions of p and q. If $\alpha_{pq,i}$ is zero, the point p and/or q is a node of the mode-shape. This method is the so-called mode superposition method, which means the response of a structure at any frequency can be approximately expressed as a linear combination of the modal shapes of some nearby modes.

For the low-density frequency spectrum of FRF, where the frequencies are separated from each other, the MDOF system can be simplified as several SDOF systems to extract the modal parameters with the assumption that the response of the system near resonance is dominated by the mode at resonance [65]. Then, the system parameters for each mode can be determined using the method in single dof system:

$$K_{s,i} = \frac{\alpha_{pq,i}}{2\xi_i \left(\frac{X_p}{F_q}\right)_{\omega=\omega_{d,i}}} \tag{2-13}$$

$$M_{s,i} = \frac{\alpha_{pq,i}(1 - \xi_i^2)}{2\omega_d^2 \xi \left(\frac{X_p}{F_q}\right)_{\omega=\omega_{d,i}}} \tag{2-14}$$

$$C_{s,i} = \frac{\alpha_{pq,i}\sqrt{1-\xi_i^2}}{\omega_{d,i}\left(\frac{X_p}{F_q}\right)_{\omega=\omega_{d,i}}}$$ (2 − 15)

2.1.2. Fluid-structure interaction (FSI)

When a quiescent fluid is considered around the body, a fluid force (F_f) appears over the surface of the body, modifying the general motion Equation (2-1) as:

$$M_s\ddot{x} + C_s\dot{x} + K_s x = F_s + F_f$$ (2 − 16)

$$F_f = -M_a\ddot{x} - C_a\dot{x} - K_a x$$ (2 − 17)

M_a, C_a, K_a are the added mass, added damping and added stiffness due to fluid force, respectively. The added mass can be interpreted as the mass of fluid accelerated due to the motion of the structure. The added stiffness describes the change in the flow-induced restoring force with the deflection of the structure. The added damping represents the energy extracted from the structure because of the work done by the fluid flow. For a rigid structure and when the fluid flow is not that too high, the added stiffness usually can be neglected. The added mass and added damping can be more significant, but the natural frequencies are mainly affected by the added mass. By neglecting the added stiffness and assuming the structure a free vibration ($F_s = 0$), Equation (2-16) and Equation (2-17) change to:

$$(M_s + M_a)\ddot{x} + (C_s + C_a)\dot{x} + K_s x = 0$$ (2 − 18)

The value of natural frequencies and damping ratio of the system for each corresponding mode-shape can be calculated as:

$$f_f = \frac{1}{2\pi}\sqrt{\frac{K_s}{M_s + M_a}}$$ (2 − 19)

$$\xi_f = \frac{C_s + C_a}{\sqrt{K_s(M_s + M_a)}}$$ (2 − 20)

Comparing Equation (2-4) and Equation (2-19), the natural frequency value a body submerged in a fluid is lower than in the vacuum due to the added mass (M_a). However, in the case of the damping ratio (Eqs. (2-3) and (2-20)), when the body is submerged in a fluid, the damping ratio not only depends on the added damping (C_a), but also the added mass (M_a). Assuming that the natural frequencies in the vacuum are practically the same as in the air ($f_v = f_a$), a dimensionless added mass factor (λ) can be introduced [16]. This factor is defined as the added mass (M_a) over the modal mass (M_s).

$$\lambda = \frac{M_a}{M_s} = \left(\frac{f_a}{f_f}\right)^2 - 1 \tag{2-21}$$

2.1.3. Numerical Modeling

According to the dynamic theory of MDOF system and finite element method, the dynamic equilibrium equation of a structure can also be expressed as following (neglecting damping):

$$[M_s]\{\ddot{x}\} + [K_s]\{x\} = \{0\} \tag{2-22}$$

The $[M]$ and $[K]$ are the mass matrix and stiffness matrix, respectively. The $\{x\}$ is the nodal displacement vector. Because low damping ratios have little effect on the natural frequencies and modal shapes, it is usually neglected in the numerical modal analysis. The structure is thought to have constant stiffness and mass effects. There are no time varying forces, displacements, pressures, or temperatures applied to the structure, therefore it is a free vibration.

For a linear system, free vibrations will be harmonic of the form:

$$\{x\} = \{\phi_i\} \cos \omega_i t \tag{2-23}$$

where the $\{\phi_i\}$ is the eigenvector representing the modal shape of ith natural frequency and ω_i is the natural frequency of ith mode. Thus, Equation (2-22) becomes

$$\left(-\omega_i^2 [M_s] + [K_s]\right)\{\phi_i\} = \{0\} \tag{2-24}$$

This equation is satisfied either if $\{\phi_i\} = \{0\}$ or if the characteristic matrix of $-\omega_i^2 [M] + [K]$ is zero. The first option is the trivial one and, therefore, is not of interest. Thus, the second one gives the solution:

$$\left|-\omega_i^2 [M_s] + [K_s]\right| = 0 \tag{2-25}$$

This eigenvalue problem can be solved for up to n values of ω_i and n eigenvectors $\{\phi_i\}$ which satisfy Equation (2-24), where n is the number of DOFs. Rather than outputting the natural circular frequencies ω_i, the natural frequencies are derived as:

$$f_i = \frac{\omega_i}{2\pi} \tag{2-26}$$

f_i is the ith natural frequency in Hz.

For the numerical simulation of the fluid-structure interaction of a structure submerged in still water based on the finite element method (FEM), an acoustic FSI technology is widely used [32, 66, 67]. In the case of water-structure coupling, the behavior of the water pressure can be described with the acoustic wave equation, known as Helmholtz's equation, which is derived from the Navier–Stokes equation of motion and the continuity equation by considering the following assumptions [68]:

• The fluid is slightly compressible (density changes due to pressure variations).

• The flow is irrotational.

• There is no mean flow of the fluid.

• Changes of mean density and pressure in different areas of the fluid domain remain small.

By considering the fluid pressure acting at the interface, the discretized equation for structural dynamics can be written as follows:

$$[M_s]\{\ddot{x}\} + [C_s]\{\dot{x}\} + [K_s]\{x\} = \{F_s\} + \{F_{fs}\} \qquad (2-27)$$

where $\{F_{fs}\}$ is the fluid pressure load vector at the fluid-structure interfaces. There is:

$$\{F_{fs}\} = -[M_{fs}]\{\ddot{x}\} = -[K_{fs}]\{p\} = [M_f]\{\ddot{p}\} + [C_f]\{\dot{p}\} + [K_f]\{p\} \qquad (2-28)$$

where $[M_f]$ is the fluid equivalent "mass" matrix, $[C_f]$ is the fluid equivalent "damping" matrix, $[K_f]$ is the fluid equivalent stiffness matrix, $[M_{fs}]$ is the equivalent coupling "mass" matrix, and $[K_{fs}]$ is the equivalent coupling "stiffness" matrix. The complete finite element discretized equations for the fluid structure interaction problem are written in assembled form as:

$$\begin{bmatrix} [M_s] & [0] \\ [M_{fs}] & [M_f] \end{bmatrix} \begin{Bmatrix} \{\ddot{x}\} \\ \{\ddot{p}\} \end{Bmatrix} + \begin{bmatrix} [C_s] & [0] \\ [0] & [C_f] \end{bmatrix} \begin{Bmatrix} \{\dot{x}\} \\ \{\dot{p}\} \end{Bmatrix} + \begin{bmatrix} [K_s] & [K_{fs}] \\ [0] & [K_f] \end{bmatrix} \begin{Bmatrix} \{x\} \\ \{p\} \end{Bmatrix} = \begin{Bmatrix} \{F_s\} \\ \{0\} \end{Bmatrix} \qquad (2-29)$$

In the modal analysis, the damping effect usually is not considered, and the structure vibrates freely. In this way, the fluid structure coupled equation can be simplified as follows:

$$\begin{bmatrix} [M_s] & [0] \\ [M_{fs}] & [M_f] \end{bmatrix} \begin{Bmatrix} \{\ddot{x}\} \\ \{\ddot{p}\} \end{Bmatrix} + \begin{bmatrix} [K_s] & [K_{fs}] \\ [0] & [K_f] \end{bmatrix} \begin{Bmatrix} \{x\} \\ \{p\} \end{Bmatrix} = 0 \qquad (2-30)$$

Therefore, for a problem involving fluid structure interaction the fluid element generates all the matrices with subscript f in addition to the coupling matrices $[M_{fs}]$ and $[K_{fs}]$. The matrices with subscript s are generated by the compatible structural element used in the model.

2.2. Systematic approach for Kaplan turbines

The dynamic behavior of Kaplan turbines with and without a crack is studied systematically from simplified blade models to the whole runner in this section. Ansys Workbench 16.2 is used to handle all the simulations.

2.2.1. Systematic approach for Kaplan turbines without crack

2.2.1.1. Dynamic behavior of simplified blade models

The investigation on simplified blade models can help us to understand the dynamic behavior of the single blade as well as the whole runner. The simplified blade model geometry is shown in Figure 2-1. It is a rectangular plate with a dimension 750mm×500mm×25mm. The front face of the

model was divided into many grids so as to easily change the fixed support position. The first six modes of these three models are shown in Table 2-1.

For a rectangular plate, the mode shapes can usually be classified into bending (B), torsion (T) and in-plane (IP) modes [67]. The torsion modes can further be classified according to the number of its horizontal nodal lines (m_H) and vertical nodal lines (n_V). A nodal line is a line which remains at rest while the other parts of the structure are in a state of vibration. These lines separate regions where (at a given moment) the structure is moving in positive and negative directions. Therefore, the mode with m_H horizontal nodal line (NL) and n_V vertical NL can be written as mode (m_H, n_V). However, due to the fixed support of investigated models, the nodal lines sometimes become complicated, and they are needed to be distinguished very carefully.
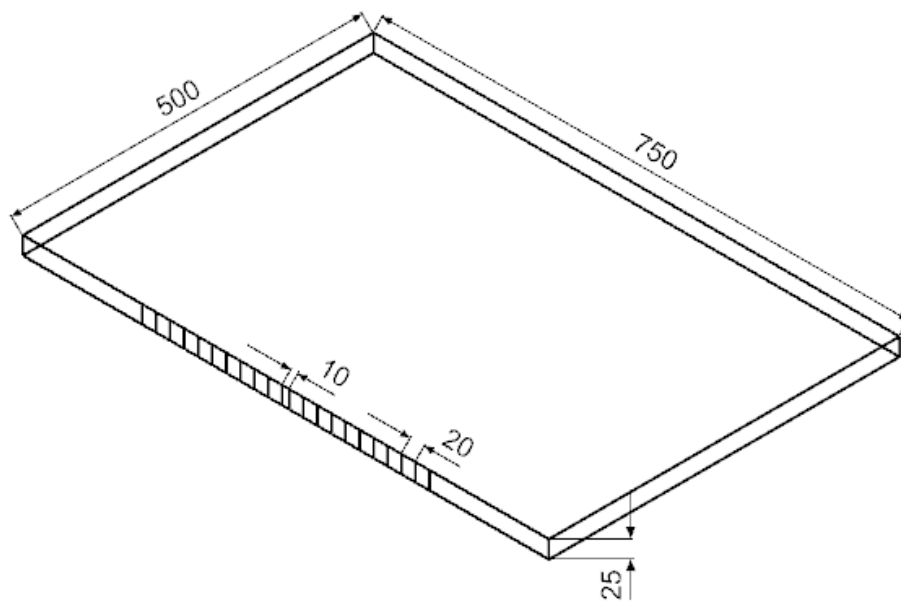

Figure 2-1. Rectangular plate model.

For the rectangular plate with symmetric fixed support (a), all the modal shapes are symmetric with the middle axis line. However, for the rectangular plate with an unsymmetric fixed support (b) and (c), all the modal shapes deflect to the side opposite to the fixed support position deviation. The larger is the deviation, the larger the mode shapes deflections are.

The support position may not only affect the modal shapes but also the natural frequencies and maximum stresses under resonance conditions. To demonstrate this, the influences of support position on the dynamic stresses under the resonance conditions of different modes are investigated through harmonic response analysis. A dynamic force with an amplitude 100 N was implemented to the left-side edge of each model. The damping ratio was set to be 0.01, and the support position moved from the symmetrical position to the right side with a step of 20 mm (the total support length kept to be 170mm). The normalized natural frequency and maximum stress changes with the support position deviation for different modes which have been shown in Figure 2-2.

Table 2-1. Modal shapes of the first six modes for different models.

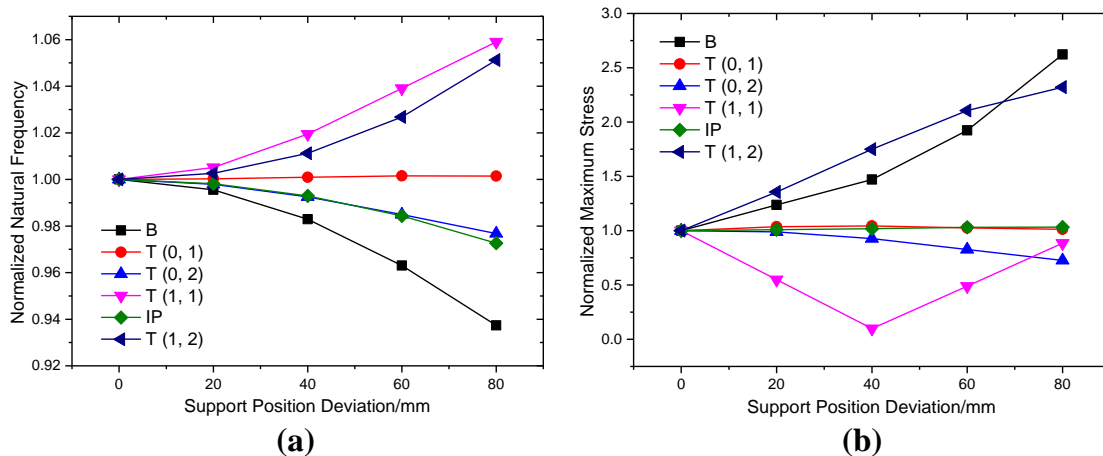|	(a) Symmetric support	(b) Support deviated 40 mm	(c) Support deviated 80 mm
B			
T (0, 1)			
T (0, 2)			
T (1, 1)			
IP			
T (1, 2)			

(a)

(b)

Figure 2-2. Normalized natural frequency and maximum stress changes with the support position deviation for different modes (a) natural frequencies (b) maximum stresses.

The influences of the support position on the natural frequencies and maximum stresses depend

on the modes. Generally, the natural frequencies are not very sensitive to the support position change. However, the maximum stresses of some modes can be very sensitive to the support position. For some particular modes concerned, the support position can probably be optimized in the real design progress of a real turbine blade, e.g., the Kaplan turbine blade, to minimize the stress level.

2.2.1.2. Dynamic behavior of single blade

This section is focused on the dynamic behavior of a single blade model. The blade model consists of the blade and the rod parts. The blade model is supported at the position where the blade connects the control system as shown in Figure 2-3.
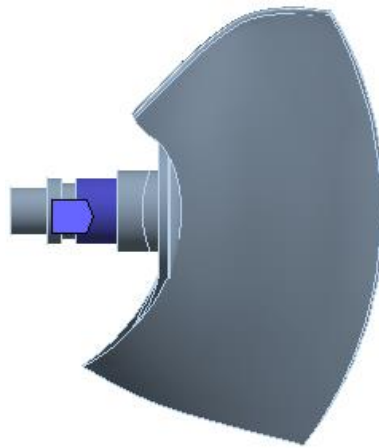

Figure 2-3. Single blade model with a fixed support.

The first six modes of this model are shown in Table 2-2. These modes are similar to those of the rectangular plate model shown in Section 2.1.1.1.

Table 2-2. Modal shapes of single blade model.

B	T (0, 1)	IP
T (0, 2)	T (1, 1)	T (1, 2)

For real Kaplan turbines, blades are assembled together by the connections with the hub and control system at the rod part. The connection stiffness may also affect the dynamic behavior of the blade. To investigate the influence of support stiffness, a model with a single blade and a layer at the rod part was used, as shown in Figure 2-4. The layer is cut from the hub with a thickness of 1mm, and its Young's modulus can vary to investigate the influence of the support stiffness. Fixed supports were given to the end face of the rod and the circumferential surfaces of the layer. The results are shown in Table 2-3. For the Bending mode and Torsion (0, 1) mode, the higher support stiffness makes the modal shapes deflect to the leading-edge side. While for rest modes, the modal shapes deflect to the trailing-edge side. The support stiffness can obviously change the balance of the blade, thus the modal shapes of different modes. But for different modes, the changes can be different.
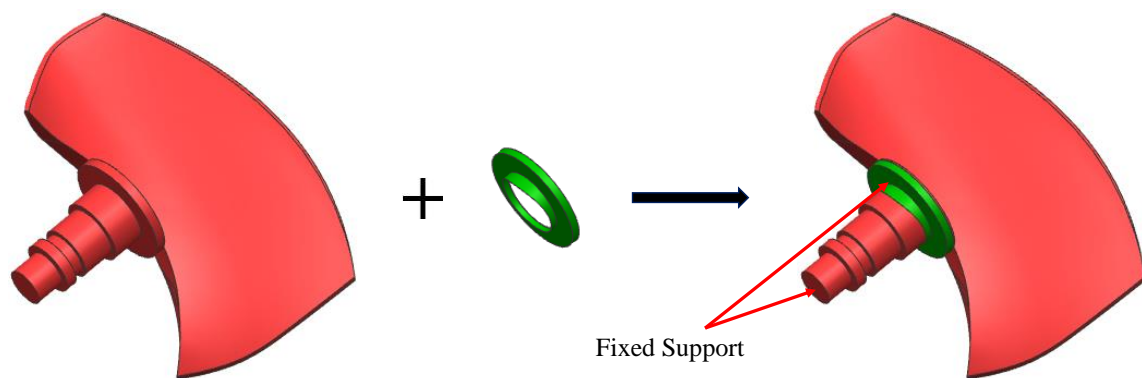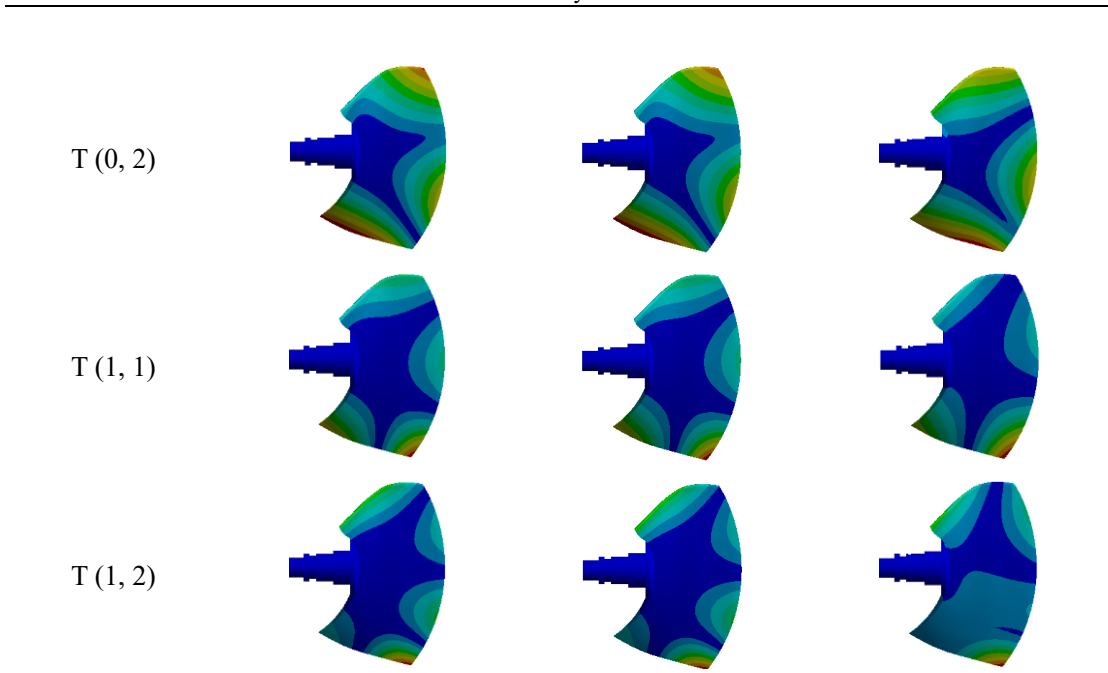

Fixed Support

Figure 2-4. Single blade model with a stiffness variable layer support.

Table 2-3. Modal shape changes with the variation of layer stiffness ratios.

	Layer stiffness 1.0	Layer stiffness 0.01	Layer stiffness 0.0001
B			
T (0, 1)			
IP			

The support stiffness may also have large effects on the natural frequencies. The natural frequency changes for different modes with the layer stiffness ratio (K) change are shown in Figure 2-5. With the reduction of layer stiffness, the natural frequencies of all modes decrease, particular for the layer stiffness ratio area between 0.01 to 0.0001, which means that the natural frequencies are sensitive to the support stiffness in this area.
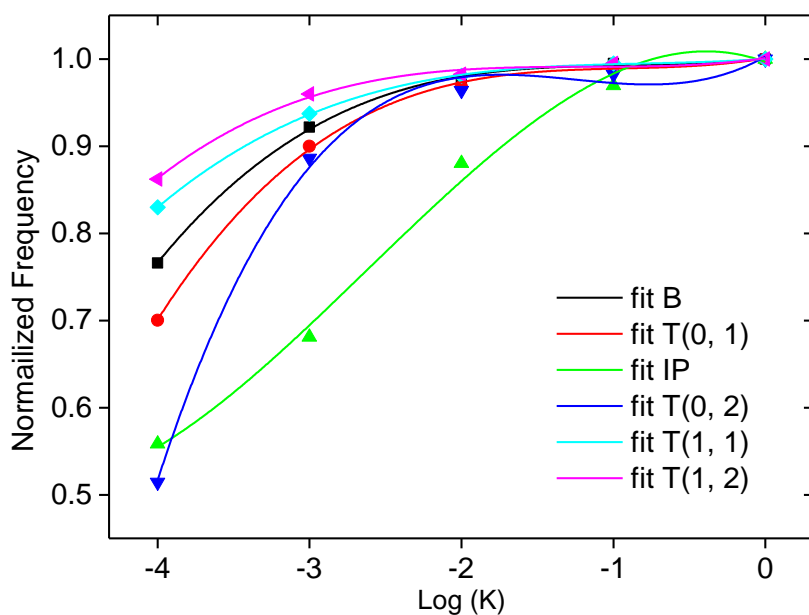

Figure 2-5. Natural frequency changes with the variation of layer stiffness.

2.2.1.3. Dynamic behavior from single blade to the whole runner

This section presents the effects of considering the hub of the runner, the shaft, the control system and the generator of a Kaplan turbine on the modal behavior of the turbine blade. The steps followed include: single blade (B), single blade + hub + shaft (BHS), single blade + hub + control system + shaft (BHCS) and single blade + hub + control system + shaft + generator (BHCSG). The

models for each step are shown in Figure 2-6. The shaft of the BHS and BHCS models only contains the part below the thrust bearing and all boundary conditions are the same as those of BHCSG except a fixed support at the top of the thrust bearing. The natural frequencies and natural frequency bands of different modes for different models are shown in Table 2-4.

All the parts of different models are merged as a whole body. The effect of turbine bearing and generator bearing is simulated as elastic supports with a foundation stiffness 6.524 N/mm³, which is equivalent to a spring stiffness $10^{10} N/m$ around bearings (this spring stiffness has been used in some other similar researches [39]). When the machine is stopped, the rotor system is laid on the support structure of the thrust bearing. Therefore, the effect of the thrust bearing is simulated as zero-displacement support in the shaft axial direction. The mesh detail of the BHCSG model is shown in Section 2.2.1.4. When all the six blades are simulated, the modes of the blades form different mode families with 6 modes in each family, thus a natural frequency band is presented for each family.
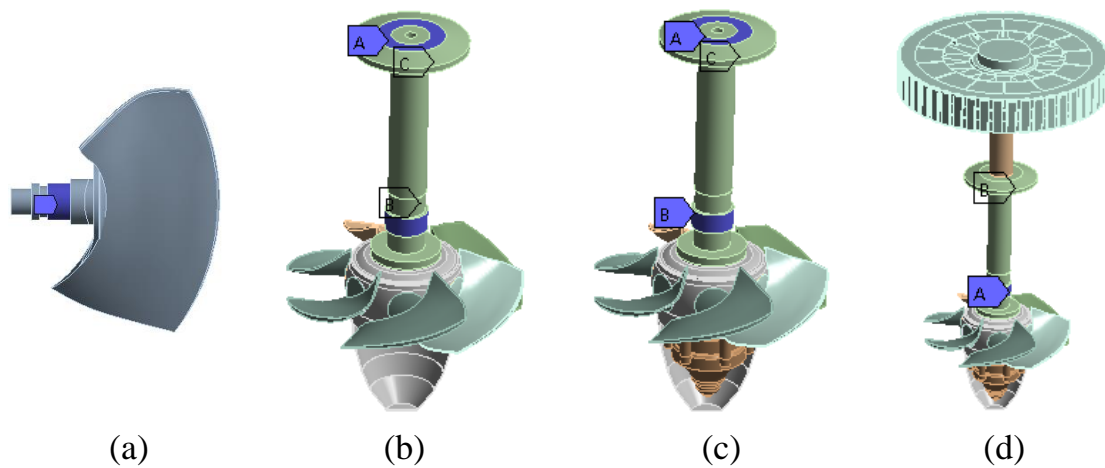

(a)   (b)   (c)   (d)

Figure 2-6. Different models investigated for each step from single blade to the whole runner (a) B (b) BHS (c) BHCS (d) BHCSG.

Table 2-4. Natural frequencies of different modes for different models (Hz).

	B	BHS	BHCS	BHCSG
Bending	57.094	51.38-59.56	49.97-60.749	51.37-60.74
T (0, 1)	64.683	71.38-75.57	72.14-76.32	71.31-76.21
IP	76.229	83.679-93.81	86.49-97.35	87.46-97.31
T (0, 2)	112.79	110.25-123.11	110.89-120.02	110.93-119.97
T (1, 1)	138	144.69-150.72	144.96-150.61	144.94-150.61
T (1, 2)	183.64	194.34-197.7	190.03-196.74	189.97-196.72

Through the comparison between the results of BHCS and BHCSG, it is easy to find that the generator nearly has no influence on the natural frequency bands of blade modes. This is because the generator nearly does not take part in the vibration cycle in Table 2-5. Therefore, the generator can be neglected in the simulation if only blade-dominated modes are concerned. The influence of the control system is a little more significant because the control system can take part in the vibration

for some mode families, but its influence on the natural frequency bands is still less than 3%.

The natural frequencies obtained through single blade are close to the corresponding natural frequency bands of the whole runner. These natural frequencies are usually located at the downstream or lower part of the corresponding natural frequency bands. Therefore, the single blade simulation can probably be used to estimate the natural frequency bands.

2.2.1.4. Dynamic behavior of the whole runner

When the runner is submerged in water, the acoustic fluid-structure interaction technology has been used to simulated the added mass effect from the water. The asymmetric solver with fluid-structure couple algorithm has been used. The density of the acoustic body is 1000 kg/m^3 and the sound speed is 1483 m/s. The water domain includes the part from the guide vanes to 125 mm downwards the hub. To simplify, all the boundaries of the water domain were set to be rigid walls. The common nodes technology has been used at the fluid-structure interfaces. The mesh sensitivity was strictly checked. When the runner is submerged in water, about $1.4 \cdot 10^5$ tetrahedral elements were used, as shown in Figure 2-7. In the modal analysis, the structural damping and the dynamic viscosity of the water have been neglected.
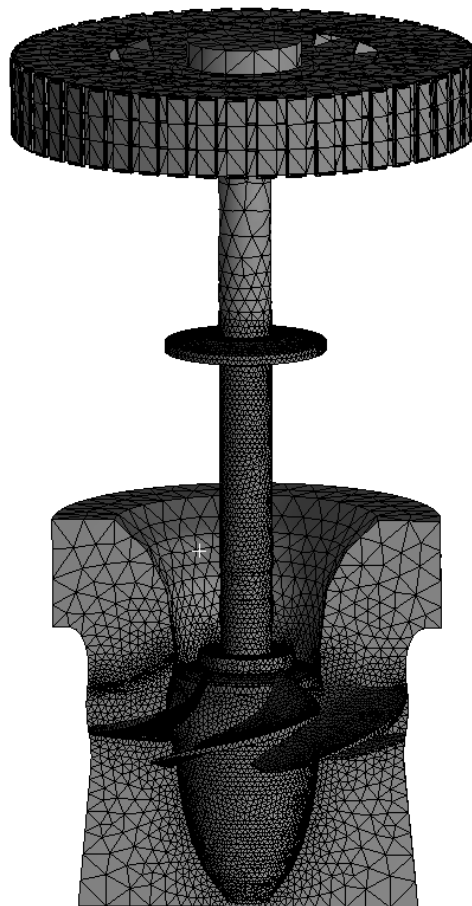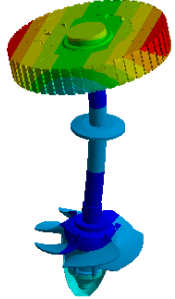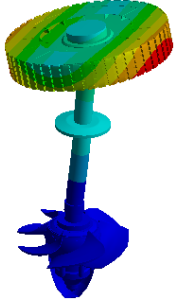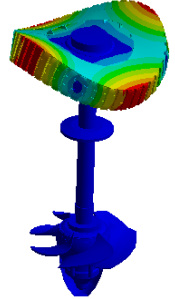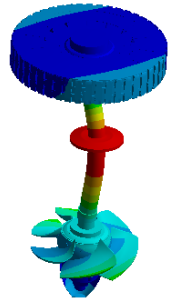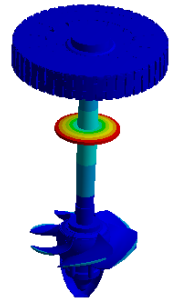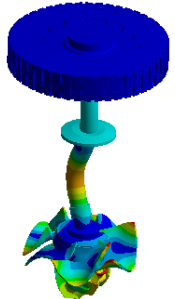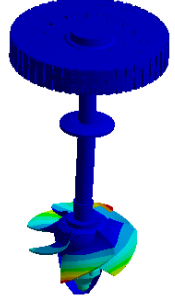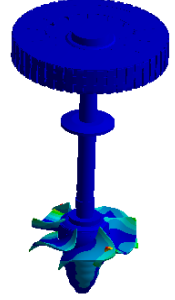

Figure 2-7. View of the mesh when the runner is submerged in water.
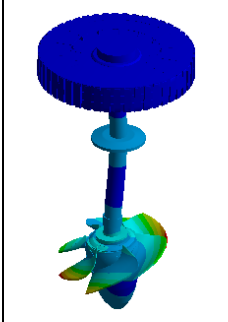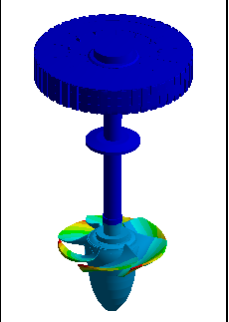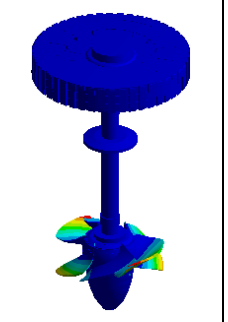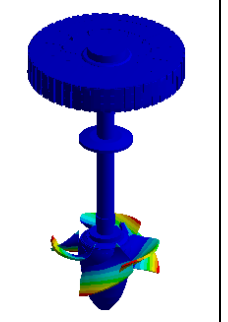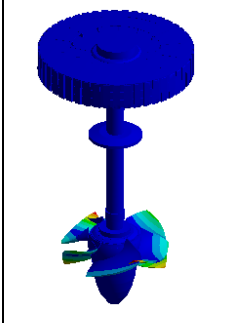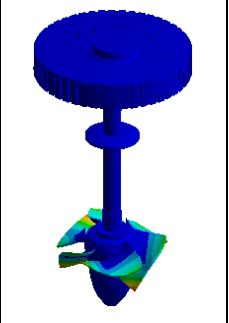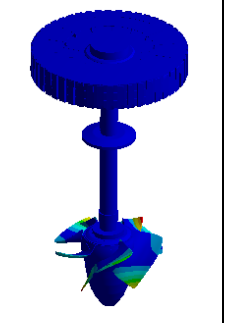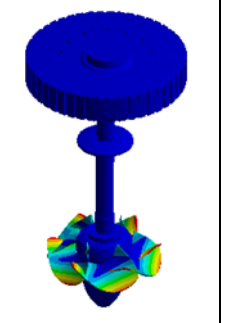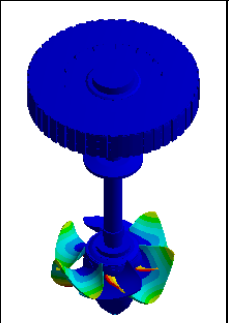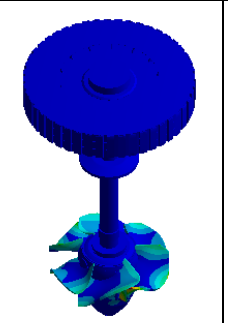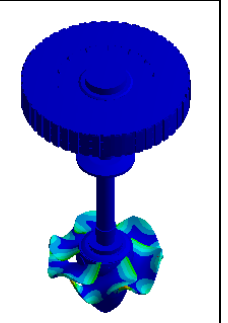
2.2.1.3.1. Structure in air

According to the maximum displacement position, the modes of the machine can usually be

divided into generator dominated (GD), shaft dominated (SD), hub dominated (HD), control system dominated (CSD) and blades dominated (BD). Some of them are listed in Table 2-5.
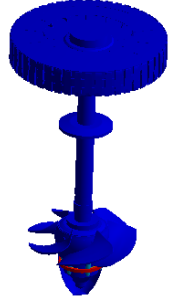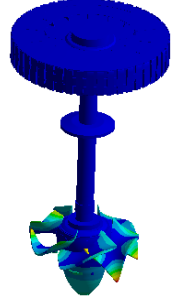
Table 2-5. Numerical modes of the whole turbine.

	1ND	0ND	2ND	3ND
Generator dominated modes (GD)				
Shaft dominated modes (SD)				
Control system dominated modes (CSD)				
Hub dominated modes (HD)				
Blade	1ND	0ND	2ND	3ND
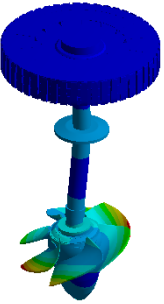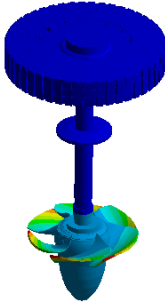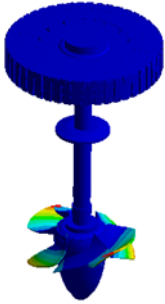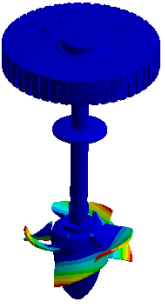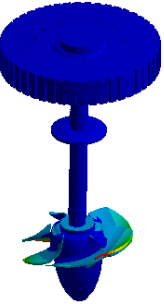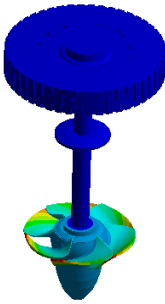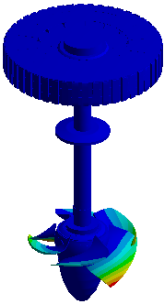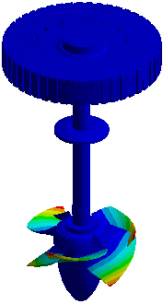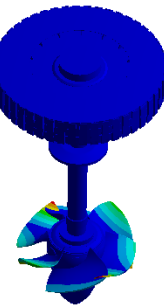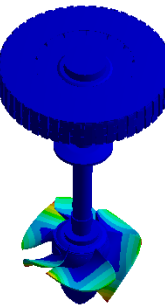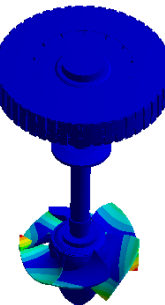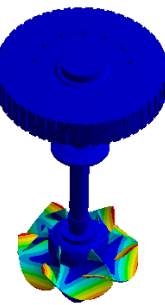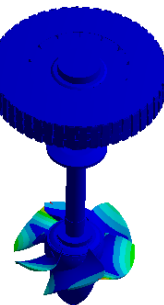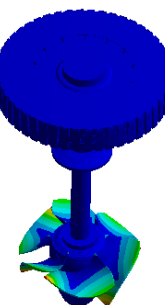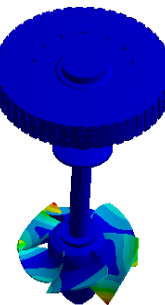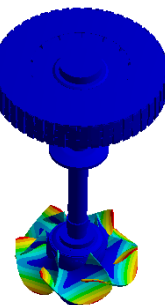
dominated (BD) Mode family Bending (B) 51.4-60.7Hz				
	2ND	3ND	1ND	0ND
Blade dominated (BD) Mode family Torsion (0, 1) 72.1-73.7Hz				
	Blade dominated Mode family In Plane 87.5-97.3Hz	Blade dominated Mode family Torsion (0, 2) 110.9-119.9Hz	Blade dominated Mode family Torsion (1, 1) 144.9-150.6Hz	Blade dominated Mode family Torsion (1, 2) 189.9-196.7Hz
Other blades dominated mode families (BD)				

The blades dominated modes can be divided into different mode families according to the mode shape of the blades, and each mode family has 6 modes, which form mode shapes with different nodal diameters (ND) (singlet 0ND, doublet 1ND, doublet 2ND and singlet 3ND). The modal shapes of the doublet modes of the same ND have a $90°$ phase shift between each other. The appearance sequences of different ND modes in different mode families can be different, which is mainly determined by the interaction intensity between the blades and hub/control system. Bending and In-Plane mode families usually have stronger interaction intensities than other mode families. The stronger interactions make the natural frequency bands of the corresponding mode families wider.

2.2.1.3.2. The effect of the surrounding water

The modal shapes of bending and Torsion (1, 2) mode families of the whole runner in air and in water are shown in Table 2-6.

Table 2-6. Modal shapes of the whole runner in air and in water.

	1ND	0ND	2ND	3ND
Blade dominated (BD) Mode family Bending In Air				
	1ND	0ND	2ND	3ND
Blade dominated (BD) Mode family Bending In Water				
	2ND	3ND	1ND	3ND
Blade dominated (BD) Mode family Torsion (0, 1) In Air				
	0ND	2ND	1ND	3ND
Blade dominated (BD) Mode family Torsion (0, 1) In Water				

Generally, for blade dominated modes, the mode shape changes from air to water are not significant. However, the appearance sequence of different ND modes in each mode family can be different in air and in water.

Some mode-shapes present higher reduction in frequency than others due to the added mass effect. The frequency reduction ratios of each ND mode in the Bending mode family and the Torsion

(0, 1) mode family are shown in Table 2-7 and Table 2-8, respectively.

Table 2-7. Frequency reduction ratios of each ND in the Bending mode family.

Mode	Natural Frequency (Hz)		FRR (%)
	In Air	In Water	
0ND	54.8	28.86	47.3
1ND	51.38	32.58	36.6
2ND	58.3	33.39	42.7
3ND	60.74	33.81	44.3

Table 2-8. Frequency reduction ratios of each ND in the Torsion (0, 1) mode family.

Mode	Natural Frequency (Hz)		FRR (%)
	In Air	In Water	
0ND	76.21	52.25	31.4
1ND	73.64	47.19	35.9
2ND	72.12	49.4	31.5
3ND	72.22	48.68	32.6

The FRR differences among different ND modes of the Bending mode family can be larger than 10%, while the differences of different ND modes of the Torsion (0, 1) mode family are less than 5%.

2.2.1.3.3. The effect of tip-clearance

Unlike Francis turbine or pump-turbine, the runner of the Kaplan turbine runner is far away from the head cover, and the only nearby surface is the chamber wall with a narrow tip clearance between them. To prevent from the tip vortex cavitation, the tip-clearance is usually designed to its technical minimum. During the optimization progress of the tip-clearance, the effect of its size on the dynamic behavior of the runner should also be known. The natural frequency change ratios of different ND modes for the Bending mode family and T (0, 1) mode family with the tip-clearance size (t) change from 2.5mm to 10mm (0.000439D to 0.00175D) are shown in Figure 2-8.
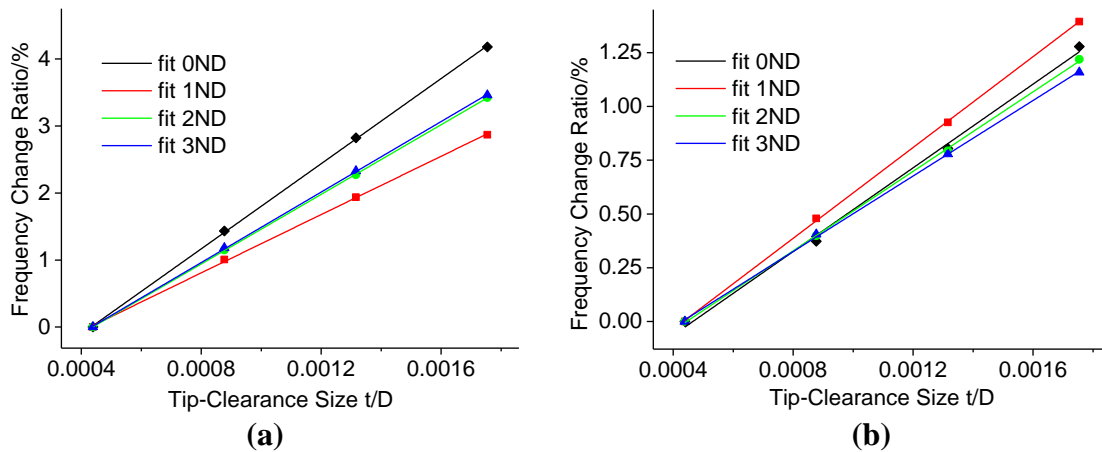
Figure 2-8. Natural frequency change ratios of different ND modes for (a) Bending mode family and (b) Torsion (0, 1) mode family with the tip-clearance size (t) change.

With the reduction of the tip-clearance size, the natural frequencies of all modes are reduced almost linearly due to the increasing added mass. The reduction can vary to some extent according to the ND and mode family. Overall, the frequency changes with the tip-clearance for all the modes are not very high. There are mainly two reasons to account for this, on the one hand, the blade is very thin, and the area of the tip face is small, on the other hand, the displacements for all the modes mainly vibrate in the axial direction and very little in the radial direction.

2.2.2. Systematic approach for Kaplan turbines with a crack

To study the influence of a crack on the dynamic behavior of a Kaplan turbine, a systematic approach has been also followed: first, the crack is modeled in a rectangular plate, and then in a single blade, as well as in the whole runner. The cracks are simulated as a narrow gap. This is a linear method to represent the crack without considering the nonlinear effect caused by the contact of crack surfaces [61].

2.2.2.1. Dynamic behavior of simplified blade models

For the simplified blade mode shown in Figure 2-1, the influence of a crack on its dynamic behavior is investigated here. The tested model with a crack is shown in Figure 2-9, where (a) shows three different crack positions (0mm, 40 mm and 80mm from the support position, respectively) and (b) shows five crack angles from $45°$ to $135°$. The modal shapes of the model with a crack at different positions and different angles are shown in Table 2-9 and Table 2-10, respectively.
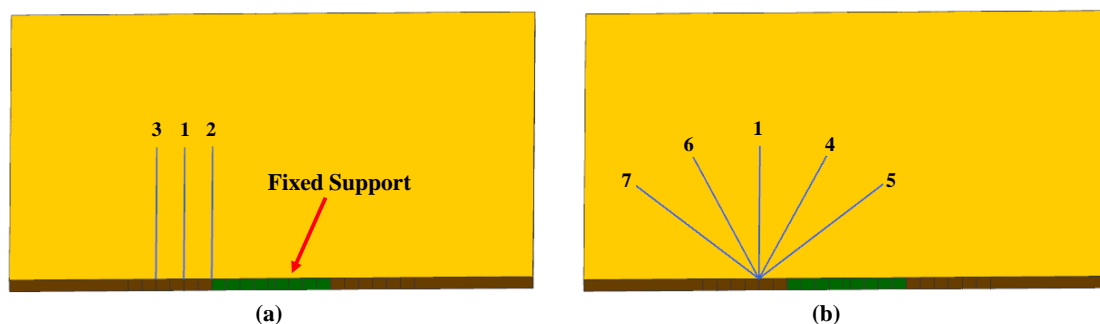
Figure 2-9. Simplified blade model with a crack. (a) different crack positions (b) different crack angles.

Table 2-9. Modal shapes of simplified model with a crack at different positions

	Crack-1 100 mm	Crack-1 200 mm	Crack-2 200 mm	Crack-3 200 mm
B				
T (0, 1)				

T (0, 2)				
T (1, 1)				
IP				
T (1, 2)				
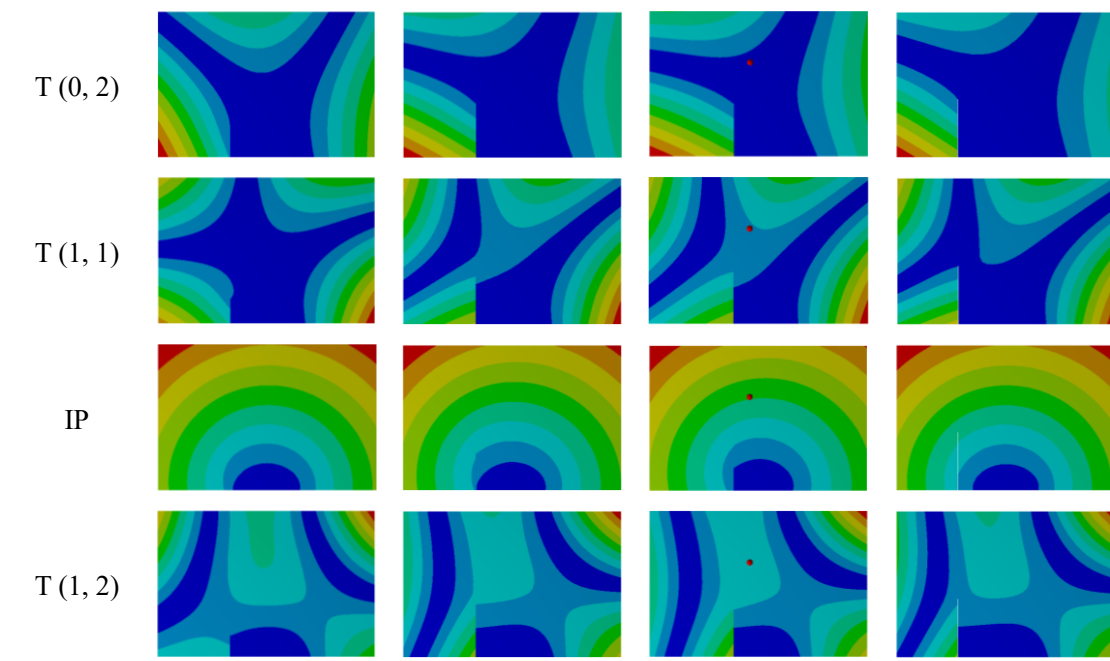
Table 2-10. Modal shapes of simplified model with a crack at different angles (200 mm long).

	Crack-1	Crack-4	Crack-5	Crack-6	Crack-7
B					
T (0, 1)					
T (0, 2)					
T (1, 1)					
IP					
T (1, 2)					
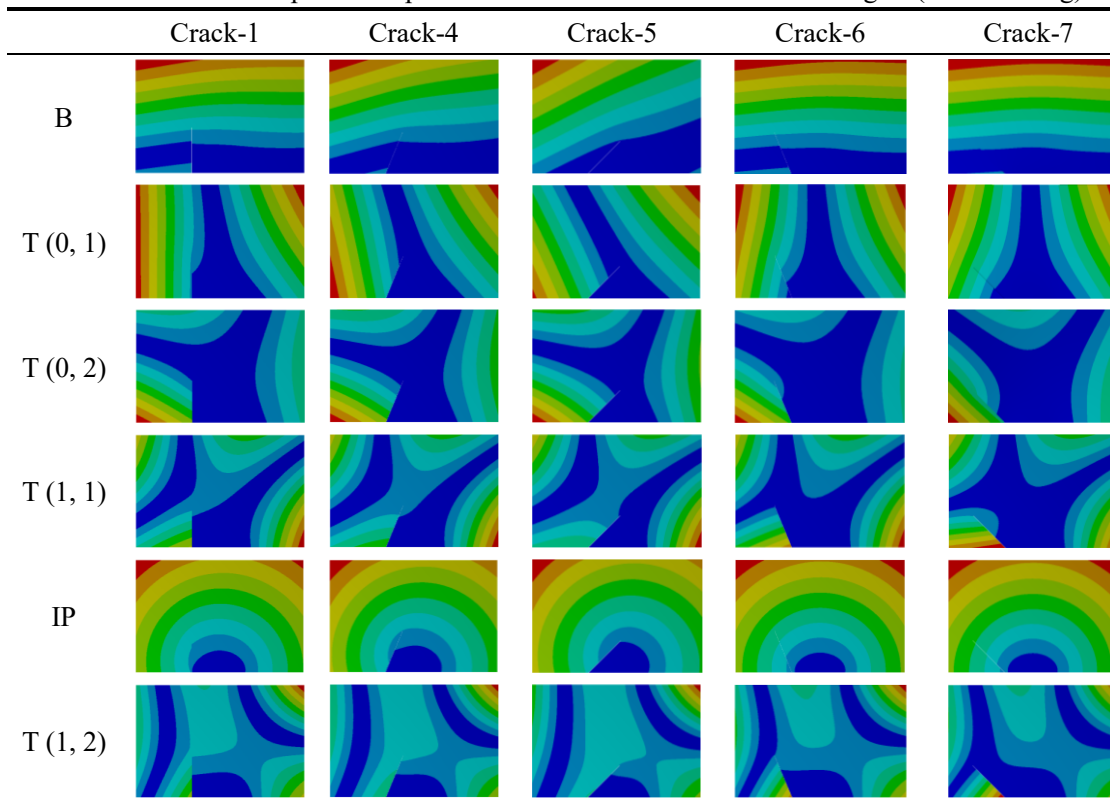
With a crack, the mode shapes of all modes deflect to the crack sided because a crack lowers the stiffness of its side. Comparing the mode shapes of all modes under a Crack-1 with a 100 mm and 200 mm the length in Table 2-9, the mode shape deflections increase with the crack length increase. From Crack-2 to Crack-1 and continuously to Crack-3, the mode shape deflections decrease, which means the deflections decrease with the crack position. From Crack-1 to Crack-6 and continuously to Crack-7, the mode shape deflections decrease, which is similar to the crack

position deviation. From Crack-1 to Crack-4 and continuously to Crack-5, the deflection changes are very complicated. The deflections of some modes increase (Bending and Torsion (0, 1)), while the deflections of some modes are very close or even decrease (T (0, 2), T (1, 1) and T (1, 2)).

Because the crack position affects the mode shape deflections, it ought to also affect the frequency reduction ratios (FRR)of different modes with the crack length increase. The FDR is defined by Equation 2-31. The frequency reduction ratios of different modes under a crack at different positions and different angles are shown in Figure 2-10 and 2-11, respectively.

$$FDR = \frac{f_{damaged} - f_{undamaged}}{f_{undamaged}} \times 100\% \qquad (2-31)$$
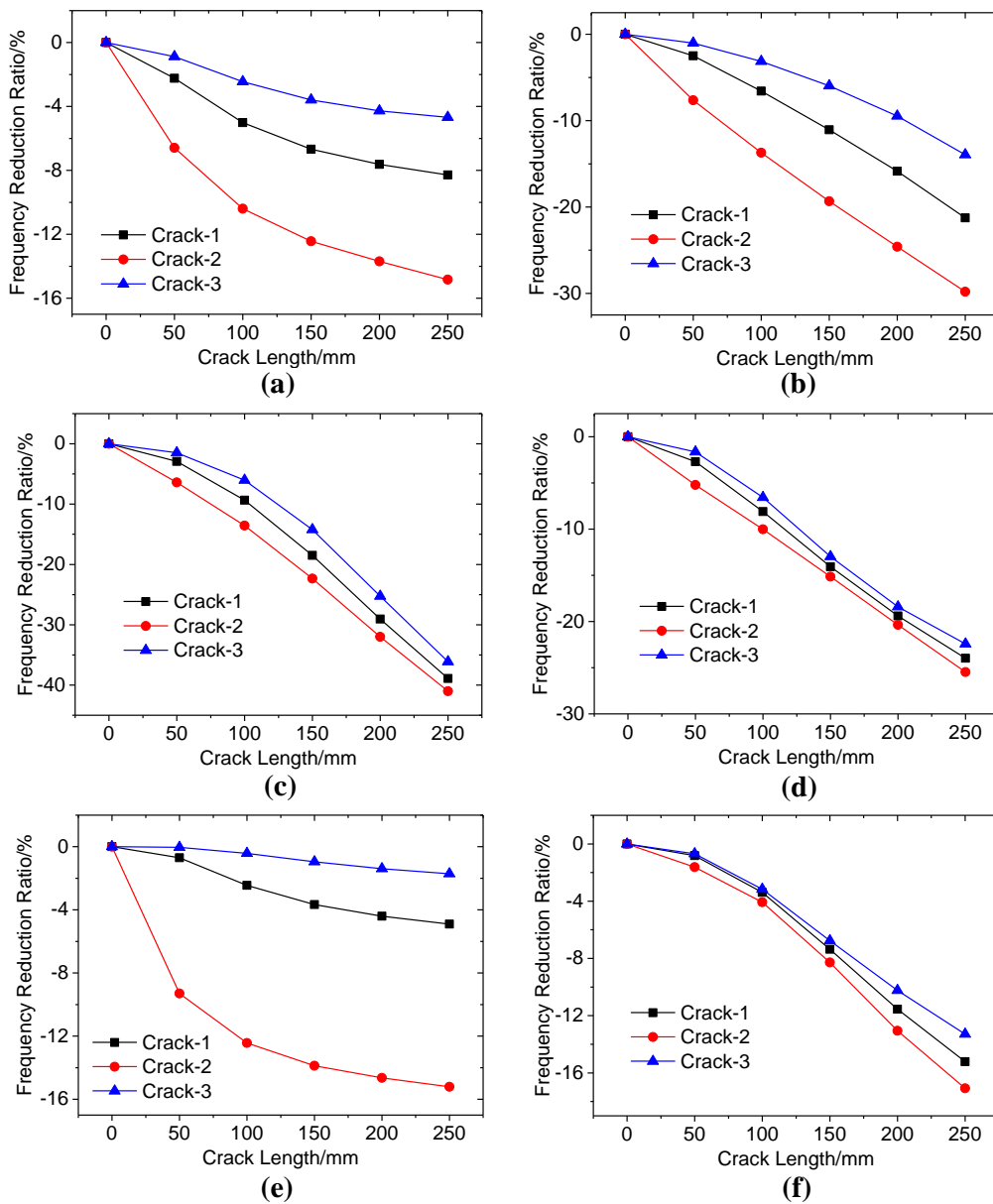
Figure 2-10 Natural frequency changes of different modes under different crack positions with the crack length increase (a) Bending (b) T (0, 1) (c) IP (d) T (0, 2) (e) T (1, 1) (f) T (1, 2).

With the crack length increase, the natural frequencies of all modes decrease. The crack positions and angles can have large influence on the frequency reduction ratios (FRR) of some modes. The FRRs change at the same time with the mode shape deflections, which means that a higher FRR represents a higher mode shape deflection.
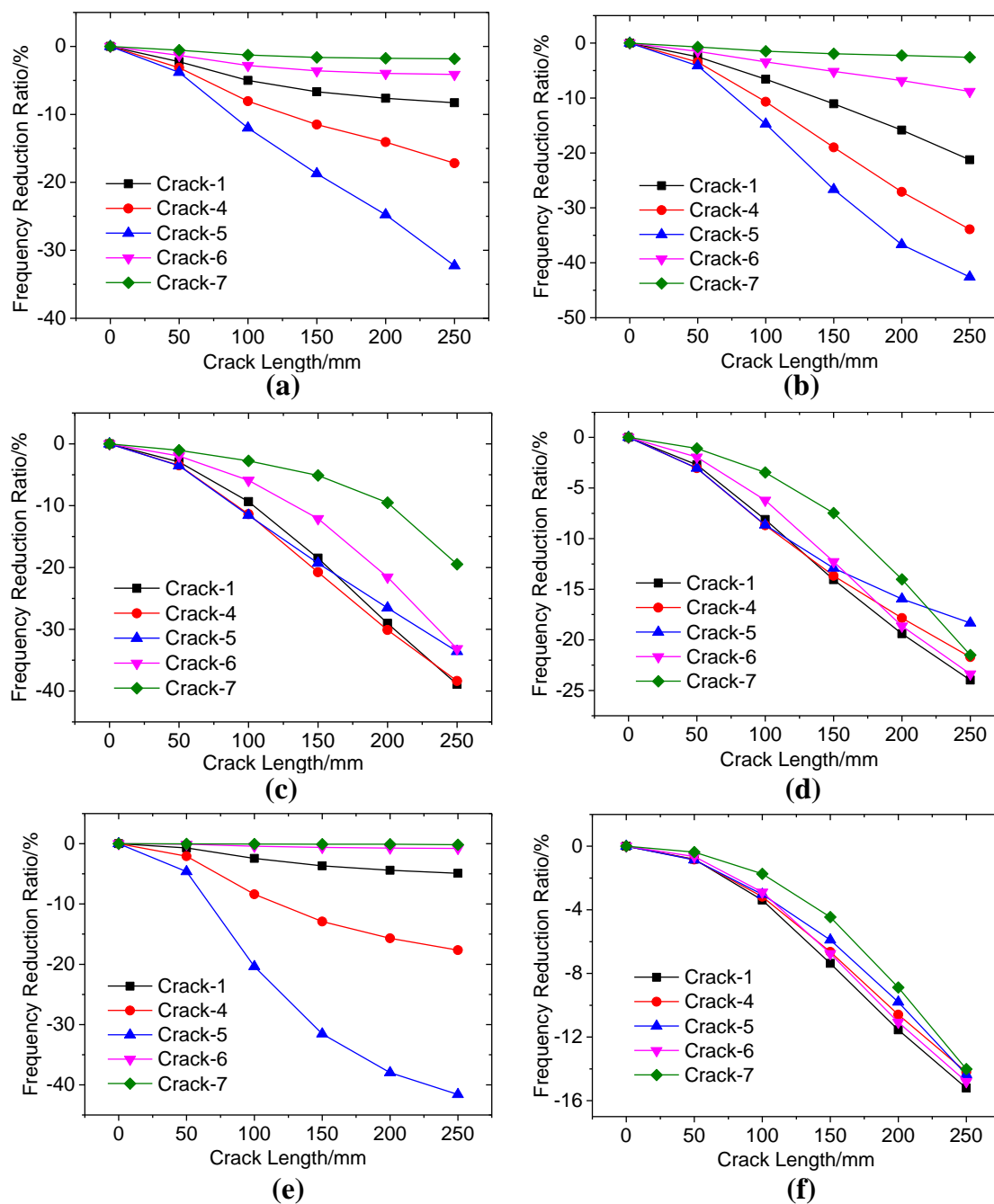
Figure 2-11. FRR changes of different modes under different crack angles with the crack length increase (a) Bending (b) T (0, 1) (c) IP (d) T (0, 2) (e) T (1, 1) (f) T (1, 2).

To better compare the mode-shapes for the different configurations, 71 monitoring points were set on the periphery of the plate, as shown in Figure 2-12. Then, the modal displacements of the

38

different configurations have been plotted for the 71 monitoring points. In Figure 2-13, the mode shape deflections due to crack length and crack position changes are clearly shown.
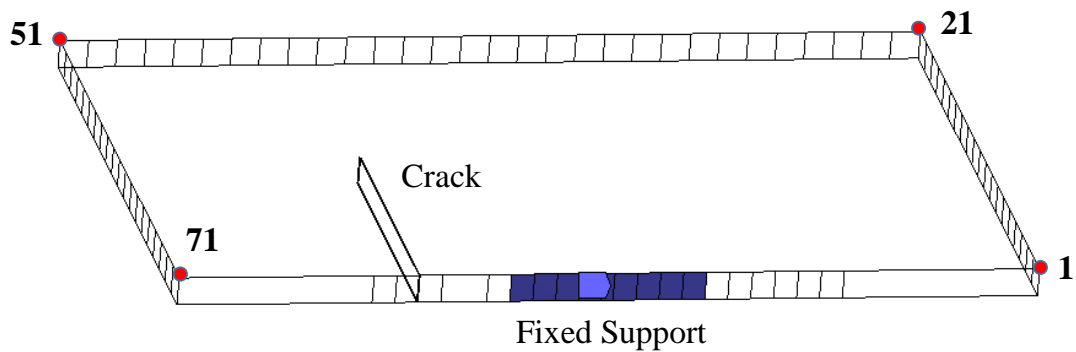
Figure 2-12. Monitoring points on the rectangular plate model.
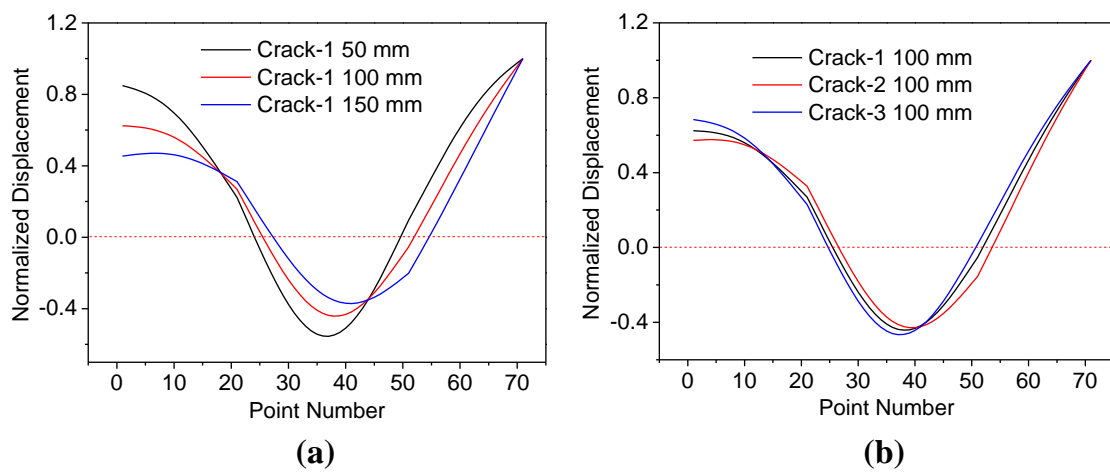
Figure 2-13. Mode shapes of T (0, 2) under different crack lengths and positions (a) different lengths (b) different positions.

2.2.2.2. Dynamic behavior of a single blade with a crack
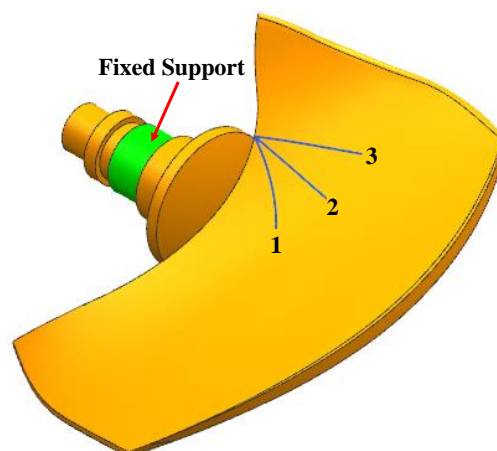
Figure 2-14. Single blade model with a crack of different paths.

This section is focused on the dynamic behavior of a single blade with a crack. Three crack paths (Crack-1, Crack-2 and Crack-3) are investigated as shown in Figure 2-14. The path of Crack-2 deviates more from the rod axis than that of Crack-1. The path of the Crack-3 is in the opposite angle than the Crack-1. The modal shapes of different modes with the different crack paths are shown in Table 2-11. As in the case of the rectangular plate, the crack makes all the modal shapes deflect to its side. These deflections increase with the crack length and decrease with the deviation of the crack path from the rod axis. These conclusions are in accordance with those obtained on simplified blade models with a crack. The FRR changes of different modes under different crack paths with the increase of crack length are shown in Figure 2-15. The same as the rectangular blade models, the FRRs of some modes (Figure 2-15) are sensitive to the crack path and length.
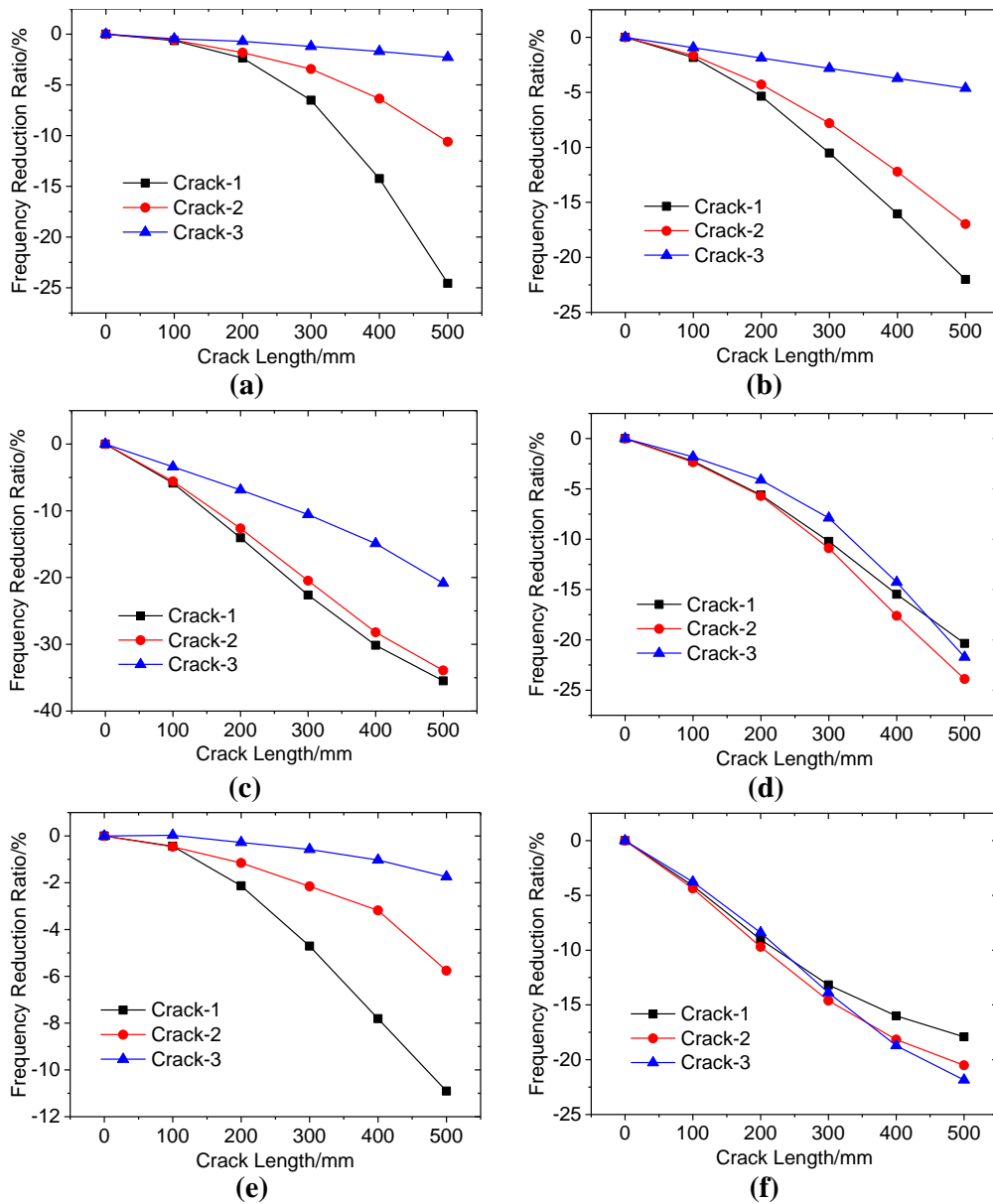
Figure 2-15. FRR changes of different modes under different crack angles with the crack length increase (a) Bending (b) T (0, 1) (c) IP (d) T (0, 2) (e) T (1, 1) (f) T (1, 2).

Table 2-11. Modal shapes of single blade model with a crack.

|	No Crack	Crack-1 200mm	Crack-1 400mm	Crack-2 400mm	Crack-3 400mm
B					
T (0, 1)					
IP					
T (1, 1)					
T (0, 2)					
T (1, 2)					
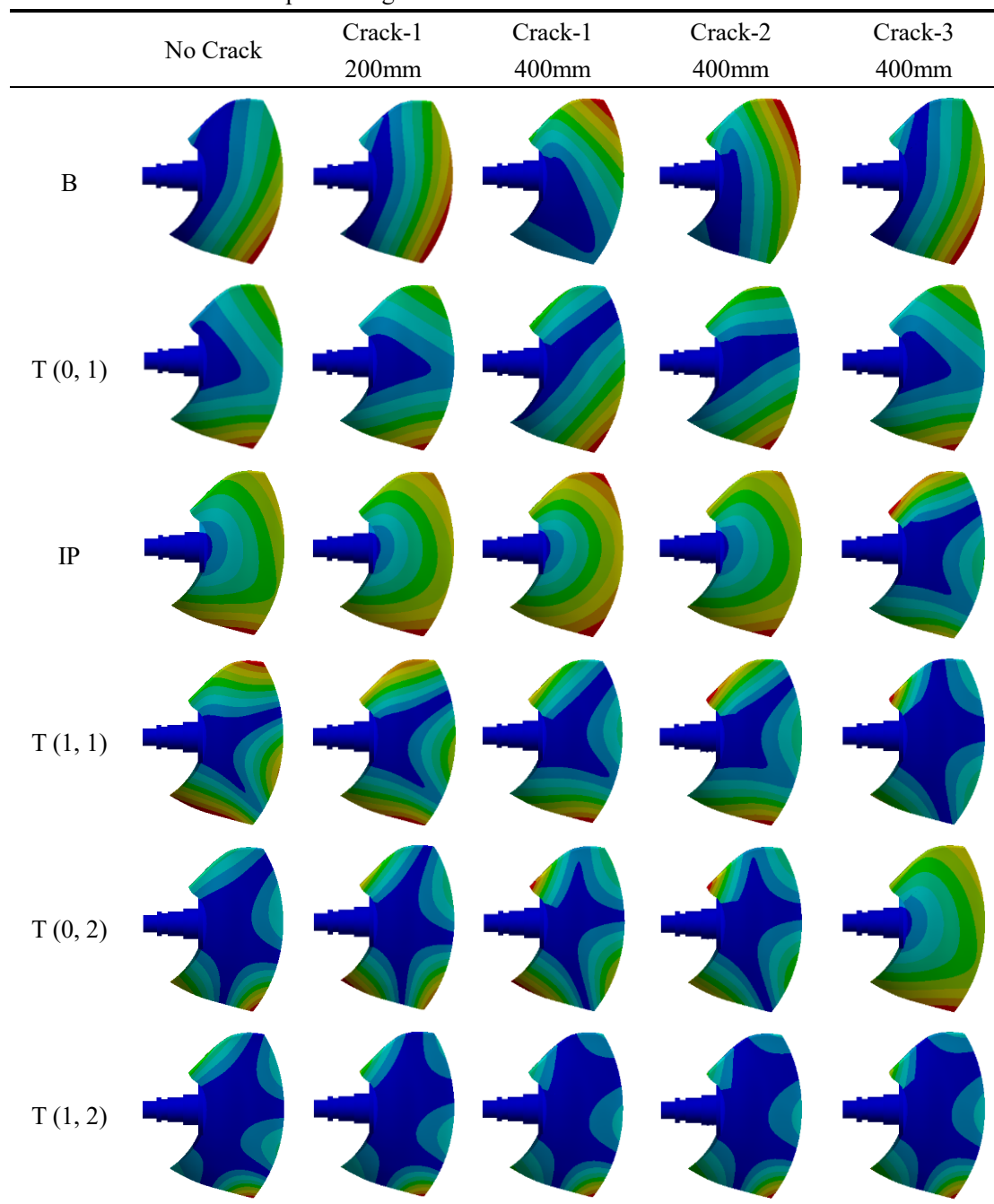
Overall, many conclusions on rectangular plates are general for Kaplan turbine blades. For this type of structures, the frequency reduction ratio of one mode due to a crack is nearly equivalent to the mode shape deflection caused by it. For real Kaplan blades, cracks usually appear at the root area [11, 69], therefore the crack position usually does not change, and only the crack angle can change. Because the FRRs or mode shape deflections may be sensitive to the crack paths (positions or angles), it is difficult to determine the crack path or length accurately through the FRR or mode shape deflection of only one mode. However, if the FRRs and mode shape deflections of more than one mode are known, the crack path and length are possible to be determined together. These conclusions are probably useful for the crack diagnostic of Kaplan turbine blades.
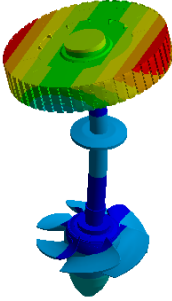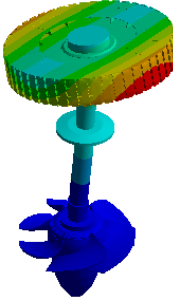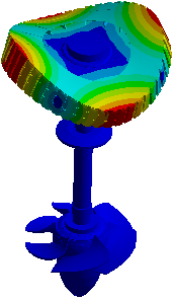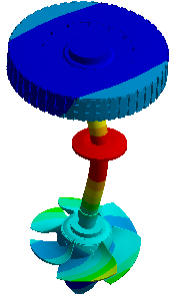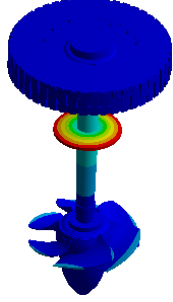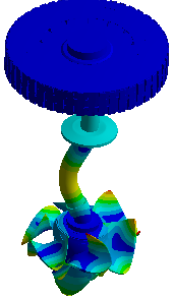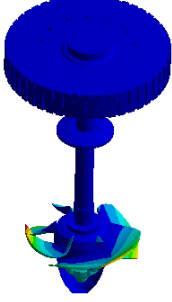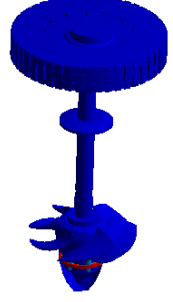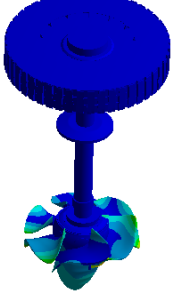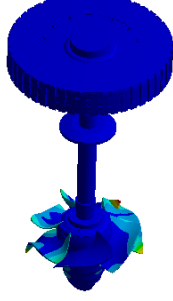
2.2.2.3. Dynamic behavior of the whole runner with a crack
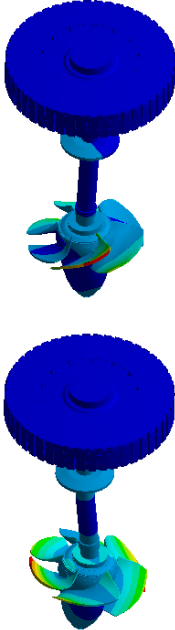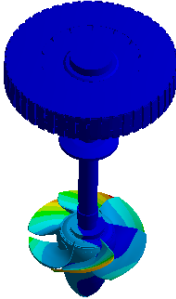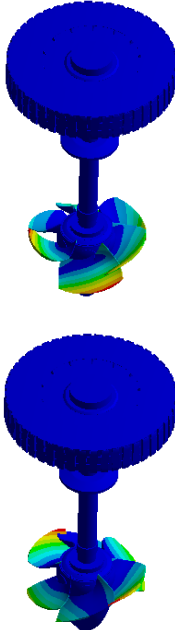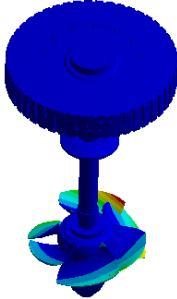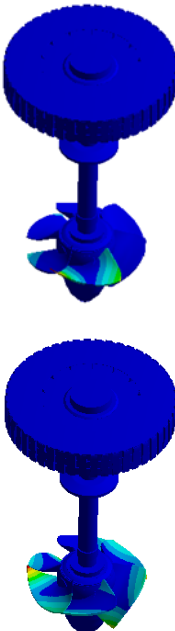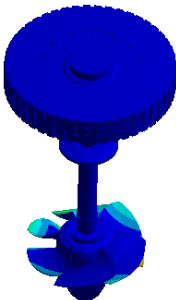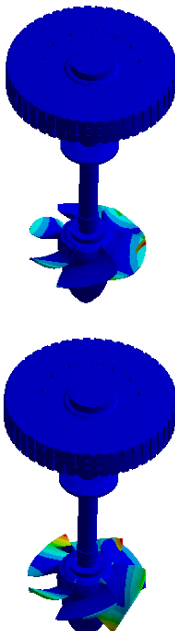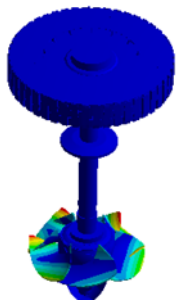
The effect of a crack on the dynamic behavior of the whole runner is investigated in the following Sections. The crack path is the same as Crack-1 shown in Figure 2-14.

2.2.2.3.1. Structure in air

Table 2-12. Modal shapes of the whole runner with a crack.
The front blade is the damaged blade.

	1ND	0ND	2ND	3ND
Generator dominated modes (GD)				
Shaft dominated modes (SD)				
Control system dominated modes (CSD)				
Hub dominated modes (HD)				
Bending	1ND	0ND	2ND	3ND

	2ND	3ND	1ND	0ND
mode family (BD) 51.4-60.7Hz				
T (0, 1) mode family (BD) 72.1-73.7Hz				

The modal shapes of the whole runner with a 300mm crack are shown in Table 2-12. For the generator, shaft, control system and hub dominated modes, the influence of the crack is small. For blade-dominated mode families, the influence of the crack is much more significant. For each mode family, there is one localized mode, which means that the maximum amplitude is concentrated on the cracked blade. The localization always occurs at the mode with the lowest frequency for each mode family. The displacement concentration of the Bending localized mode is lower than that of the T (0, 1) localized mode.

43

(a)   **(b)**
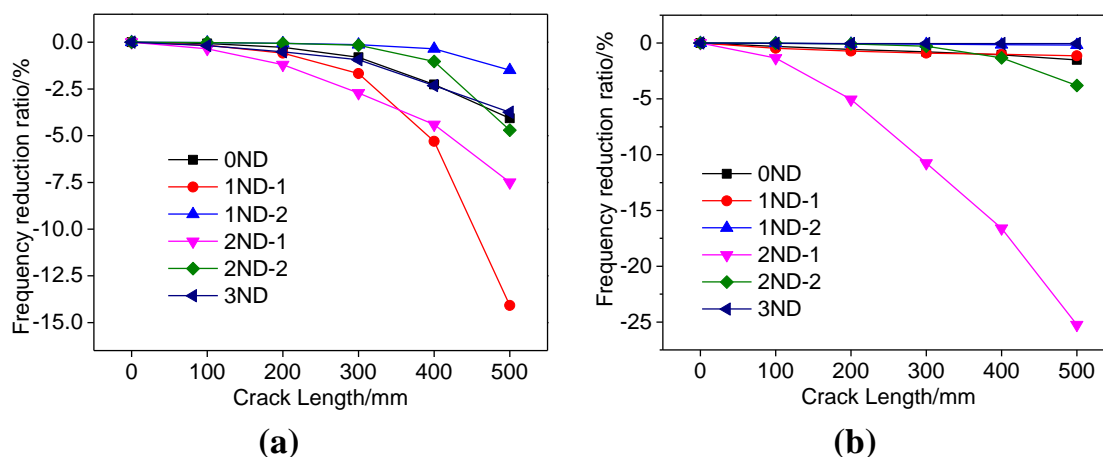
Figure 2-16. Frequency reduction ratios of different ND modes for the first and second mode families. (a) Bending mode family (b)T (0, 1) mode family.

The frequency reduction ratios of different ND modes of the Bending and T (0, 1) mode families are shown in Figure 2-16. The localized modes have the highest frequency reduction ratios for each mode family. Apart from the localized mode, the frequency reduction ratios of all other modes are small, even when the crack length is very high.

2.2.2.3.2. The effect of the surrounding water

In air, the 1ND mode of Bending mode family has the lowest frequency, while in water, the lowest frequency appears at 0ND. The modal shapes of the Bending mode family under a 500 mm crack in water are shown in Figure 2-17.
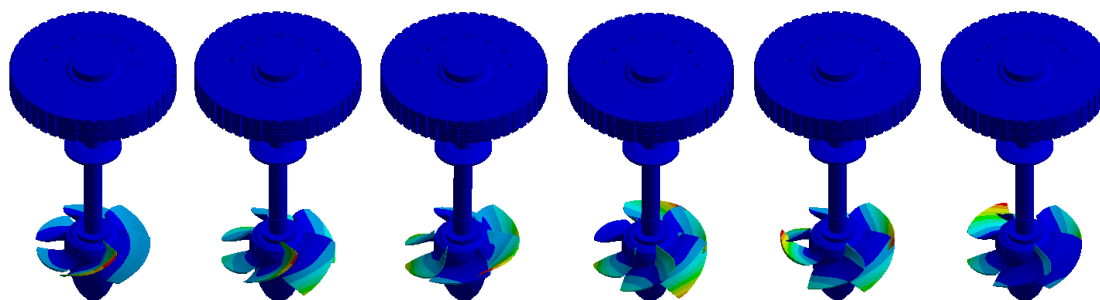
Figure 2-17. Modal shapes of the Bending mode family under a 500 mm crack in water from lower frequency (left) to higher frequency (right).

The frequency reduction ratios of the localized Bending and T (0, 1) modes both in air and in water are shown in Figure 2-18. When the crack length is very high, the frequency reduction rations of the localized Bending mode in air and in water can be quite different (Figure 2-18 (a)). This is due to the blades/hub interaction intensity differences in air and in water, which make the coupling stiffness in air and in water different. However, for the localized T (0, 1) mode, the frequency reduction ratios are very close in air and in water as shown in Figure 2-18 (b).

(a)   **(b)**
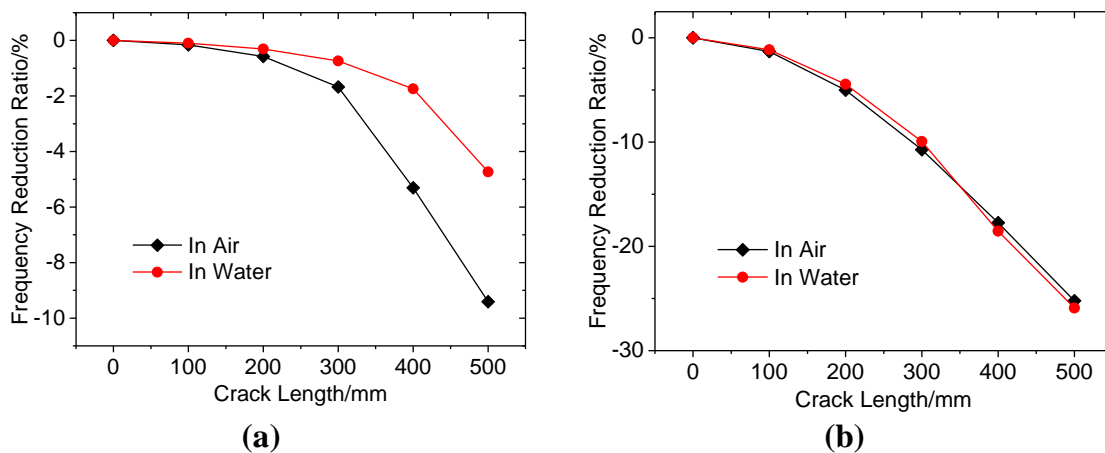
Figure 2-18. FRR of the localized mode in air and in water for the Bending mode family (a) and T (0, 1) mode family.

2.2.2.3.3. The effect of tip-clearance

The effect of tip-clearance size on the frequency reduction ratios (FRR) of localized Bending and T (0, 1) under a 300mm crack has been shown in Figure 2-19.
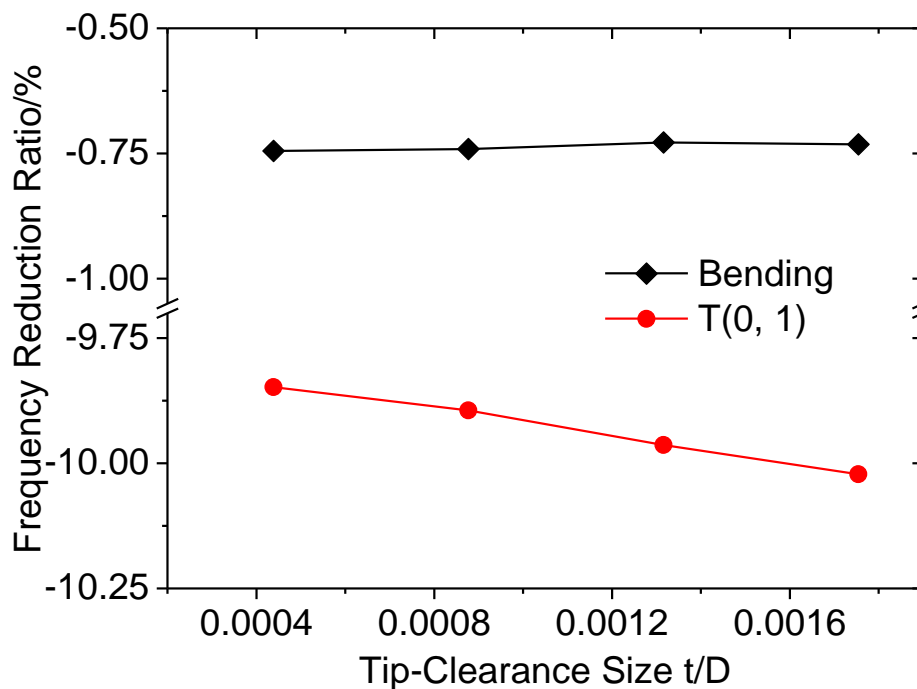
Figure 2-19. FRR changes of the localized modes with the variation of tip-clearance size.

The tip-clearance size can have some influence on the FRR, however, the influences for all mode families are less than 1%, and therefore can nearly be neglected.

2.2.2.3.4. Forced response of the runner with and without a crack

To better monitor the crack appearance, it is necessary to know the effect of a crack on the forced response of the runner. The harmonic response of the runner under a 1000N force on the damaged blade with a damping ratio 0.01 has been carried out. The vibrational response on two

monitoring points (A at the turbine bearing and B at the thrust bearing Figure 2-20) due to a crack has been investigated. The forced response (velocity) changes of the two points both in radial and axial directions below 200 Hz have is shown in Figure 2-21, Figure 2-23 and Figure 2-24, respectively. Some vibration peaks have been marked as ① to ⑦ in Figure 2-22, and the corresponding modes of these peaks have been shown in Figure 2-22.
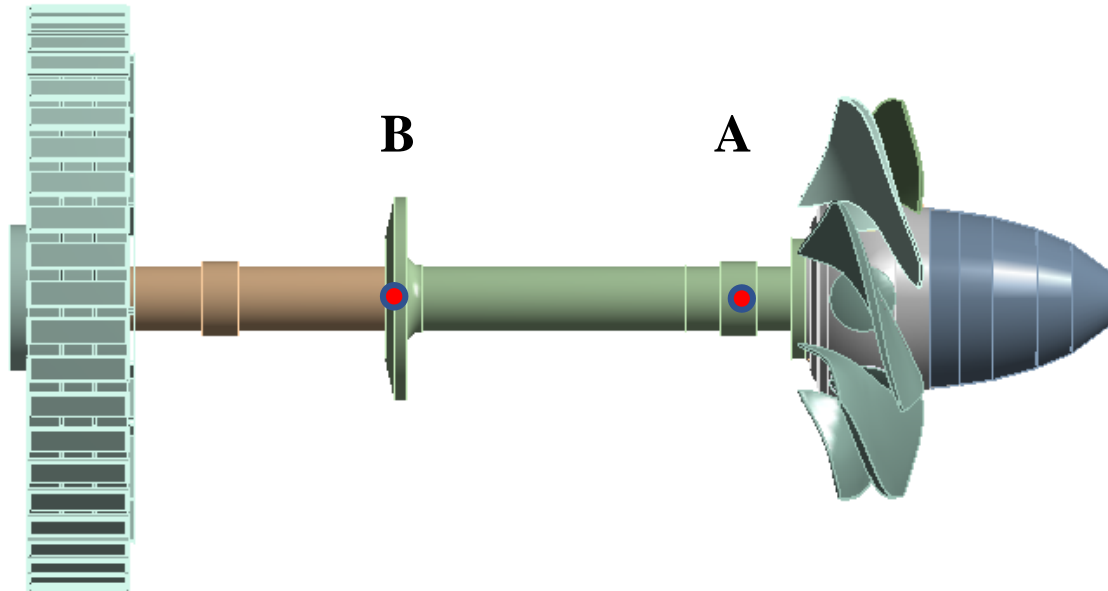
Figure 2-20. Positions of monitoring points.

The vibration peaks marked in Figure 2-21 appear in all the monitoring points and in both radial and axial directions. The vibration peaks ① to ⑦ correspond to a hub dominated mode, a shaft dominated mode, the localized Bending mode, a control system dominated mode, the localized IP mode, the localized T (0, 2) mode and a hub dominated mode, respectively (see Figure 2-22). For the peaks corresponding to hub, shaft and control system dominated modes, the high vibration amplitudes are obviously due to the high modal displacements at the monitoring points, and with the increase of crack length, the vibration amplitudes can increase or decrease significantly. The vibrations of some localized blade dominated modes are much higher than those of the mode without crack. The vibration amplitude changes of the monitoring point B are less significant than those of A, which is probably because B is closer to the runner.

However, all these results consider that the runner is a rigid body, with the blades assembled together, in the real case the blades may have different stiffness support due to the control system and this assumption may not be completely right. This will be discussed in the experimental study presented in Chapter 3.
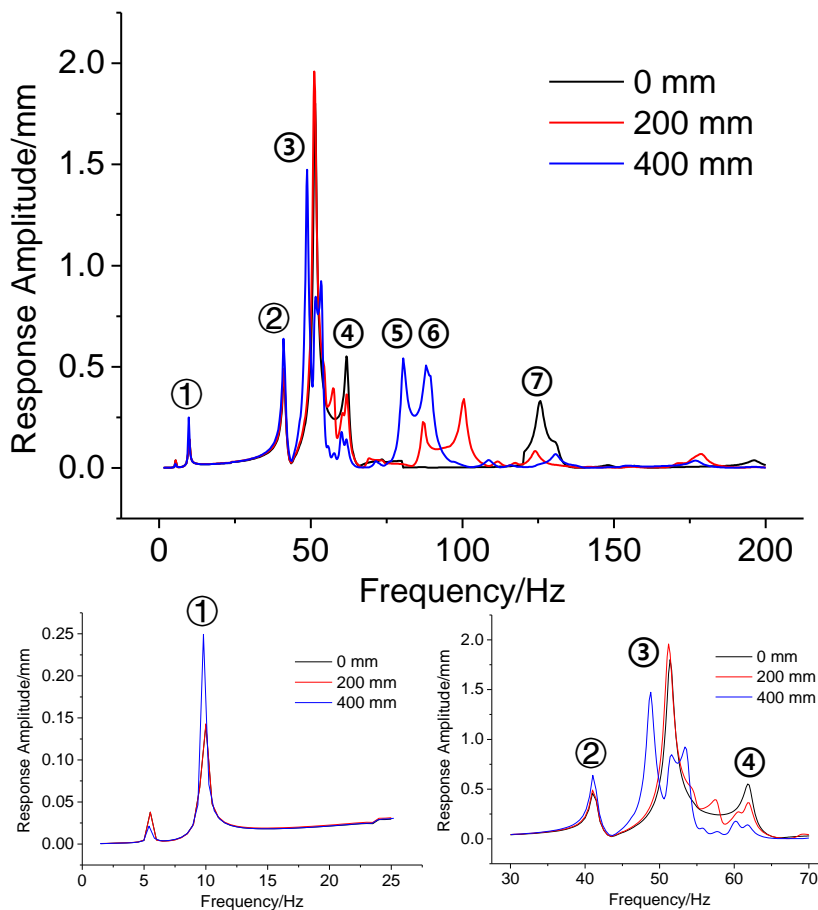
Figure 2-21. Forced response of monitoring Point-A in radial direction.
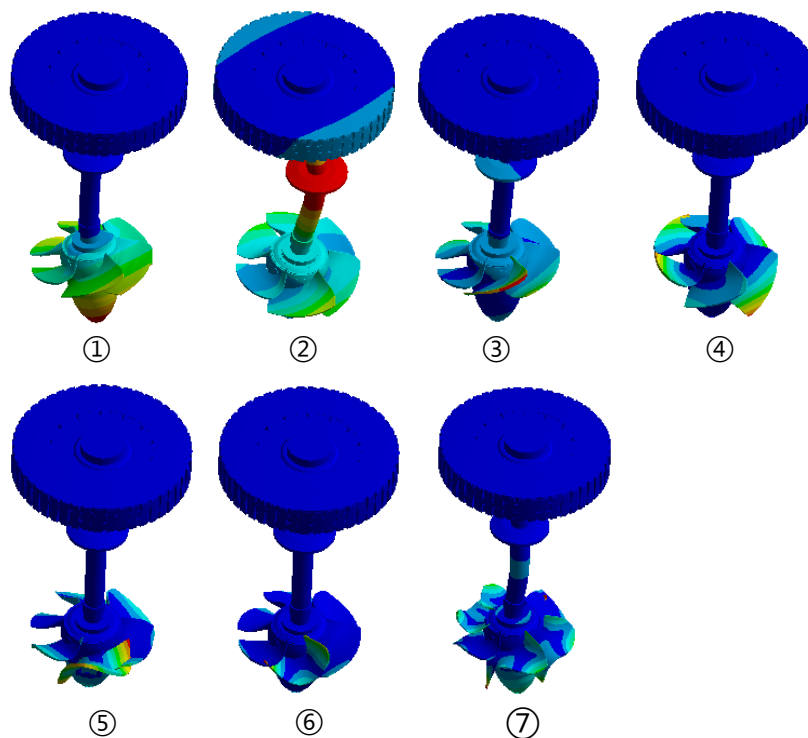
Figure 2-22. Modes corresponding to the vibration peaks shown in Figure 2-24.
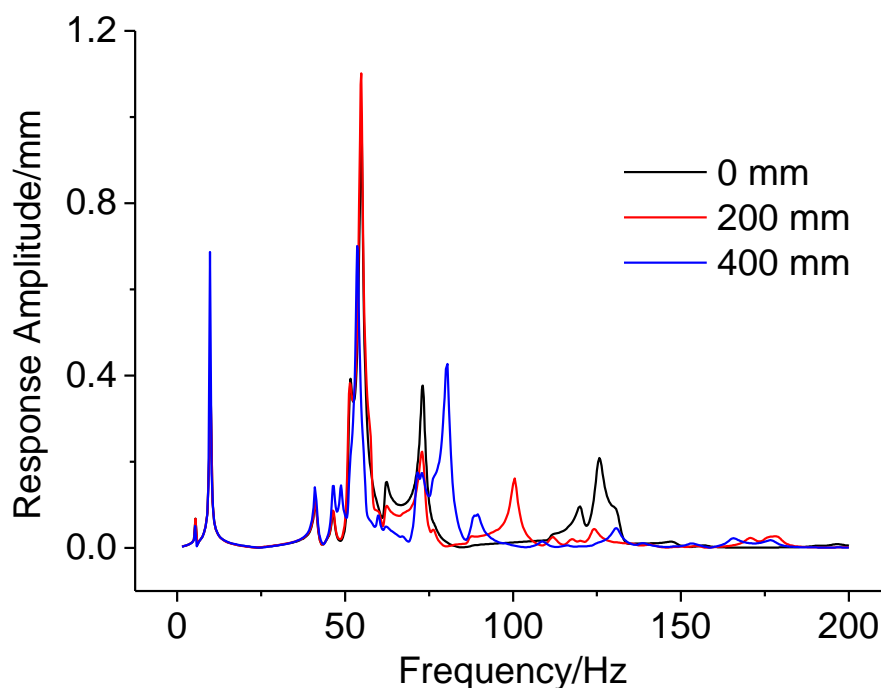
Figure 2-23. Forced response of monitoring Point-A in axial direction.
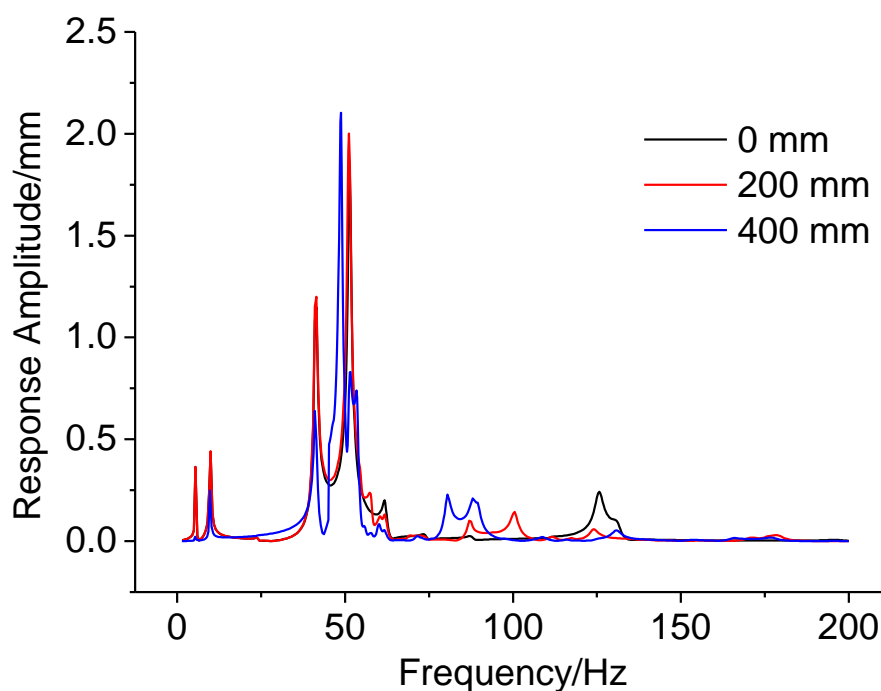
Figure 2-24. Forced response of monitoring Point-B in radial direction.

2.3. Crack modelling of a Francis runner model

The investigation presented in this section have been published in the paper "Zhang M, Valentin D, Valero C, et al. Numerical study on the dynamic behavior of a Francis turbine runner model with a crack[J]. Energies, 2018, 11(7): 1630". It is based on studying the changes due to a crack in a Francis runner using as a reference the investigation done in the Kaplan turbine. Only the

most relevant results are included in this section, the rest of the information can be found in the aforementioned paper.

2.3.1. Simulation setup
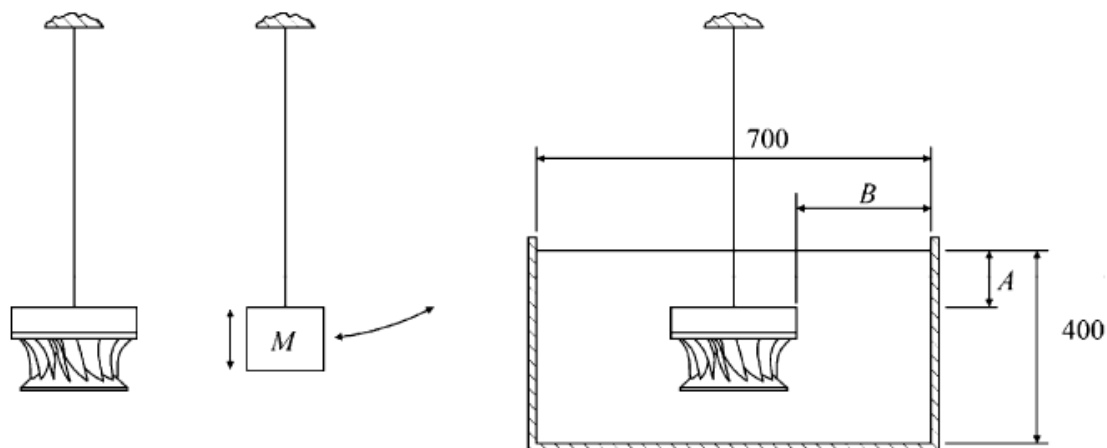
Figure 2-25. Schematic of the test rig with the runner in air (left) and submerged inside water (right), all the dimensions in mm [16].

First, the intact runner model will be validated by comparing its modal analysis results in air and water with the experimental results in [16]. The test rig in [16] in air and in water is shown in Figure 2-25. The acoustic FSI technology is used to simulate the added mass effect from surrounding still water [32, 68]. The material property of the acoustic body can be seen in Table 2-13. When the runner is submerged in water, common nodes technology is used at all the FSI interfaces, and the Asymmetric solver is used in the simulation.

In the experiment done in [16], the runner was hung by a low natural frequency rope, which means the runner can be seen as without support. When submerged in water, the distances A and B shown in Figure 2-25 are 100mm and 45mm, respectively. At this distance, the added mass effect is not affected by the distance changes to the surfaces of the water domain [16]. The upper surface of the water domain was set as zero-pressure surface (referring to the atmospheric pressure), and all other outside boundaries of water domain were set as rigid walls. The mesh sensitivity is strictly checked, and when the runner is submerged in water, 192,391 tetrahedral elements are used. The comparison between the numerical and experimental results in [16] can be seen in Table 2-14, and a good agreement has been obtained.

Based on the validation of the intact runner model, a crack is created at the intersection line between one blade and the crown from inside to outside, a location that has been shown to be prone to the appearance of cracks in Francis turbines [13]. The crack is represented as a narrow gap, and this is a linear method that has been used in the literature before [58, 60]. The total length of the intersection line is approximately 120 mm, and the crack length will vary from 0 mm to 100 mm. The mesh density at the crack tip has been especially increased as shown in Figure 2-26. When submerged in water, the water at the crack clearance is neglected. The effects of the crack on the dynamic behavior of the runner will be investigated.
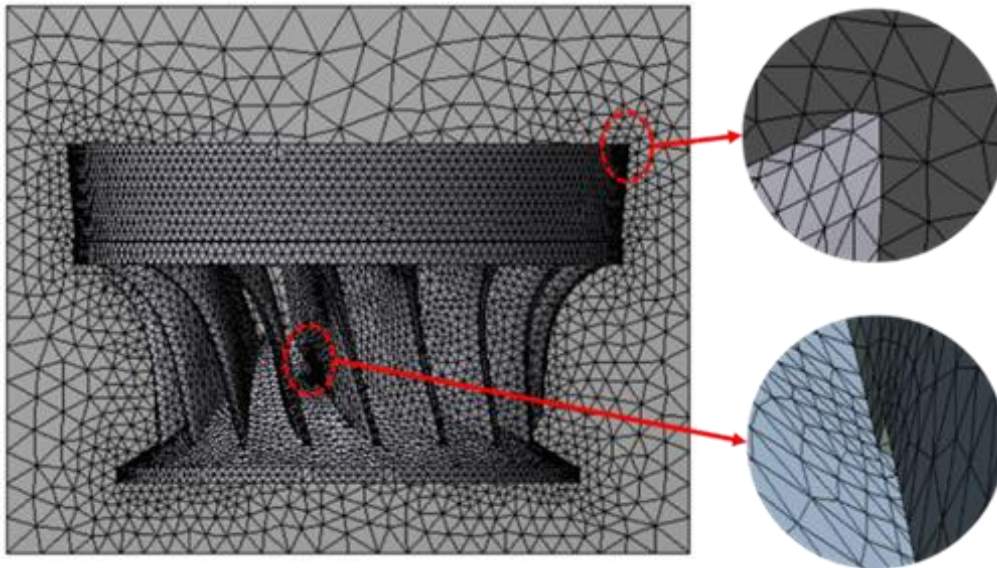
Figure 2-26. View of the mesh when the Francis runner is submerged in water.

Table 2-13. Properties of the acoustic body.

Properties	Sonic speed	Density
Value	1483 m/s	1000 kg/m^3

Table 2-14. Results of the experimental and numerical modal analysis.
SIM-AIR: Simulation in air (unit: Hz). EXP-AIR: Experiment in air. SIM-RATIO: SIM-WATER/SIM-AIR.

	In Air		In Water		Ratio	
	SIM-AIR	EXP-AIR	SIM-WATER	EXP-WATER	SIM-RATIO	EXP-RATIO
2ND	357.00	373.51	275.89	279.50	0.773	0.748
0ND	408.38	417.50	374.73	370.50	0.907	0.887
3ND	475.98	487.53	338.26	331.25	0.711	0.679
4ND	563.50	573.75	369.36	359.00	0.656	0.626
1ND	606.20	616.75	489.62	481.50	0.808	0.781
5ND	634.85	649.75	391.65	400.00	0.617	0.616

2.3.2. Results and discussion

2.3.2.1. Natural frequencies and modal shapes

The modal shapes without a crack, with a 60 mm crack and with a 100 mm crack in the air and water can be seen in Table 2-15 and Table 2-16, respectively. For each simulation case, the modal displacement is divided into nine levels from high to low so that they can be compared together. The changes in both the natural frequencies and the frequency-reduction ratios with the crack length in air and water can be seen in Figure 2-27 and Figure 2-28, respectively.

The modal shapes are a little bit different in air and in water for the same ND modes with the same crack length, which has also been shown in [32]. This may be mainly because the blades and

the band suffer from different added mass factors [16] in water. Due to the modal shape changes from air to water, the frequency changes with the crack length in air and water increase will also be very different, as shown in Figure 2-27 and Figure 2-28. Therefore, the Francis turbine in water can be seen as a new bladed-disk structure with the band, crown and blades having different densities.

From the modal shapes and natural frequencies, one of the doublet modes of each ND will change more than the other one. Generally, for actual turbines, there are no substructures that are without any deformations. Therefore, there are no modes that are completely unaffected by the crack. In the following parts, the modes changing relatively more are referred to as changed modes(C-Mode), and modes changing relatively less are referred to as unchanged modes (UC-Mode).

(a)   (b)
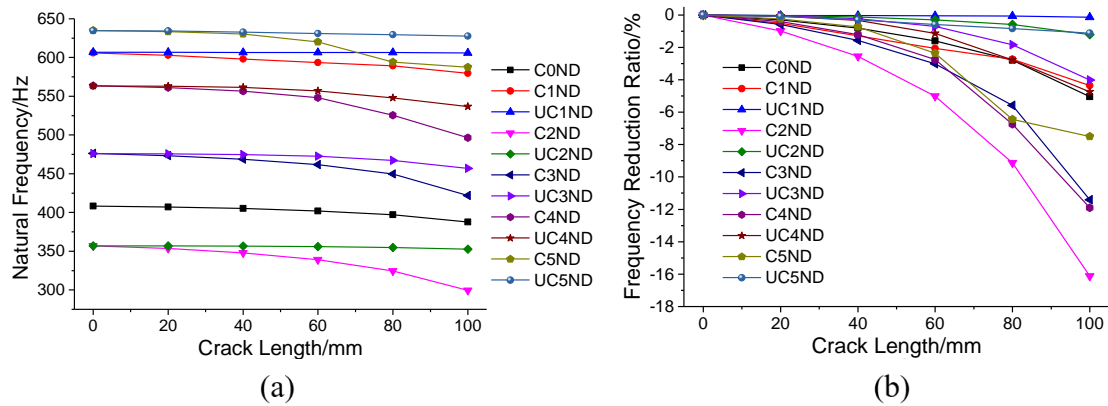
Figure 2-27. Natural frequency changes and change ratios in air (a) Natural frequencies (b) Frequency change ratios.

Table 2-15. Modal shape changes in air.

	No Crack		Crack 60mm		Crack 100mm	
	C-Mode	UC- Mode	C-Mode	UC-Mode	C-Mode	UC-Mode
0 ND		High Low		Damaged Blade		
1 ND						
2 ND						
3 ND						

| 4 ND | |

| (a) | (b) |
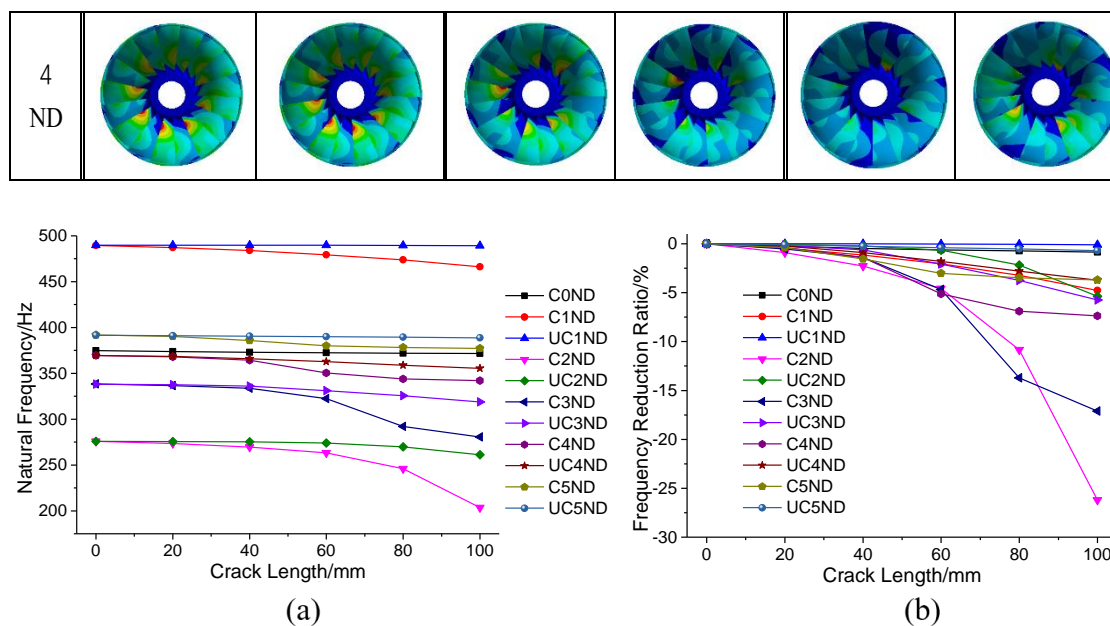
Figure 2-28. Natural frequency changes and change ratios in water (a) Natural frequencies (b) Frequency change ratios.

Table 2-16. Modal shape changes in water.

	No Crack		Crack 60mm		Crack 100mm	
	C-Mode	UC-Mode	C-Mode	UC-Mode	C-Mode	UC-Mode
0 ND		High / Low		Damaged Blade		
1 ND						
2 ND						
3 ND						
4 ND						

For most ND modes, the changed mode usually originates from the one with low deformation on the damaged blade, and the damaged blade is close to the zero-displacement node. In contrast,

for the 1ND and 8ND modes, which have nearly zero deformation blades, the changed mode usually originates from the one with high deformation on the damaged blade, and the damaged blade is far from the zero-displacement node.

The modal shape changes with the increase in crack length are not that regular. For all the unchanged modes, the modal shapes may also become distorted to some extent with the increase in crack length. Apart from the unchanged 1ND, which has low deformation at the damaged blade, the damaged blade is prone to have a large deformation close to the beginning part of the crack.

For the changed modes, the modal shape changes are even more irregular than those of the unchanged modes. Sometimes, under certain crack lengths, the highest deformation may appear at blades near the damaged blade, but when the crack length is very large, it will finally transmit to the damaged blade, like the changed 2ND and 3ND mode in air.

For the unchanged modes, the frequency reduction ratios are usually lower than 5% when the crack length is 100 mm. For some modes, such as the unchanged 1ND, the frequency reduction ratio can be as low as 0.1%. For the changed modes, the localized mode usually has a relatively high-frequency reduction ratio. When the crack length is 100 mm, the frequency reduction ratios of the localized 2ND can be as high as 16% in air and 26.5% in water. Though the changed 3ND mode in air has a high deformation concentration on the damaged blade when the crack length is 100 mm, its frequency reduction ratio is much lower than the localized 2ND. However, when in water with a crack length of 60 mm, the frequency reduction ratio of the 3ND mode is higher than that of the localized 2ND mode.

As mentioned earlier, when the changed modes are close to other modes with the reduction of frequencies, the modal shapes will become similar to those modes. This phenomenon may have large effects on the frequency reduction ratios of the changed modes. In water, this phenomenon can be more significant than in air because the frequencies of different modes are closer. For the changed 3ND, 4ND and 5ND modes in water, as well as the changed 5ND mode in air, when this phenomenon occurs with an increase in crack length, the frequency reduction rate is greatly decreased.

Overall, the natural frequency changes for all ND modes are small when the crack is not long enough. This is due to two main reasons. On the one hand, though the band is like a thin ring, the couplings between neighboring sectors are still very high. On the other hand, the blades are firmly constrained by the band and the crown, which may reduce the stiffness reduction ratio. For different modes, the frequency reduction ratios can vary significantly.

2.3.2.2. Quantitative description of modal shape changes

The modal shape change due to a crack can also be described using a Fast Fourier Transform (FFT) of the modal shape. The first step of this procedure is to choose the sample point to represent the modal shape change. First, the sample point is chosen as the intersection point of the trailing edge and the band for each blade. Therefore, 17 sample points were obtained, and the modal displacement variation of these 17 points for each mode was used for FFT. The FFT results of the

changed 2ND, unchanged 2ND, unchanged 3ND and changed 3ND in air for crack lengths of 0 mm, 60 mm and 100 mm are shown in Figure 2-29(a), (b), (c) and (d), respectively. Each modal shape can be seen to be synthesized by different ND harmonic waveforms with different magnitudes. For each ND, its value was plotted by the percentage of its magnitude to the sum of the magnitudes of all ND waveforms.
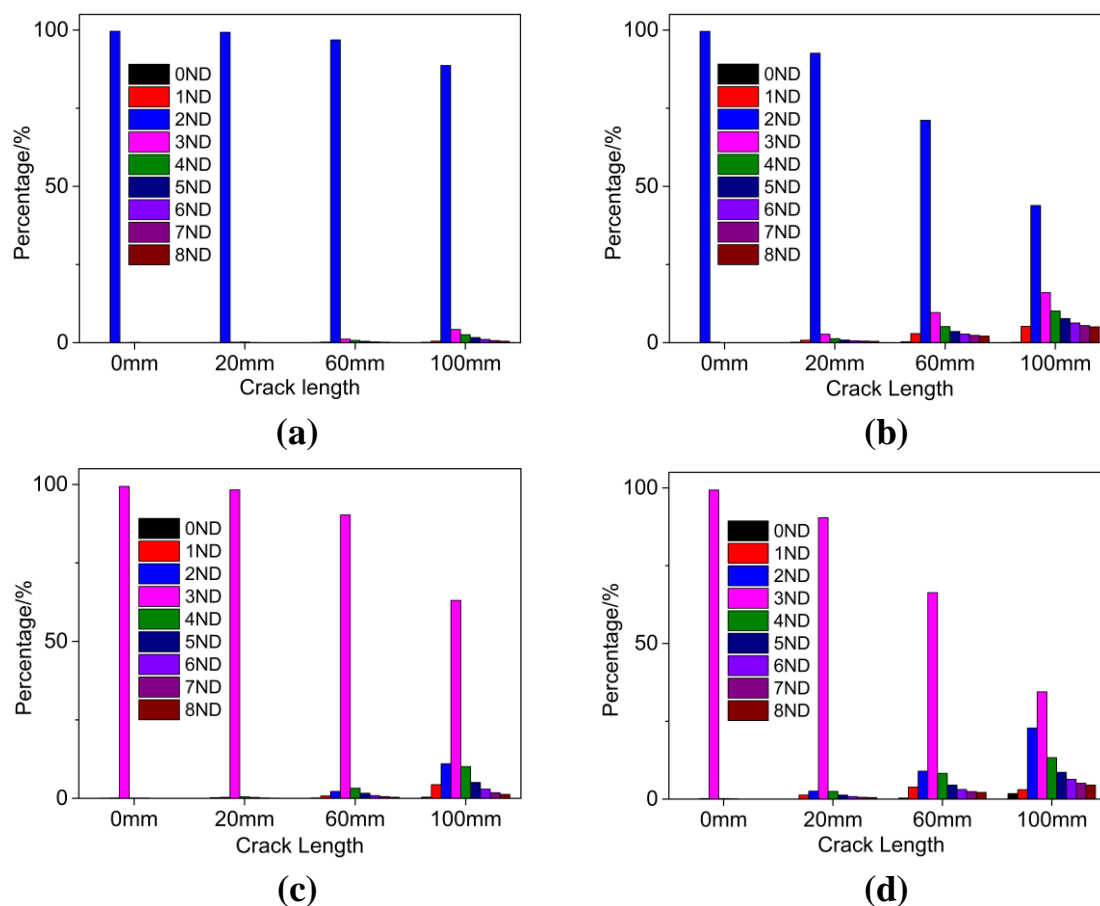
Figure 2-29. FFT results of different modal shapes (a) Unchanged 2ND (b) Changed 2ND (c) Unchanged 3ND (d) Changed 3ND.

Without a crack, each modal shape clearly contains only one waveform. With the increase in crack length, the percentage value of this original waveform decrease, and other ND waveforms appear with increasing percentage values. For the unchanged modes, the decrease in the original ND waveform and the increase other ND waveforms are insignificant, while for the changed modes, they are much more significant, particularly for the localized mode and the mode with a strong deformation concentration on the damaged blade (like the changed 3ND in Figure 2-29(d)). The values of the new appearing ND waveforms usually decrease with their separation from the original ND waveform.

For a Francis turbine, the excitation from the hydraulic force is due to the rotor-stator interaction and the excitation is order-excitation [22]. To make the runner resonant, both the frequency and the ND of the excitation should be in accordance with the runner mode. When a crack is present, other ND waveforms start to appear. This means that the mode now can not only be

excited by the original ND excitation but also be excited by other ND excitations. However, the FFT value change may depend on the sample points positions because with the crack, the deformations on the blades, particular the damaged blade, become very uninform. With other groups of sample points, the FFT results may vary a lot and become not that regular. Using those sample points may be not appropriate because of the unregular deformation change on the damaged blade, and it may be better to use the sample points on the band.
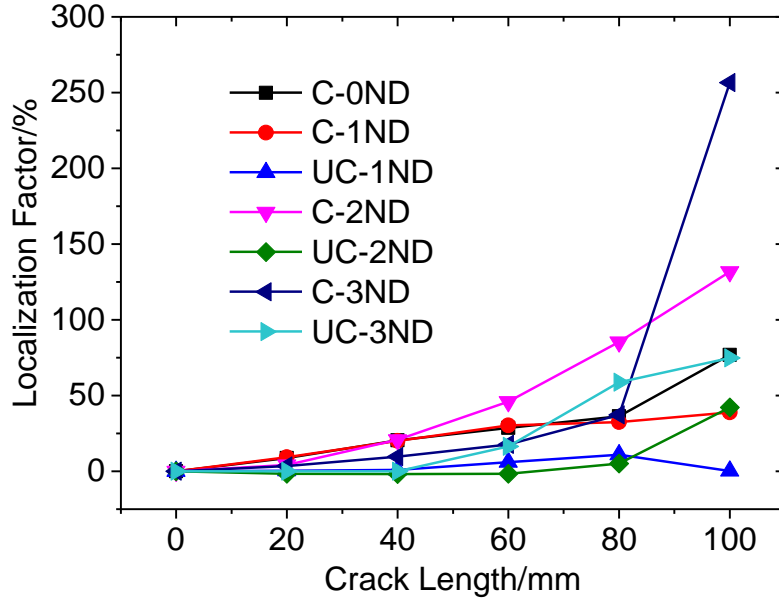
Figure 2-30. LF value changes with the crack length.

The maximum response under order excitation not only depends on the FFT value change but also depends on the Localization Factor(LF) [71] change. The LF is defined as:

$$LF = \frac{U_{1\,max} - U_{0\,max}}{U_{0\,max}} \times 100\% \qquad (2-32)$$

Where $U_{0\,max}$ is the maximum dimensionless modal displacement of one mode without crack calculated by dividing the maximum modal displacement of all the blades with the sum of maximum modal displacement on each blade. $U_{1\,max}$ is the maximum dimensionless modal displacement of the mode with a crack. The LF is an estimation of the energy percentage change of the blade with maximum deformation compared with the energy of the whole structure for one mode due to the crack, and it is also an estimation of the maximum frequency response function (FRF) [65] change for one mode under unit energy excitation. With damage, the deformation will have concentrations to some blades, which will induce the increase of the LF value. From Figure 2-30, for most of the modes, the LF will increase with the crack length increase. The increases for changed modes are much more significant than the unchanged modes due to higher deformation concentrations. The localized mode and modes with high deformation concentrations on the damaged blade are prone to have high LF value increases.

2.3.2.4. Crack monitoring challenges

For the researched Francis turbine mode, when the crack length is high, the frequency reduction ratios can be as high as 20% (mainly referring to the localized mode or the modes with strong deformation concentrations on the damaged blade). However, when the crack is not that large, the natural frequency reduction ratios are usually less than 10%. Another very important thing is that the current monitoring system is usually at the bearing of the turbine. The vibration of the runner must be transmitted to the bearing through the shaft, and the vibrations are also easily confused with the bearing effect. The response used in this paper is the maximum response of the runner, which is also used in many other papers [59, 72, 73]. However, due to the vibration transmitting to the monitoring system, the equivalence between the maximum local response increase due to a crack and the vibration increase captured by the monitoring system is still doubtful.

For the Francis turbine shown in Figure 1-4(a), its modal behavior is still not that clear, and the crown may have a high deformation. The higher deformation at the crown will greatly increase the coupling stiffness, which will cause the natural frequency reduction ratios and the response changes to be much lower [58]. This will greatly increase the monitoring difficulty and may be the reason why a so large crack is sometimes not detected by the monitoring system.

2.4. Summaries

2.4.1. On the dynamic behavior of a prototype Kaplan turbine without damage

The dynamic behavior of a prototype Kaplan turbine runner without damage has been researched numerically, and the results have been summarized as follows:

The research on simplified blade models shows that the modal shapes are mainly determined by the support position and stiffness. The support position of the blade can be optimized to reduce the dynamic stress of the blade. For the single blade model, the support stiffness can have some influences on the modal shapes. The natural frequencies of the single blade become very sensitive to the support stiffness when it is lower than some value. For the real Kaplan turbine, the blades are assembled together with non-firm connections, which means the connection stiffness of different blades can be different.

The modes of the prototype turbine can be generator, shaft, hub, control system or blade dominated. Each blade dominated mode family has six modes (the same with the number of blades). The mode families are just the modes obtained on the single blade model. The generator has little influences on blade dominated modes, and a single blade model can probably be used to predict the natural frequency band of each mode family. However, these conclusions are only valid when the runner is considered as a rigid body.

The surrounding water has small influence on the modal shapes of blade dominated modes. The natural frequencies decrease in the case of the water with a different reduction ratio depending on the mode-shapes. In addition, with the decrease of the tip-clearance size, the natural frequencies of all the modes decrease slightly.

2.4.2. On the dynamic behavior of a prototype Kaplan turbine with damage

The dynamic behavior of a prototype Kaplan turbine runner with damage has been investigated numerically. The main conclusions are the following:

The research on simplified blade models shows that a crack makes the modal shapes deflect to its side because it lowers the stiffness. This deflection increases with the crack length increase. The crack path can affect the frequency reduction ratios significantly. These conclusions are also validated on the single blade model.

When considering the runner as a rigid body with the blades assembled together, the crack causes one mode to localize for each blade dominated mode family. This means that the maximum amplitude is concentrated in the damaged blade. The localization usually occurs at the mode with the lowest natural frequency within the mode family. The tip-clearance size nearly has no influences on the frequency reduction ratios of the localized modes.

Forced response analysis has been done by applying a force on the damaged blade, and the responses of two points in the turbine bearing and in the thrust bearing have been monitored. When a crack occurs, the differences in amplitude due to the crack are detected from the bearings, especially in the axial direction. This information may be useful for crack monitoring under working conditions.

2.4.3. On the effect of a crack on the dynamic behavior of a Francis runner model

The modal behavior and forced responses of a Francis runner model with a crack have been studied numerically. Similar methodology than for the Kaplan turbine have been used. For the studied Francis runner model, there is usually only one localized mode, and when the crack length is high, strong localization can occur. The localized mode or the modes with strong deformation concentrations on the damaged blade usually have the highest natural frequency reduction ratios. The modal shapes and frequency reduction ratios in water are different from those in the air.

To analyze the changes in the mode-shapes due to the crack, a FFT analysis of the band deformation have been performed. Different components appear in the FFT when the crack is present, which means that the mode-shape changes considerably. In addition, a localization factor has been also calculated, revealing which mode-shapes are more affected by the crack.

However, the natural frequency reduction ratios are not so high when the crack is not large enough. These are the reasons why the crack is difficult to be monitored in this type of runner. This research can provide some useful results to take into account in order to try to perform crack monitoring during operation.

57

CHAPTER 3. Experimental Study

In this chapter, the dynamic behavior of the prototype Kaplan turbine runner has been studied experimentally to validate the numerical analysis presented in Chapter 2. Experimental modal analysis has been done on the damaged blade and on the undamaged blade. The instrumentation, signal processing and test procedures are introduced first. Then, the frequency response functions and coherence are checked. At last, the experimental results about the natural frequencies, mode shapes and damping ratios of the damaged and undamaged blades are presented.

3.1. Instrumentation

Experimental Modal Analysis (EMA) was done on the Kaplan turbine with one damaged blade as shown in Figure 1-9 to Figure 1-11. The most popular method for experimental modal analysis is the hammering method. This method can also be divided into the rolling hammer method and the rolling accelerometer method [74]. The rolling accelerometer method was used in this experiment. The blade was impacted using an instrumented hammer (Dytran 5802A, 220 μV/N) and the response was measured using some accelerometers (Kistler 8752A, 100 mV/g) located on the blades and turbine bearing. Both accelerometer and hammer were connected to a Bruel & Kjaer (LAN XI Type 3053) acquisition system which recorded the signals in the time domain.
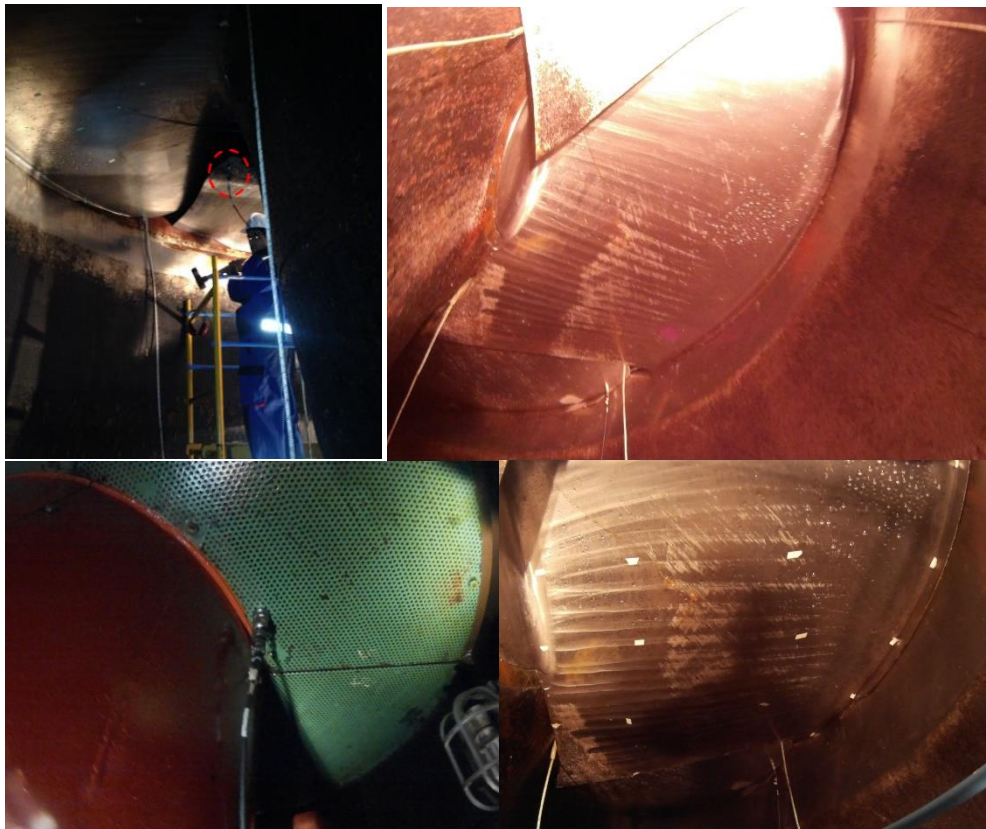
Figure 3-1. Experimental Modal Analysis.

3.2. Signal Analysis

To analyze every point, a frequency response function (FRF) between the accelerometers and the hammer was computed. The Frequency response Function (FRF) can be calculated by transforming Equation (2-1) in the frequency domain (jω) by means of the Fourier Transform:

$$\{X(j\omega)\} = [H(j\omega)]\{F(j\omega)\}$$

$\{X(j\omega)\}, \{F(j\omega)\}$ are the corresponding x(t) and F(t) in frequency domain. Thus, the FRF, or relationship between $\{X(j\omega)\}$ and $\{F(j\omega)\}$, is the matrix $[H(j\omega)]$. The impact and measurement were repeated for each measurement position. Both the impact and measurement

59

signals will be transformed in the frequency domain by means of the Fast Fourier Transform (FFT) and the FRF H_1 calculated averaging according to the standard method:

$$[H(j\omega)]_1 = \frac{\sum_1^{Na}\{X(j\omega)\} \cdot \{F(j\omega)\}^*}{\sum_1^{Na}\{F(j\omega)\} \cdot \{F(j\omega)\}^*} \tag{1}$$

The average in a frequency domain of three impacts was used taking 8 s of time signal and a frequency resolution of 0.125 Hz (400 Hz maximum frequency analyzed). The coherence function, which is usually used to estimate the influence of the noise and nonlinear effect during the EMA, was also computed between the accelerometer and the hammer in order to ensure the accuracy of the experimental testing. When the noise and nonlinear effect are low, the coherence function is close to 1. In that way, one FRF was obtained for every point where the accelerometer was located. Using all the FRFs of different measurement points, an operational deflection shape (ODS) [75] of the runner can be obtained in order to obtain the mode-shapes of the structure.

3.3. Test procedure
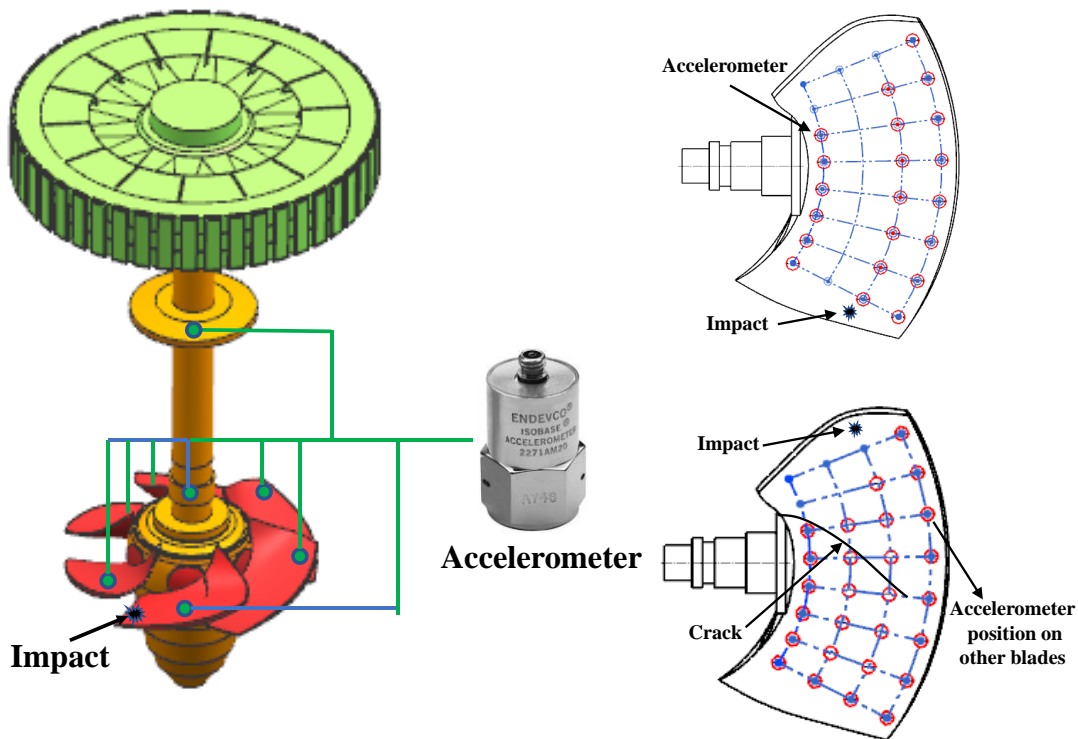
Figure 3-2. Accelerometer distributions and positions

Eight accelerometers were used in the EMA. Each blade had one, and the other two were located on the turbine bearing in the radial direction and axial direction, respectively. Apart from the impacted blade, the positions of accelerometers on other blades and turbine bearings kept fixed with the same positions on each blade. For the impacted blade, the impact position was always impacted in the same point, and the accelerometer was moved to different positions (21 for the undamaged blade and 27 for the damaged blade) in order to represent the mode-shape of the blade for every natural frequency. This method is called roving accelerometer. Three impacts were done

in every position of the accelerometer in order to compute the average of them. The positions where the accelerometer was placed are shown in Figure 3-2. The impact position on the undamaged blade is close to the trailing edge, and that on the damaged blade is close to the leading edge.

3.4 Experimental results

3.4.1. Frequency response function and coherence of the blade measurement points

3.4.1.1. Impact on the undamaged blade

Figure 3-3. Frequency response function of the blade measurement points (impact on the undamaged blade). (a) overlaid FRF of all the measurement points on the blades (b) the point on the impact blade with the same position with the points on non-impact blade (c) one point on a non-impact blade.

The FRFs of the measurement points on the blades when the impact was on the undamaged blade are shown in Figure 3-3. (a) is the overlaid FRFs of all the measurement points on the blades, (b) is the FRF of the point on the impact blade with the same position as the accelerometers on other blades and (c) is the FRF of one measurement point on one non-impacted blades. There are five modes detected below 200 Hz, and these five modes can also be clearly detected by the measurement

points on other blades. The response amplitudes of all the modes of the measurement points on the non-impacted blades are much lower than those of the measurement point with the same position on the impact blade.

The coherences of the leading-edge tip point and the point with the same position with the points on other blades, as well as a point on other blades are shown in Figure 3-4. All the coherences of the measurement points on the blades are close to 1 at resonant frequencies, even those from the points on non-impact blades, which ensures the accuracy of the FRFs.

Figure 3-4. Coherences of different measured points (impact on the undamaged blade). (a) leading-edge tip point on the impact blade (b) the point on the impact blade with the same position with the points on non-impact blade (c) one point on a non-impact blade.

3.4.1.2. Impact on the damaged blade

The FRFs of the measurement points on the blades when the impact was on the damaged blade are shown in Figure 3-5. There are four modes detected below 200 Hz, and these modes can also be detected by the measurement points on the non-impacted blades.
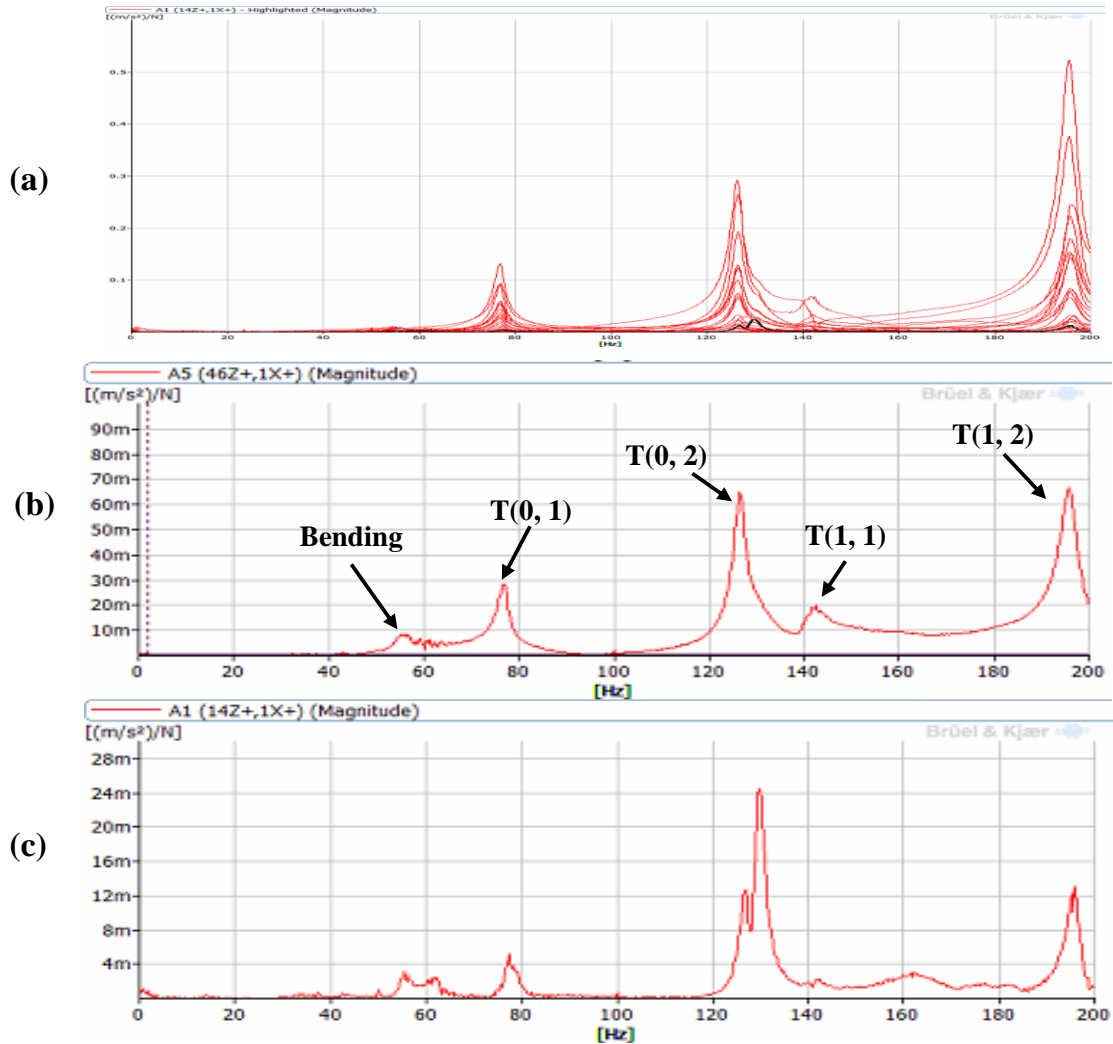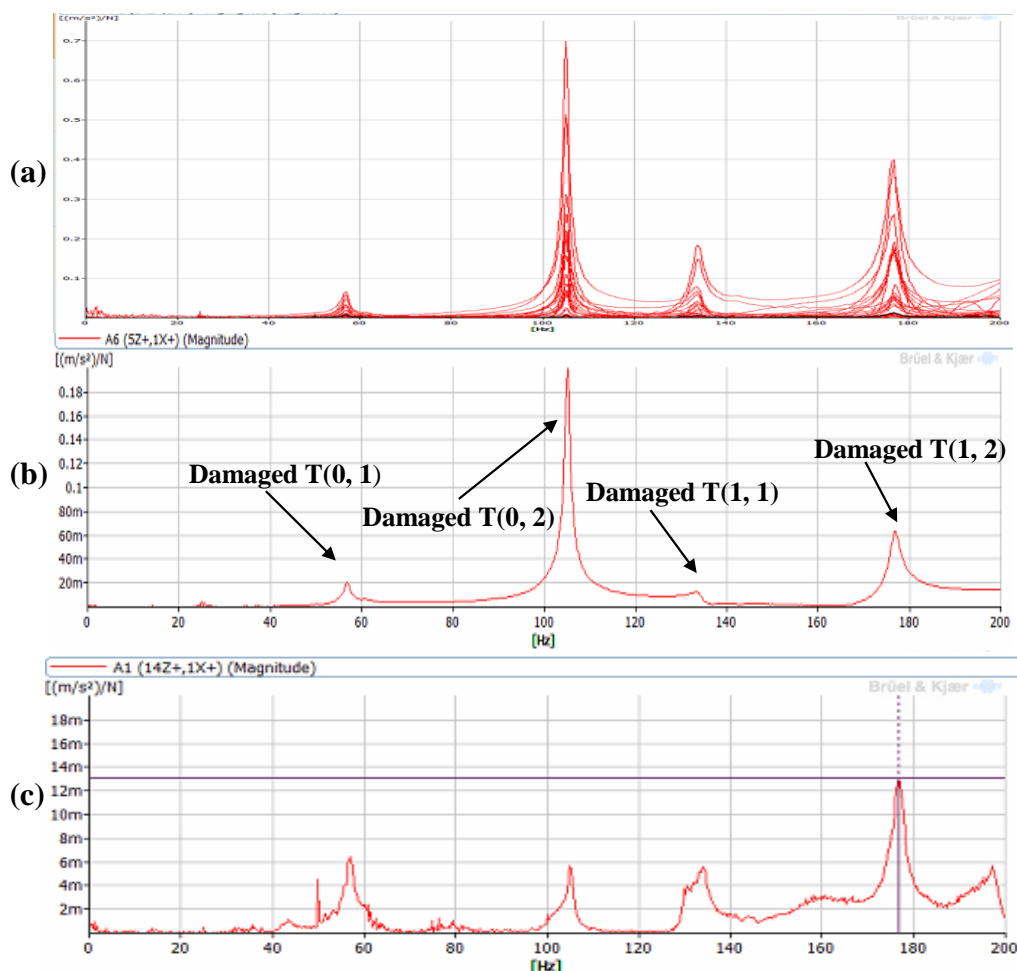
Figure 3-5. Frequency response function of the blade measurement points (impact on the damaged blade). (a) overlaid FRF of all the measurement points on the blades (b) the point on the impact blade with the same position with the points on non-impact blade (c) one point on a non-impact blade.

The coherences of the leading-edge tip point and the point with the same position with the points on other blades, as well as a point on other blades are shown in Figure 3-5. The coherences of all the points are close to 1 at resonant frequencies.

3.4.2. Natural frequencies and mode shapes

An ODS model was built in Bruel & Kjaer Reflex software to represented the Kaplan turbine. This model consists of six blades and part of the turbine bearing. A single blade model was built specially to analyze the response of the impacted blades. The frequencies and mode shapes (including the bearing points) detected by impacting the undamaged blade and the damaged blade are shown in Table 3-1. These modes have been matched to the numerical modes obtained on single blade in Section 2.2.1.2.
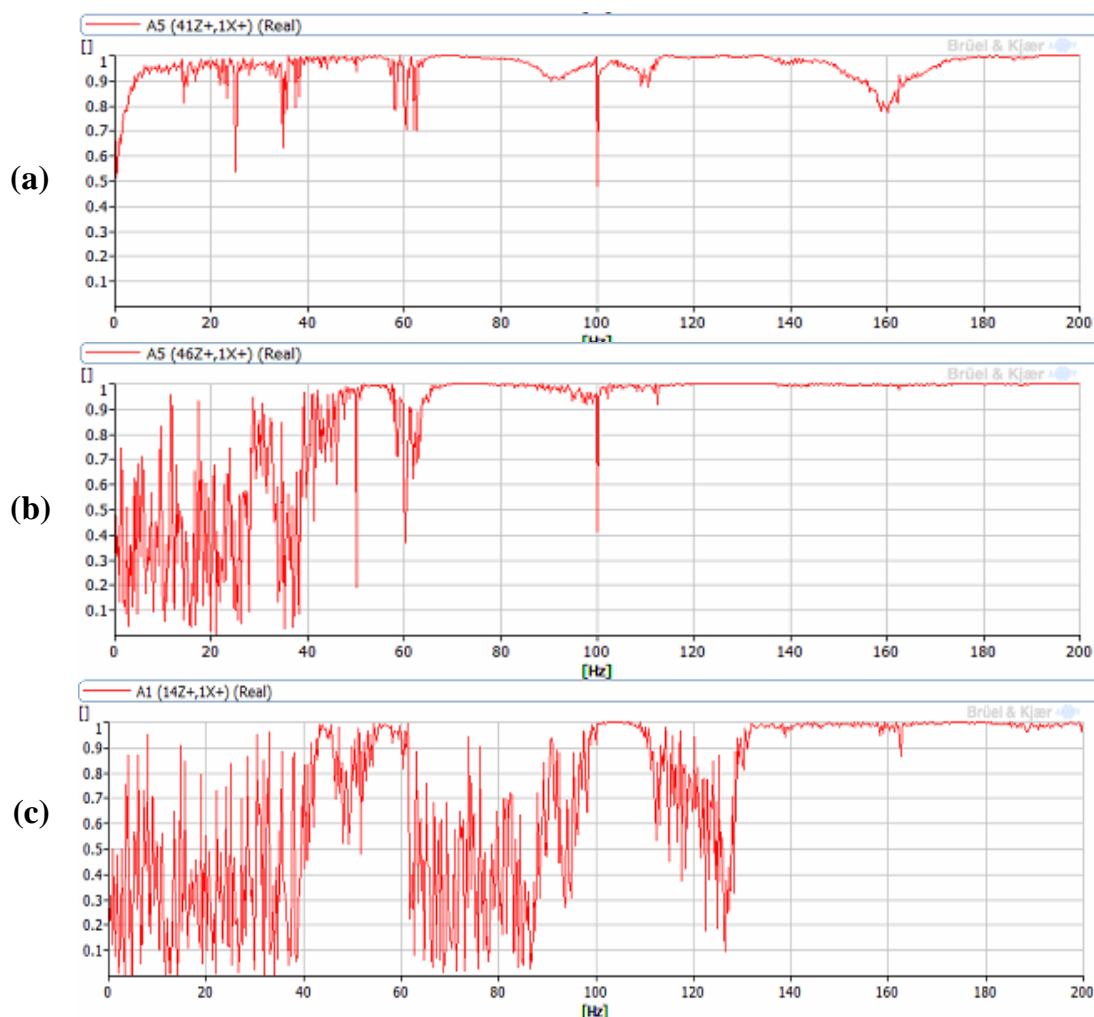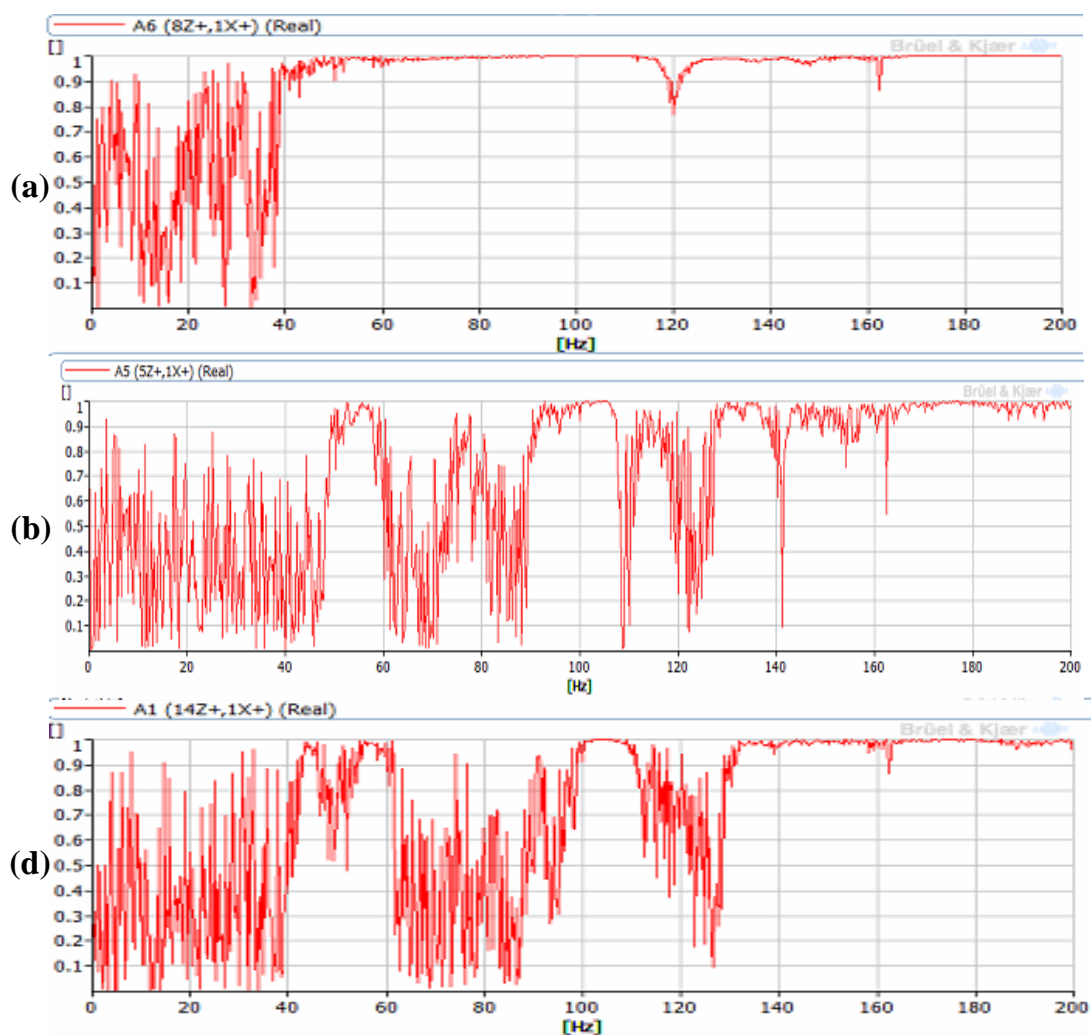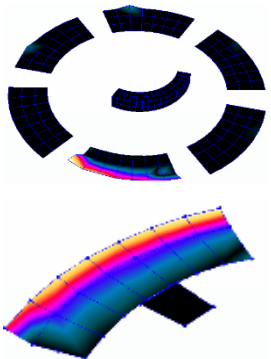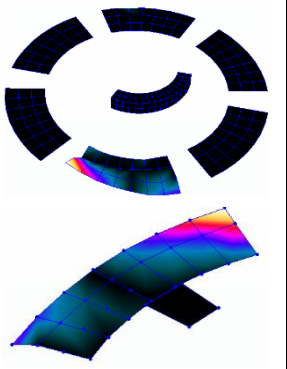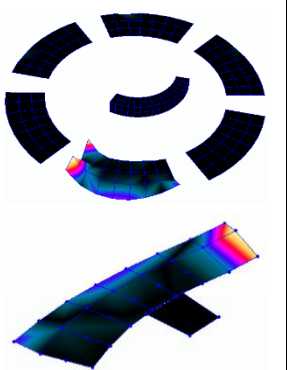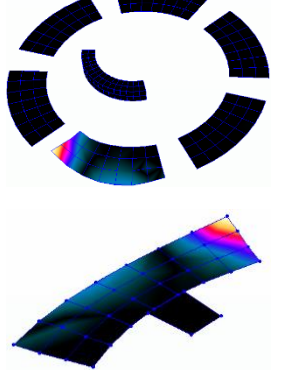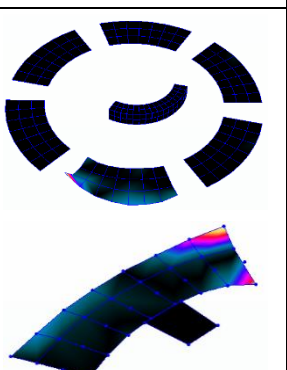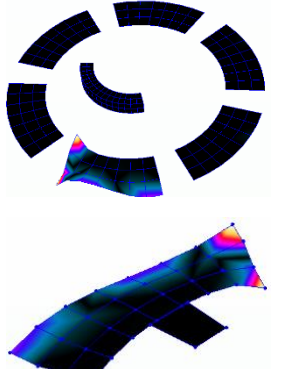
Figure 3-5. Coherences of different measured points on the blade (impact on the undamaged blade). (a) leading-edge tip point on the impact blade (b) the point on the impact blade with the same position with the points on non-impact blade (c) one point on a non-impact blade.

Table 3-1. Experimental frequencies and mode shapes for the undamaged and damage blades.

Mode	Undamaged Blade		Damaged Blade		FRR
	Freq [Hz]	Modal Shape	Freq [Hz]	Modal Shape	
B	55.47			Not Detected	N/A

T (0, 1)	77.44		56.7		0.267
T (0, 2)	126.39		105.3		0.167
T (1, 1)	141.26		133.6		0.054
T (1, 2)	195.46		176.55		0.097

The responses of the measurement points on the non-impacted blades and bearing are very low, which have also been shown in the FRFs in Figure 3-2 and Figure 3-4. The response amplitudes of different modes of the measurement points on non-impacted blades normalized to the response amplitude of the point on the impact blade with the same position are shown in Figure 3-6, in which the blades are marked by numbers in the anti-clockwise. The undamaged blade is B5, and the

damaged blade is B6. For all the modes, the responses on the impact blade are much higher than in the other blades, particular when the impact was on the damaged blade. The reason of this can be the loose connections between the blades and hub/control system. Therefore, mode-shapes families that were found in the numerical simulation are actually not appearing. This means that the runner cannot be considered as a rigid body and that every blade vibrates independently.

The frequency reduction ratios (FRR) of each mode are also shown in Table 3-1. Under a so large crack, the FRRs of some modes seem to be abnormally low with the lowest 0.054 for the T (1, 1) mode. The possible reason of this can be the nonlinear effect due to the contact of crack surfaces, which can provide some stiffness. However, it is better to validate this through the comparisons with numerical results, which are shown in Chapter 4. Due to the crack, the mode shapes of all the modes deflect to the crack side, and their detailed comparisons with numerical results are also shown in Chapter 4.
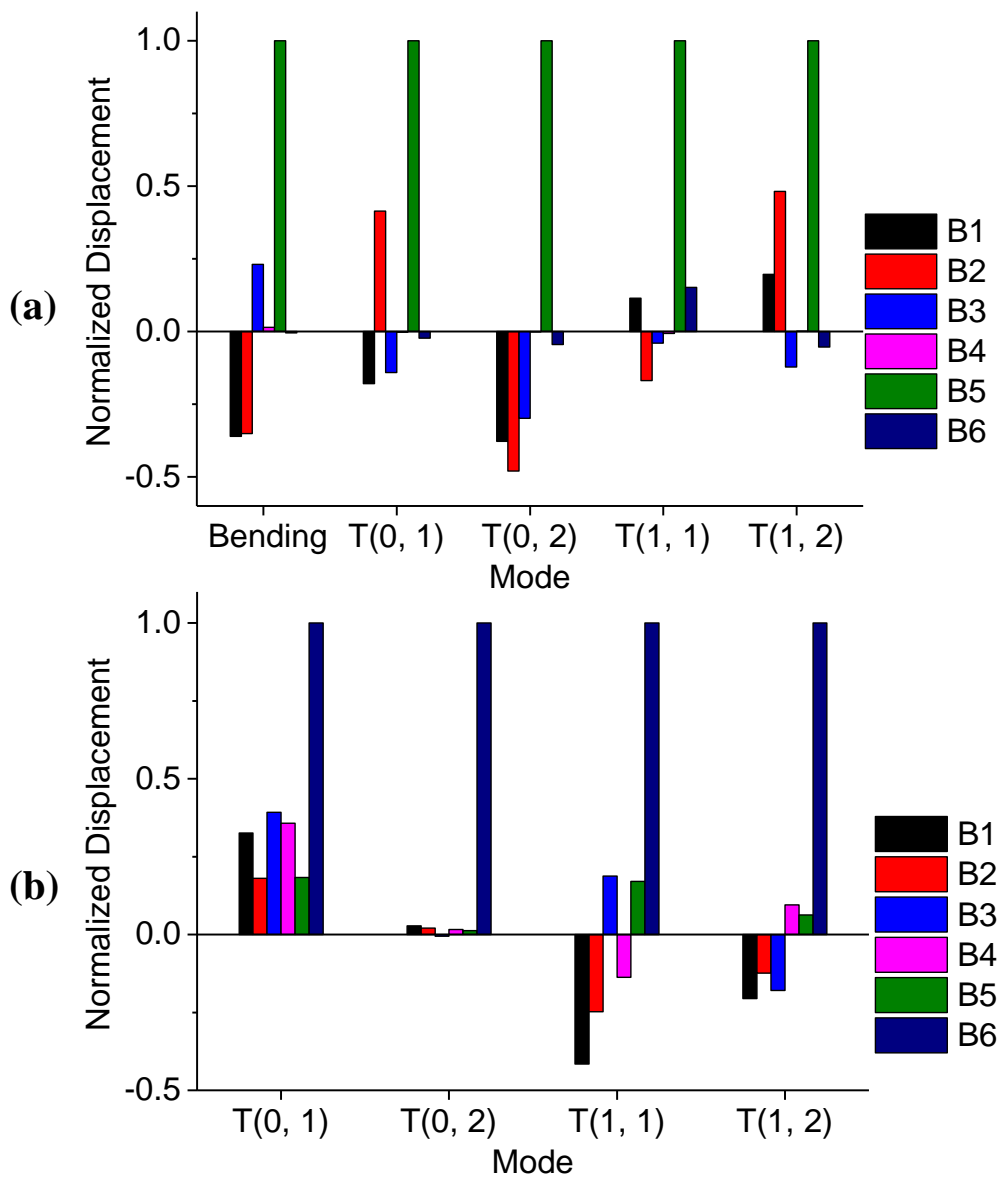
Figure 3-6. Normalized blade displacement of different modes. (a) impact on the undamaged blade (b) impact on the damaged blade.

3.4.3. Transmission to the bearings.
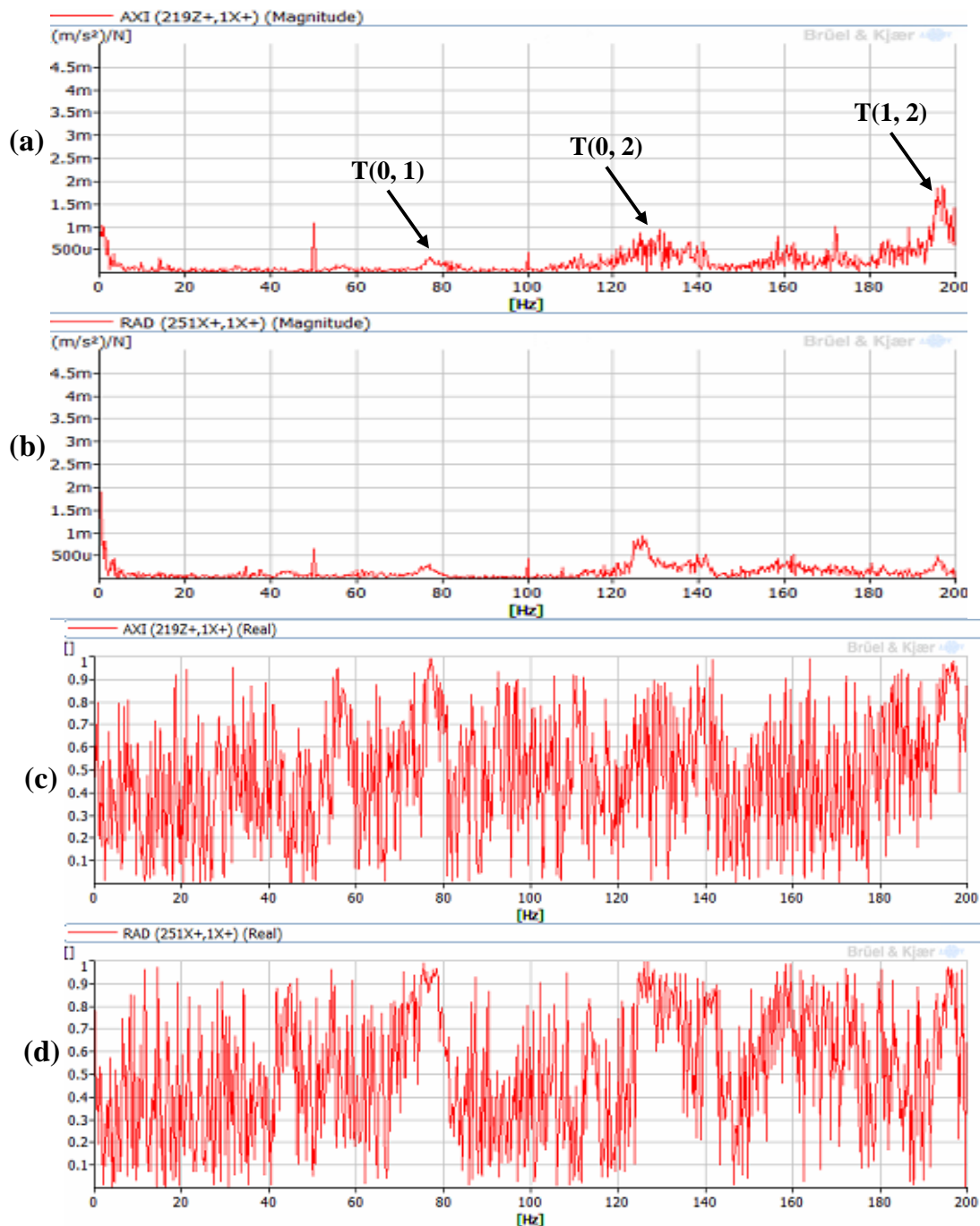
Figure 3-7. FRFs and Coherences of the measurement points on the turbine bearing (impact on the undamaged blade). (a) FRF in axial direction (b) FRF in radial direction (c) coherence in axial direction (d) coherence in radial direction.

The monitoring systems of hydraulic turbines usually measure vibration at the turbine bearings. Therefore, to study the response transmission from the runner to the bearing is very important for the crack monitoring. The FRFs and coherences of the measurement points on the bearing when the impact was on the undamaged blade are shown in Figure 3-7. Those ones when the impact was on

the damaged blade are shown in Figure 3-8.

When the impact is on the undamaged blade, only three blade dominated modes below 200 Hz can be detected by the point in axial direction, and two in radial direction. The detected modes in axial and radial directions are the same. The amplitudes of some detected modes in axial direction are higher than those in radial direction. The coherences of these two points are much worse than those on the blades, but they still approach to 1 at the detected resonant frequencies.
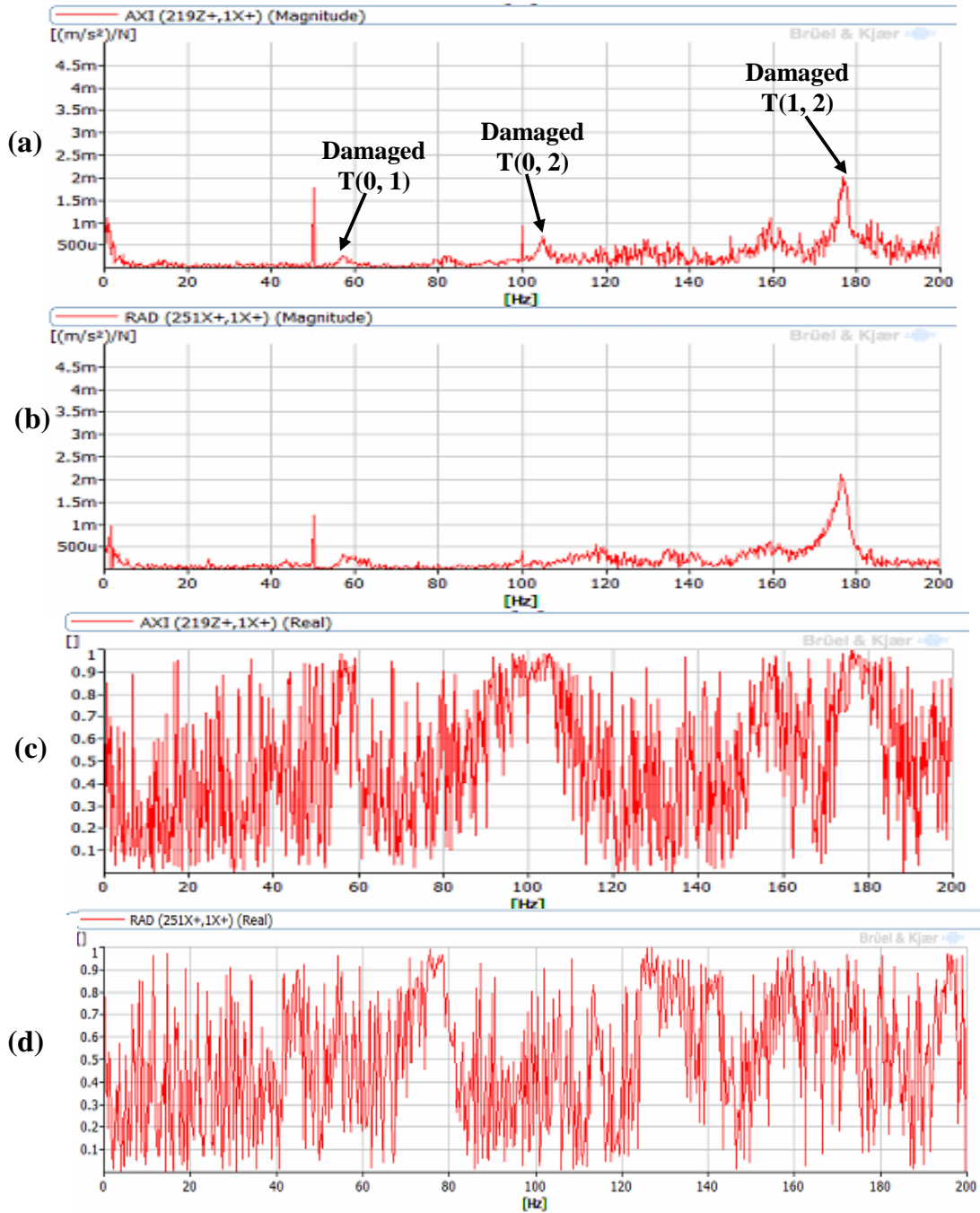
Figure 3-8. FRFs and Coherences of the measurement points on the turbine bearing (impact on the damaged blade). (a) FRF in axial direction (b) FRF in radial direction (c) coherence in axial direction (d) coherence in radial direction.

When the impact is on the damaged blade, there are only three blade dominated modes below 200 Hz that can be detected by the point in axial direction and two in radial direction. The coherences approach to 1 at the detected resonant frequencies. Overall, the response transmission to the bearing in axial direction is better than that in radial, and this is probably because the blade dominated modes mainly vibrate in axial direction. This conclusion has also been reached with the numerical model in section 2.2.2.3.4.

Even it seems that some modes can be detected from the bearings, the amplitudes of the FRFs are not so high which will make difficult to detect them under working conditions. In addition, the reduction of frequencies due to the crack are not so high (less than 26%), which will also make difficult to detect the crack in its first stage of developing.

3.5. Summaries

In this chapter, the dynamic behavior of the Kaplan turbine runner with and without damage has been studied experimentally. The experimental modal analysis has been done through the roving accelerometer method. The damaged blade and one undamaged blade have been analyzed. Accelerometers have been located on every blade, as well as on the turbine bearings and thrust bearings. Using all the FRFs of the different measurement points, the operational deflection shape (ODS) of both the damaged and undamaged blades have been obtained. Coherences between the measurement points and hammer have been checked to ensure the accuracy of the experiment. The natural frequencies and mode shapes of the modes below 200 Hz detected by impacting the damaged blade and by impacting the undamaged blade have been presented.

The frequency reduction ratios of some modes can be abnormally low under a so large crack, which is possible due to the nonlinear effect caused by the contact of crack surfaces. The crack makes all the mode shapes deflect to the crack side.

All the modes detected show that the response concentrate on the impact blade, which indicate that each blade behave independently. The responses of the runner can be transmitted to the turbine bearing, and some modes of the runner can be detected by accelerometers in the bearing in the axial and radial directions. The responses in the thrust bearing in axial direction are higher than those in the radial direction, and more modes are detected, which may indicate that measuring the bearing response in axial direction is better than in radial direction for the crack monitoring.
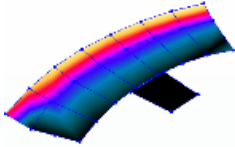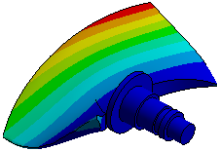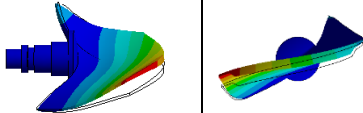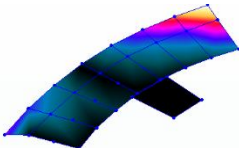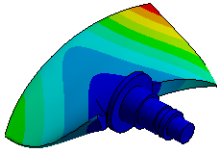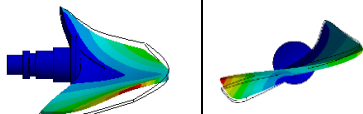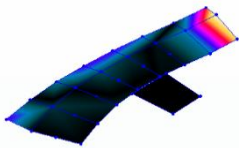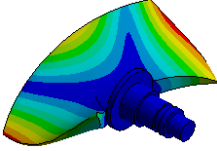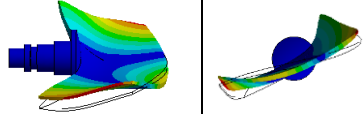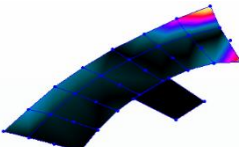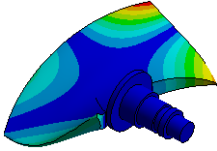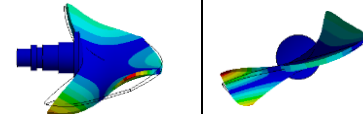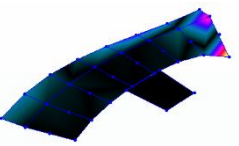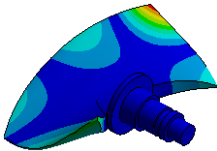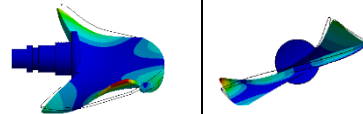
CHAPTER 4. Comparison between the experimental and numerical results

In this chapter, the experimental and numerical results on the Kaplan turbines are compared. The differences between the experimental and numerical results are also analyzed. Based on the validation of the numerical models, failure analysis on the damaged blade is also done, and an uncommon failure reason in Kaplan turbines due to the rubbing between the blades and chamber wall is revealed. The content of the failure analysis part has been published in in the paper" Zhang M, Valentín D, Valero C, et al. Failure investigation of a Kaplan turbine blade[J]. Engineering Failure Analysis, 2019".

4.1. Comparison between numerical and experimental results

4.1.1. Natural frequencies and mode shapes without crack

Table 4-1 Experimental and numerical modes of the undamaged blade.

	Experimental Results		Numerical Results		Freq Error [%]
Mode	Freq [Hz]	Modal Shape	Freq [Hz]	Modal Shape	
B	55.47		57.09		2.93
T (0, 1)	77.44		64.68		-16.4
T (0, 2)	126.39		112.79		-10.7
T (1, 1)	141.26		138		-2.31
T (1, 2)	195.46		183.64		-6.05
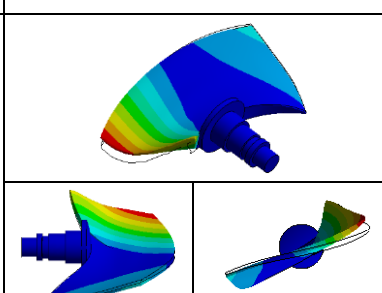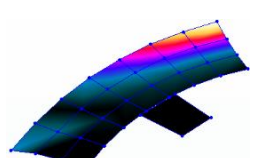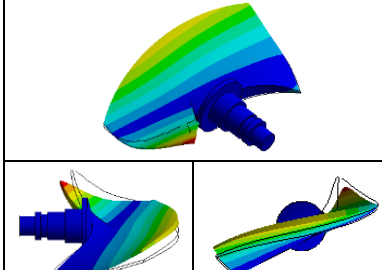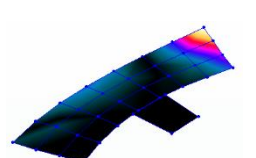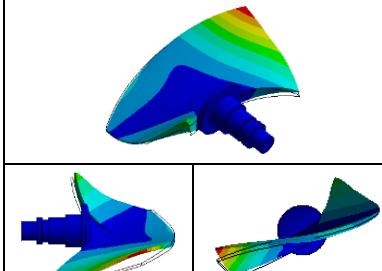
Because the experimental results show that each blade of the turbine runner behaves intendedly,

71
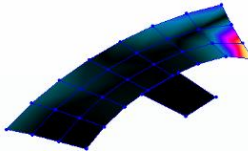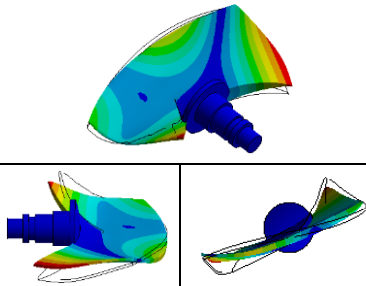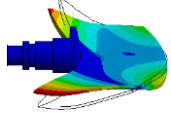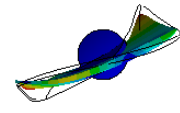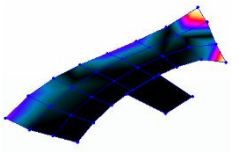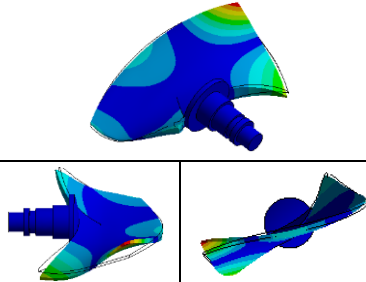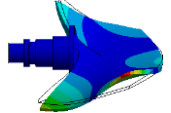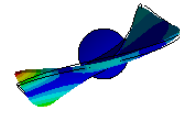
the experimental results on the impact blades are directly compared with the numerical results on the single blade in Section 2.2.1.2 and 2.2.2.2.

The experimental natural frequencies and modal shapes of the undamaged blade have been shown in Table 4-1. Apart from T (0, 1) mode with a frequency error 16%, the errors of all other modes are less than 11%. The frequency errors can be caused by geometry errors or boundary condition errors. The experimental and numerical mode shapes of all the modes are very similar. It is hard to compare the experiment and the simulation mode-shapes just with the picture of the deformation, hence the points that are measured in the experiment are directly compared with the same points in numerical simulation. Only points in the periphery of the blade are considered since the maximum deformation is located in this zone. Figure 4-1(a) show the points selected to compare the mode-shapes. Results obtained are plotted from Figure 4-1(b) to Figure 4-1(f). The displacement has been normalized with the point with maximum displacement in both experimental and numerical cases. A good correlation is found between the experiment and the numerical model for the mode-shapes.

4.1.2. Natural frequencies and mode shapes with a crack

Table 4-2. Experimental and numerical modes of the damaged blade.

Mode	Experimental Results		Numerical Results		Freq Error [%]
	Freq [Hz]	Modal Shape	Freq [Hz]	Modal Shape	
B		Not Detected	37.14		N/A
T (0, 1)	56.7		46.42		-18.1
T (0, 2)	105.3		69.35		-34.1

| T (1, 1) | 133.64 | | 104.2 | | -22.1 |
| T (1, 2) | 176.55 | | 148.05 | | -16.1 |

The experimental modal shapes and frequencies, as well as the numerical modal shapes and frequencies of the damaged blade with a 600mm crack, are shown in Table 4-2. The Bending mode is not detected by the experiment probably due to its low response. The largest frequency error goes to as high as 34.1%. The detailed mode shape comparisons are shown in Figure 4-2, where the larger discrepancies are clearer. The experimental and numerical frequency reduction ratios are shown in Table 4-3. All the experimental FRRs are much lower than numerical ones, with the lowest FRR 0.054 under a so large crack. The reason of this ought to be the nonlinear effect due to the crack surfaces contact, which provides some stiffness and lowers all the FRRs. Through Figure 4-1 and Figure 4-2, the mode shape deflections due to the crack are clear both for the experimental and numerical results.

Table 4-3. Frequency reduction ratios of different modes due to the crack.

	Bending	T (0, 1)	T (0, 2)	T (1, 1)	T (1, 2)
FRR.EXP	N/A	0.267	0.167	0.054	0.097
FRR.SIM	0.349	0.282	0.385	0.245	0.194

In order to improve the numerical results, the non-linear effect of the crack should be considered. One option to take into account this effect is to consider the crack as a material with lower stiffness than the blade material. This will be done as a future step in the investigation.

73
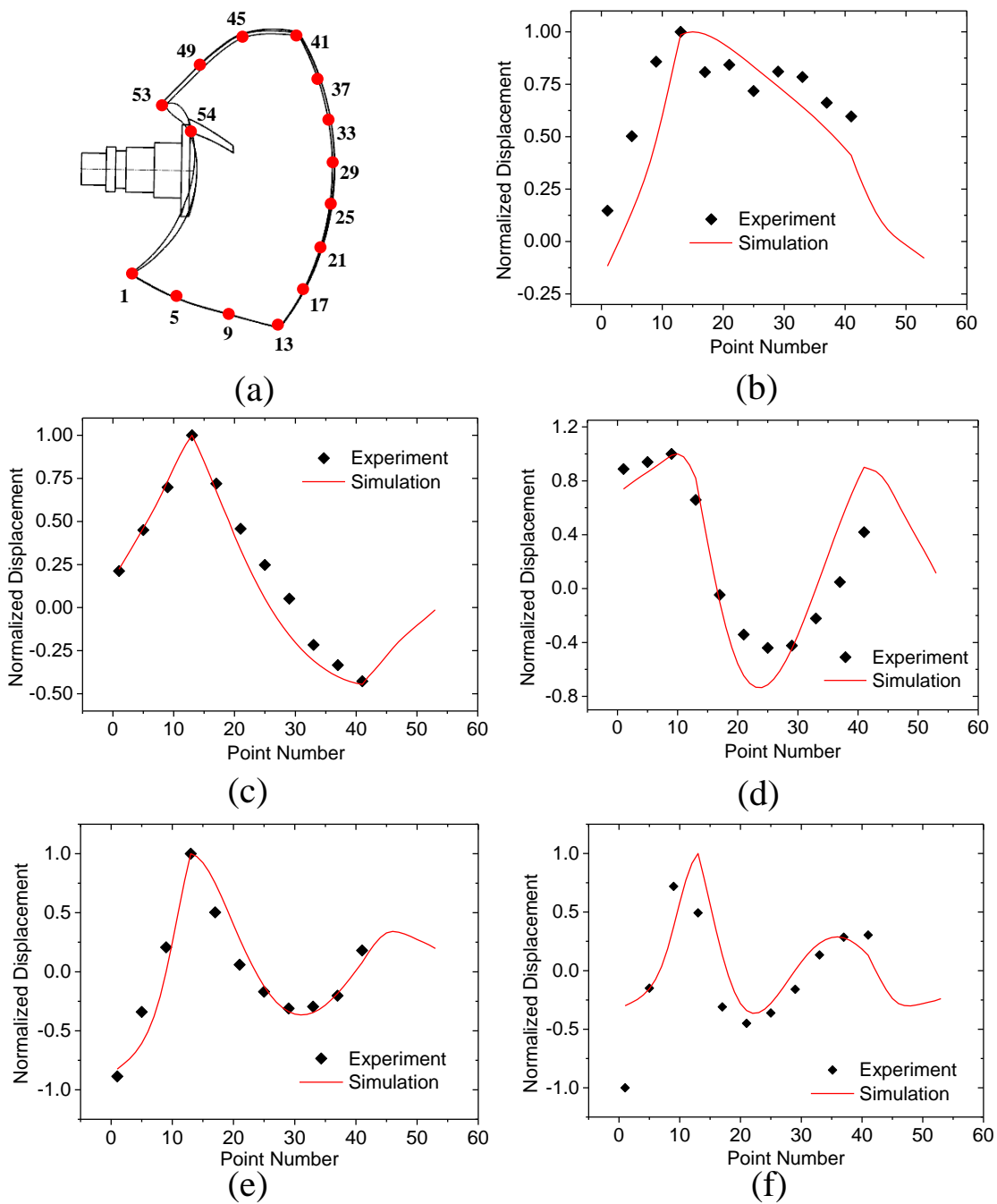
Figure 4-1. Comparison between experimental and numerical displacements along the outside edges of the undamaged blade. (a) Points number. (b) Bending. (c) T (0, 1). (d) T (0, 2). (e) T (1, 1). (f) T (1, 2).
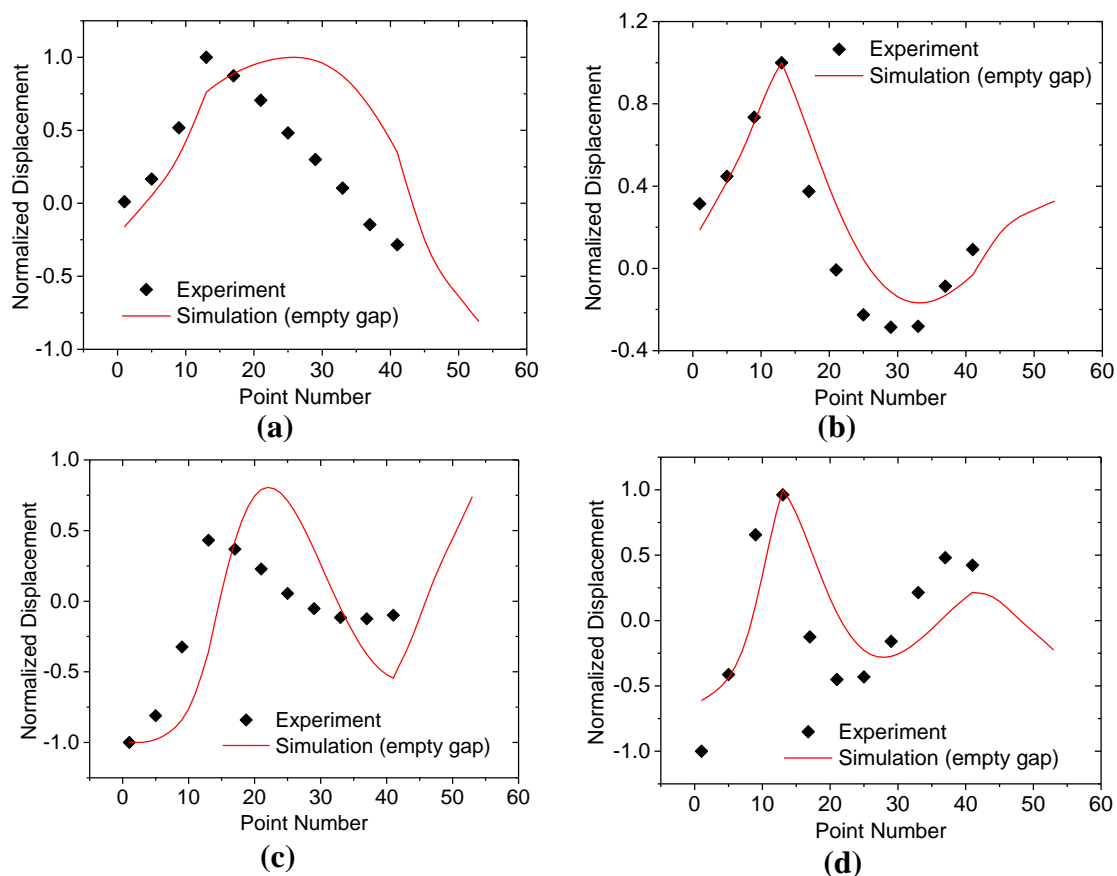
Figure 4-2. Comparison between experimental and numerical displacements along the outside edges of the damaged blade. (a) T (0, 1). (b) T (0, 2). (c) T (1, 1). (d) T (1, 2).

4.2. Failure analysis of the damaged blade

The content of this section has been published in the paper" Zhang M, Valentín D, Valero C, et al. Failure investigation of a Kaplan turbine blade[J]. Engineering Failure Analysis, 2019". Therefore, only a summary of this investigation is included here.

Periodically, vibration monitoring is carried out to supervise the condition of the turbine. This procedure consists of measuring the vibration on some accessible points of the machine allowing the detection of abnormal vibrational behavior and, in some cases, incipient damage. For this case, data was measured in the bearings in axial and radial directions. In one of the measurements, the vibration monitoring system detected an increase in the overall vibration levels, as well as a clear change in the spectra. Therefore, the machine was stopped and inspected.

The inspection of the runner showed a large crack starting from the leading-edge side root hole of one of the blades (Figure 1-11). A detail of the crack is seen in Figure 4-3, where the beach marks can be also discerned. The beach marks show that the damage was caused by a fatigue problem.

<p align="center">(a)   (b)</p>

Figure 4-3. Detail of the crack. (a) From the pressure side. (b) From the suction side.
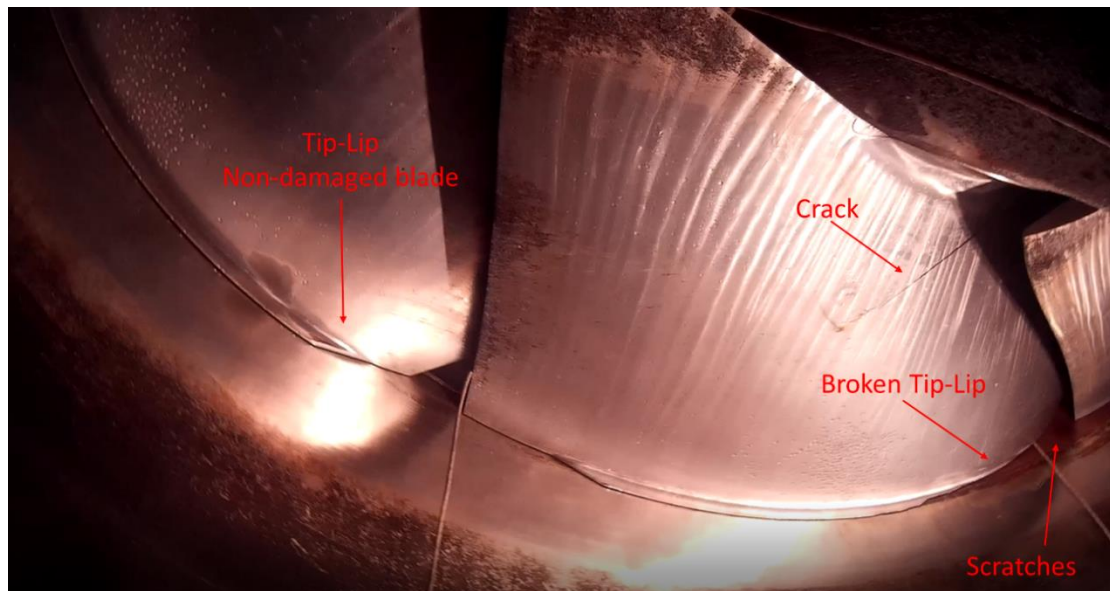
Figure 4-4. View of the runner from below. Non-damaged blade (left) and damaged blade (right).

Moreover, some scratches were found on the whole perimeter of the stationary wall and the tip-lip of the damaged blade was also found broken (see Figure 4-4 and Figure 4-5). This fact leads one to think that contact between the tip-lip of the blade and the wall occurred. To better understand how the blade was broken, a further investigation using a numerical blade model is carried out in the following sections.

<div align="center">(a)   (b)</div>
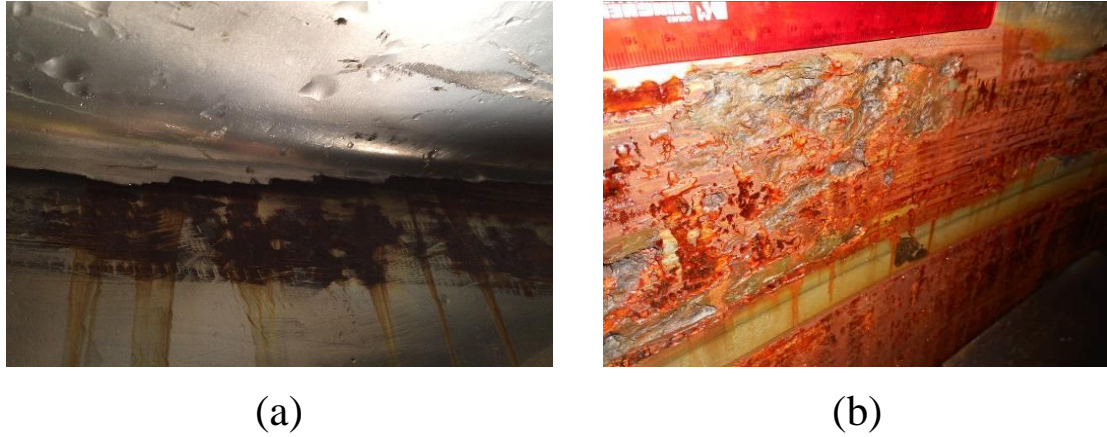
Figure 4-5. Detail of the broken tip-lip and scratches in the stationary wall. (a) Detail of the broken tip-lip. (b) Detail of the scratches in the wall.

4.2.1 Analysis of the machine vibration

As mentioned above, the machine was monitored periodically by analyzing vibration in the bearings. Analyzing the vibration overall levels as well as the spectra of every measured point, the status of the machine can be evaluated. However, first, it is essential to understand the origin of the vibration in the turbine.

Vibrations generated by Kaplan turbines can be of mechanical origin or of hydraulic origin. Mechanical origin forces are mainly the centrifugal forces, which depend on the distribution of the rotating mass and on the rotational speed. The hydraulic forces can be divided into two types: the static loads and the hydrodynamic loads. The static load is caused by the mass-flow passing through the runner and therefore they are higher for higher generating powers [23]. The hydrodynamic loads are mainly due to the rotor-stator interaction (RSI), although they can also provide from other hydraulic phenomena such as vortex rope, tip vortex or Vortex-shedding [25, 26, 76-78].

The RSI arises from the interference between the rotating blades of the runner and the stationary guide vanes [22]. In Kaplan turbines, RSI is not as important as in Francis turbines or Pump-turbines, but it still exists. Viewed from the stationary frame, the RSI frequency depends on the rotating speed of the runner (f_r), the number of rotating blades (Z_b) and the order of harmonics (n):

$$f_{b,n} = n \cdot Z_b \cdot f_r \qquad\qquad (4-1)$$

The excitation shape corresponding every $f_{b,n}$ is the superposition of several excitation modes (k) that can be calculated with the following expression:

$$k = m \cdot Z_v - n \cdot Z_b \qquad\qquad (4-2)$$

where Z_v is the number of guide vanes and m the order of harmonics from the rotating view. Higher amplitudes are expected for lower |k|. Therefore, for a Kaplan turbine, the highest amplitude is obtained normally for m = 1 and n = 2 to 4. The sign of k indicates the rotation of the pressure

pulsation. If it is positive the pressure pulsation rotates in the same direction than the runner and if it is negative, it rotates in the opposite direction.
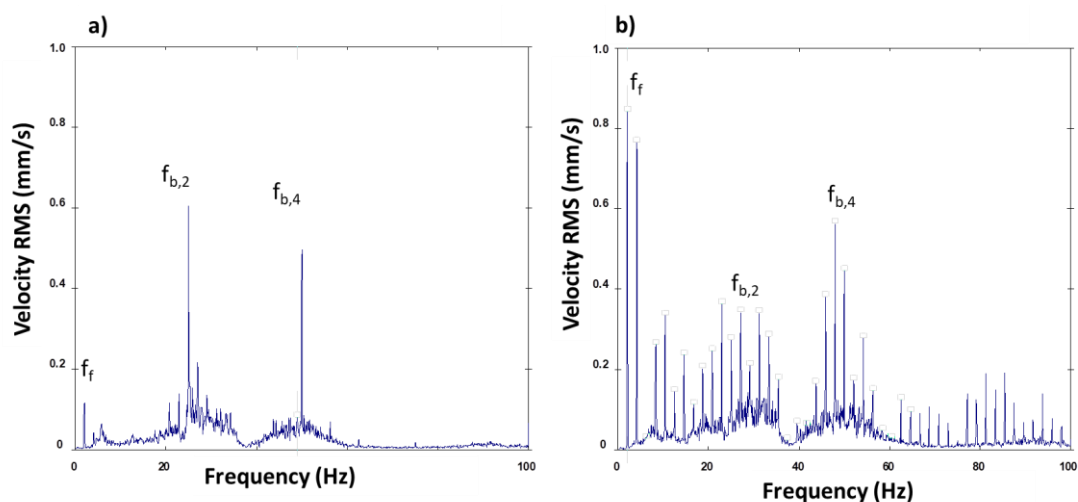
Figure 4-6. Comparison between the spectra before damage and with damage. Turbine bearing. a) Without damage b) With damage.
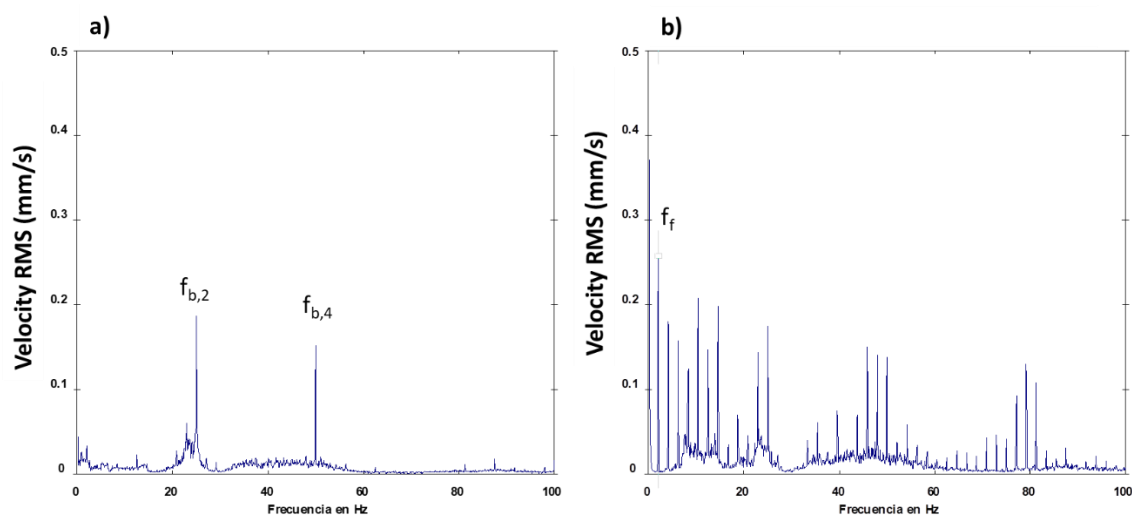
Figure 4-7. Comparison between the spectra before damage and with damage. Generator bearing. a) Without damage b) With damage.

Figure 4-6(a) shows a typical vibration signature of a Kaplan turbine in a turbine bearing without any damage. The vibration signature for the generator bearing without any damage is seen in Figure 4-7(a). Three peaks can be clearly identified: f_f, $f_{b,2}$ and $f_{b,4}$. However, a sudden increase in the harmonics related to the f_f was found when the blade was broken (see Figure 4-6(b) and Figure 4-7(b)). The unbalance, related to the f_f increased considerably in comparison with the one with the machine in good condition (Figure 4-6(a) and Figure 4-7(a)). These symptoms coincide with a severe unbalanced rotating machine and with a blade contacting in the stationary wall during operation.

The overall vibration levels of all the measured points also increased considerably. Figure 4-8 shows these levels for the turbine bearing and the generator bearing. After the reparation of the blade, the symptoms observed with the broken blade disappeared.
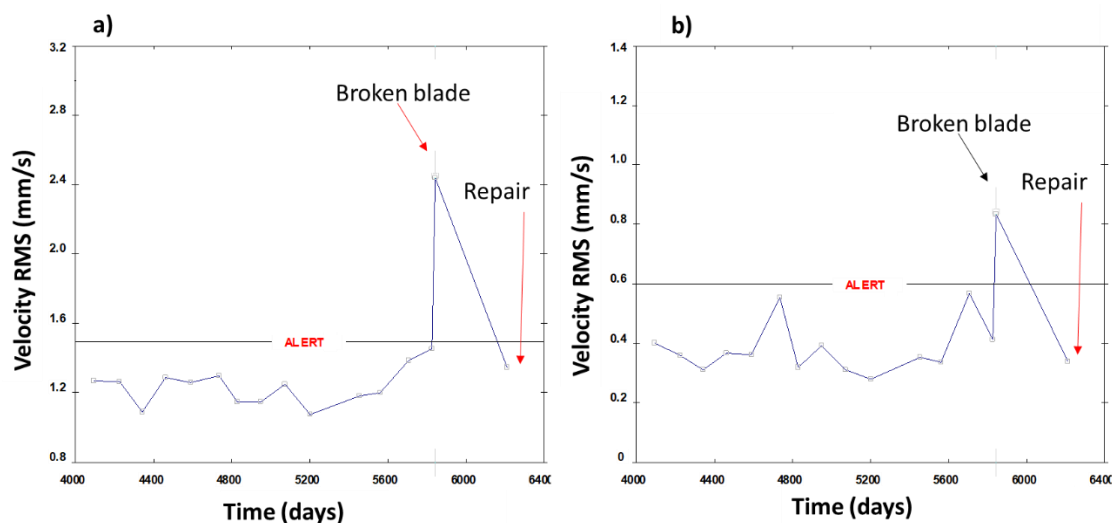
Figure 4-8. Overall vibration levels along the time. a) Turbine bearing. b) Generator bearing.

4.2.2 Numerical Simulation

A numerical model of a single blade has been built up in order to simulate the stress distribution in the blade. This numerical model considers the rod, the blade and the tip-lip (see Figure 4-9). Compared with the blade model in Figure 2-4, the tip-lip and two root holes were added to the current model to calculate the local stress in those areas better. The material used in the simulation is still stainless steel (density of 7750 kg/m^3, Young's Modulus of 193GPa and Poisson's ratio of 0.31). The blade is fixed at the rod using a totally fixed support. The mesh sensitivity was strictly checked and the mesh density at the root holes, which are the typical stress concentrator points, was especially increased. Finally, about 1.4×10^5 tetrahedral elements were used, as shown in Figure 4-9.

First, a numerical modal analysis was performed, and the results were compared with experimental values (see Table 4-1) to validate the numerical model. Though the tip-lip and two root holes were newly introduced, they do not change the natural frequencies and modal shapes too much compared with those of the blade model in Figure 2-4. Therefore, a good agreement between the numerical results and experimental results can be expected and is not listed here anymore. Once the numerical model was validated, the typical pressure distribution over the blade was applied in the model. This pressure distribution was applied according to values reference [25] (see Figure 4-10(a)). Moreover, the rotating speed was introduced to the blade to consider the inertia effects. The stress distribution was obtained for this pressure distribution, which corresponds to normal operation of the machine. After that, one tangential force and one radial force were applied in the blade tip, just where it was found broken in the prototype (see Figure 4-10(b)). These forces model the behavior of contact with the stationary wall. As the value of these forces was not known, different values were tested to see the influence of those forces on the stress distribution over the blade.

79
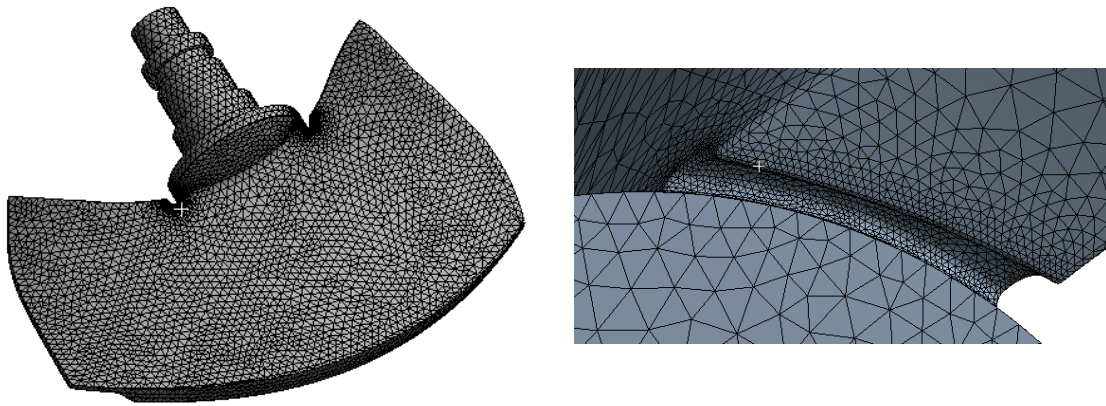
Figure 4-9. View of the mesh.

3.64E+05	
3.04E+05	
2.44E+05	
1.84E+05	
1.24E+05	
0.64E+05	
0.04E+05	
-0.56E+05	
-1.16E+05	
-1.76E+05	
-2.36E+05	

(a)   **(b)**
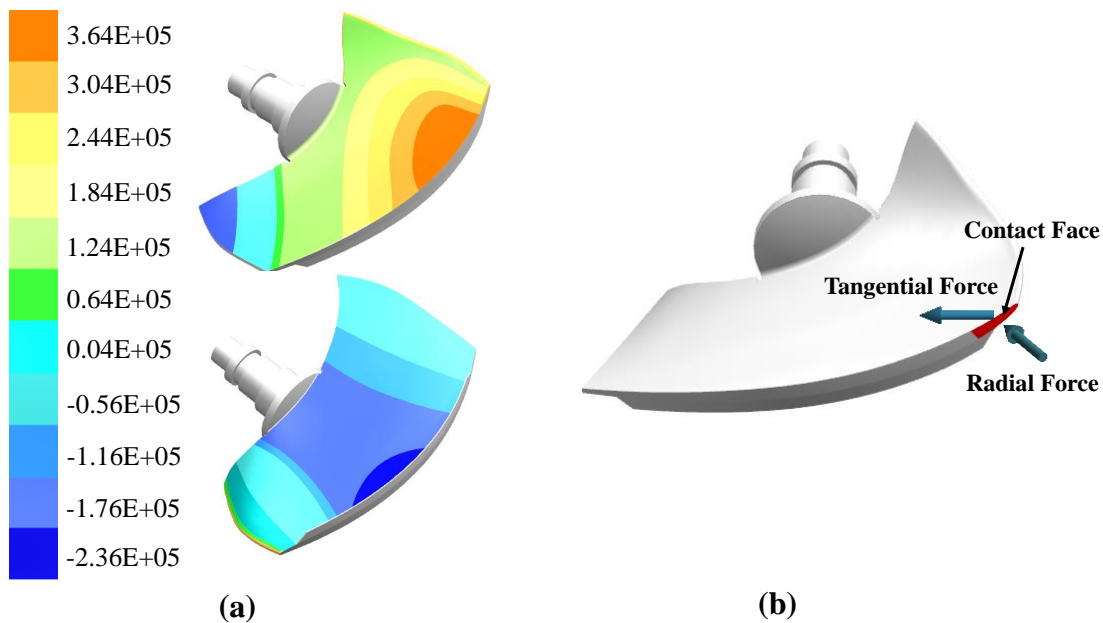
Figure 4-10. (a) Pressure pattern (unit: Pa). (b) Contact forces.

4.2.3 Dynamic response of the blade

To determine the effect of rubbing on the stress distribution of the blade and its relationship with the crack appearance, a static structural analysis of the blade was performed. To do so, first, a typical pressure distribution in Kaplan turbines is applied to the structure and then, a contact force was applied in the tip of the blade, as explained in Section 4.2.2.

4.2.3.1. Stress distribution under normal operating conditions

Once the pressure pattern over the blade is applied, the stress distribution due to this pressure is obtained. Therefore, this displacement corresponds to the normal operating conditions of the machine and it is shown in Figure 4-11(a). The stress distribution of the blade is also shown in Figure 4-11(b). It is observed that the maximum stress in the blade is located in the zone where the crack started in the machine. The stress distribution matches with other previous results obtained in other Kaplan turbine prototypes [23].

4.2.3.2. Stress distribution under rubbing

To model the rubbing, a radial force and a tangential force were applied to the blade (see Figure 4-10(b)). The value of these forces is not known, hence different values were tested in the simulation. Figure 4-12 shows how the value of these forces affect the maximum stress value located in the root of the blade, where the crack started. The stress in the figure is normalized against the value found without any rubbing (Figure 4-11(b)). It is seen that for the contact forces from 10^6N to 10^7N, the stress value increases drastically. From the case of the scratched wall and broken tip-lip, the contact force in this researched case ought to be very high. Therefore, with the appearance of these tangential and radial forces the stress in the root increases and it demonstrates the appearance of the crack in the blade.

However, not only the stress in this point increases but also the stress distribution changes due to the appearance of a tangential and radial force in the blade tip. Figure 4-13 shows the displacement and stress distribution due to the different values of tangential and radial forces. It can be observed that the stress is also higher in the zone of the tip-lip, just where it was also found broken. This fact demonstrates why this part was also found broken in the machine inspection.

(a) **(b)**
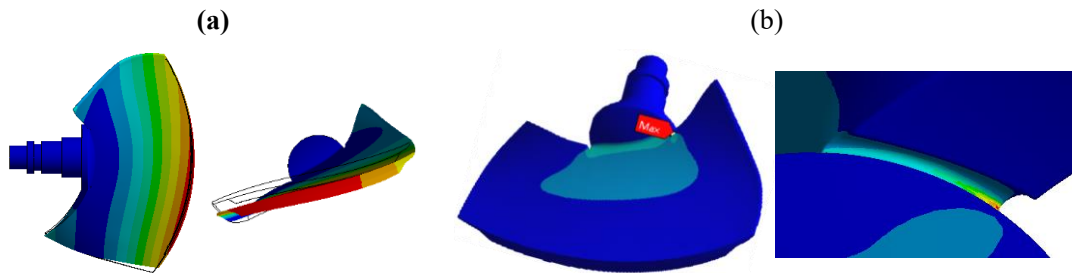
Figure 4-11. (a) Displacement under normal operating conditions. (b) Stress distribution of the blade under normal operating conditions.
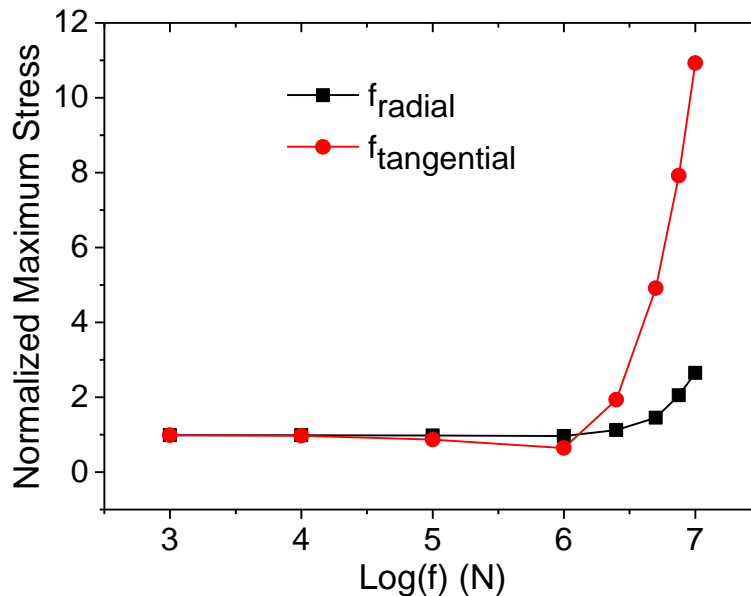
Figure 4-12. Normalized maximum stress changes with contact force.
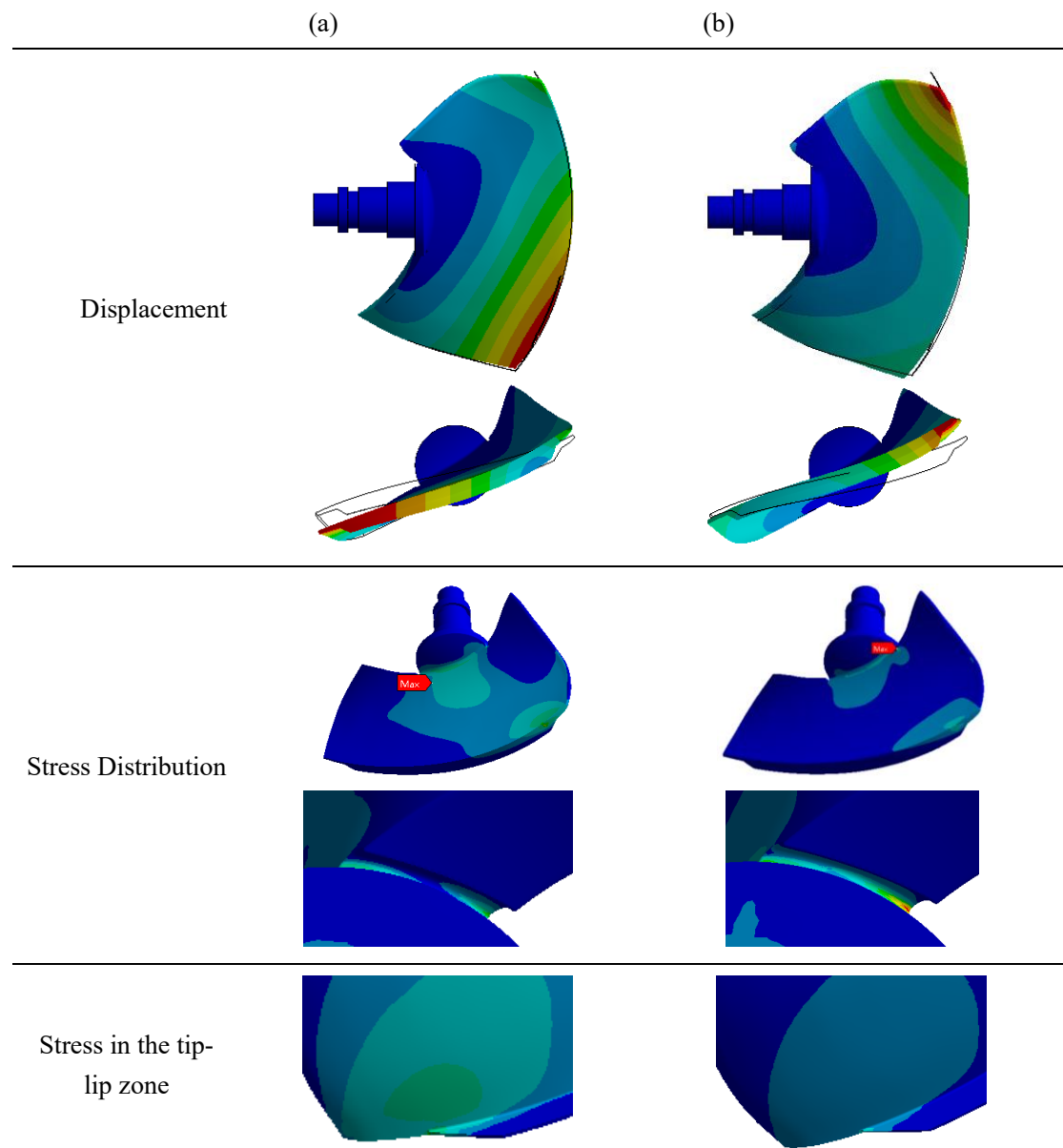
Figure 4-13. Displacement and stress distribution (a) Tangential force value of 10^6N. (b) Radial force value of 10^7N.

4.3. Summaries

In this chapter, the experimental and numerical results on the Kaplan turbine have been compared together to validated the numerical results. The experimental natural frequencies and mode shapes on the undamaged blade are close to the numerical results. The experimental mode shapes on the damaged blade are similar to the numerical mode shapes on the damaged blade. However, when using a narrow gap to simulate the real crack, the numerical frequency reduction ratios due to the crack can be much higher than experimental ones, which is probably due to the nonlinear effect induced by the crack surfaces contact. The nonlinear effect can make the frequency reduction ratios of some modes abnormally low even when the crack is very large.

Failure analysis on the large crack shown in Figure 1-11 has been done to find out the causes

that provoked it. The large crack generated an increase in the vibrations of the machine that was detected by the monitoring system. After the inspection, beach marks were found on the crack surfaces, which indicated that the crack was caused by fatigue. At the same time, some scratches were found on the chamber wall and the tip-lip near the leading-edge was broken. The vibration spectra showed that the vibration amplitude at the rotor rotation frequency increased drastically. All these symptoms showed that there had been a contact between the damaged blade and the wall. To study the effect of a contact force at the blade tip on the maximum stress, a more specific blade model with two root holes and the tip lip was created and used for static structural analysis. The newly built model has been validated by comparing its natural frequencies and mode shapes with the experimental results. The hydraulic pressure at a normal operation point and centrifugal force due to the rotation have also been considered in the stress analysis. Results showed that with the increase of the contact force, the stress at the leading-edge root hole increases drastically. A high-stress area also appeared at the tip-lip zone. Therefore, it ought to be the high contact force that caused the crack and broken tip-lip to occur.

CHAPTER 5. Conclusions and Future Perspectives

This chapter presents the major conclusions and contributions of this thesis work. The applications of the results are explored, and some future work is proposed.

5.1 Contributions and Conclusions

Summing up all the investigations carried out in this thesis and the obtained results, several contributions and conclusions can be achieved, as described in following paragraphs.

5.1.1. On the dynamic behavior of a prototype Kaplan turbine without damage

The modes of prototype turbines can be generator, shaft, hub, control system or blade dominated. The generator has little influences on blade dominated modes, and a single blade model can probably be used to predict the natural frequencies of the Kaplan runner.

The balance of the blade can be changed by the support position, which can be optimized to reduce the dynamic stress of the blade. The support stiffness can have some influences on the modal shapes because it can change the balance of the blade. The natural frequencies of the single blade become very sensitive to the support stiffness when it is lower than some value.

The surrounding water can change appearance sequences of each mode. With the decrease of the tip-clearance size, the natural frequencies of all the modes will decrease slightly.

5.1.2. On the dynamic behavior of a prototype Kaplan turbine with damage

A crack lowers the stiffness of the blade and therefore its natural frequencies. The mode-shapes are also affected by the crack. For some modes, the frequency reduction ratios can be very low even if the crack length is very large, which is probably due to the nonlinear effect induced by the crack surfaces contact. A crack will make the mode shapes deflect to its side. The crack path and length can have influence on mode shape and frequency. The value of the natural frequency can decrease up to 25% for some cases changes due to a crack.

The frequency reduction ratios of the localized modes in water can be different from those in air depending on the mode-shape. The tip-clearance size nearly has no important influences on the frequency reduction ratios.

Forced response analysis has been performed to investigate the response changes due to a crack on the blade. Due to the more significant vibration amplitude and frequency changes of the localized blade dominated modes, they are most useful for crack monitoring. The vibration amplitude change trends are common for all the monitoring points on the shaft in both radial and axial directions, but they are more significant for lower position monitoring points in axial direction. Some modes can be clearly detected from the shaft when the crack on the blade is large.

5.1.3. On the effect of a crack on the dynamic behavior of a Francis turbine runner model

For the studied Francis runner model, there is usually only one localized mode, and when the crack length is high, strong localization can occur. The localized mode or the modes with strong deformation concentrations on the damaged blade usually have the highest natural frequency reduction ratios. The modal shapes and frequency reduction ratios in water are different from those in the air. The modal shape of a changed mode may become similar to another mode when their frequencies are close. The forced response and natural frequency changes are usually small when

85

the crack is not large enough, which is the reasons why the crack is difficult to be monitored in this type of runner.

5.1.4. Failure analysis of the damaged Kaplan turbine blade

The large crack on the turbine blade researched in this thesis generated an increase in the vibrations of the machine that was detected by the monitoring system. After the inspection, beach marks were found on the crack surfaces, which indicated that the crack was caused by fatigue. At the same time, some scratches were found on the chamber wall and the tip-lip near the leading-edge was broken. The vibration spectra showed that the vibration amplitude at the rotor rotation frequency increased drastically. All these symptoms showed that there had been a contact between the damaged blade and the wall. To study the effect of a contact force at the blade tip on the maximum stress, a more specific blade model with two root holes and the tip lip was created and used for static structural analysis. The newly built model has been validated by comparing its natural frequencies and mode shapes with the experimental results. The hydraulic pressure at a normal operation point and centrifugal force due to the rotation have also been considered in the stress analysis. Results showed that with the increase of the contact force, the stress at the leading-edge root hole increases drastically. A high-stress area also appeared at the tip-lip zone. Therefore, it ought to be the high contact force that caused the crack and broken tip-lip to occur.

5.2. Future Perspectives

According to the work presented in this thesis, some improvement and extension can be prospected in the following directions:

5.2.1. On the crack monitoring

Though the forced responses on different runner models with and without a crack have been done in this thesis, and the changes of either the maximum response on the runner or the response amplitude of the monitoring points on the shaft have been obtained, crack monitoring technologies based on the real vibration measurement still need to be developed to better monitor the crack appearances. The changes on the modal behavior are not substantial to be detected by the current monitoring systems, therefore this point still has to be improved.

5.2.2. On the damping ratio changes due to a crack

The experiment on the Kaplan turbine showed that a large crack has a potential to reduce the damping ratios of some modes and increase it for other modes. Considering the complexity of the damping mechanism, the damping ratio changes with the crack length increase in Kaplan turbines, as well as other types of hydraulic turbines, still need more experimental researches. Moreover, the added damping ratio changes due to a crack are also of interest.

REFERENCES

1.   IEA, I.E.A., *KEY ELECTRICITY TRENDS 2017 BASED ON MONTHLY DATA.* Monthly Electricity Statistics, 2018.

2.   Raabe, J., *Hydraulic Machinery and Systems*.

3.   Trivedi, C., B. Gandhi, and C.J. Michel, *Effect of transients on Francis turbine runner life: a review.* Journal of Hydraulic Research, 2013. **51**(2): p. 121-132.

4.   Liu, X., Y. Luo, and Z. Wang, *A review on fatigue damage mechanism in hydro turbines.* Renewable and Sustainable Energy Reviews, 2016. **54**: p. 1-14.

5.   Huang, X., et al., *Fatigue analyses of the prototype Francis runners based on site measurements and simulations.* IOP Conference Series: Earth and Environmental Science, 2014. **22**(1).

6.   Dorji, U. and R. Ghomashchi, *Hydro turbine failure mechanisms: An overview.* Engineering Failure Analysis, 2014. **44**: p. 136-147.

7.   Lyutov, A., et al., *Modelling of a Francis Turbine Runner Fatigue Failure Process Caused by Fluid-Structure Interaction.* IOP Conference Series: Earth and Environmental Science, 2016. **49**.

8.   Luo, Y., et al., *Fatigue of piston rod caused by unsteady, unbalanced, unsynchronized blade torques in a Kaplan turbine.* Engineering Failure Analysis, 2010. **17**(1): p. 192-199.

9.   Egusquiza, M., et al., *Failure investigation of a Pelton turbine runner.* Engineering Failure Analysis, 2017. **81**: p. 234-244.

10.   Egusquiza, E., et al., *Failure investigation of a large pump-turbine runner.* Engineering Failure Analysis, 2012. **23**: p. 27-34.

11.   Frunzaverde D, C.V., Nedelcu D, et al. , *Failure analysis of a Kaplan turbine runner blade by metallographic and numerical methods.* Proceedings of the 7th WSEAS International Conference on FLUID MECHANICS (FLUIDS'10), University of Cambridge, UK., 2010: p. 60-67.

12.   Urquiza, G., et al., *Failure analysis of a hydraulic Kaplan turbine shaft.* Engineering Failure Analysis, 2014. **41**: p. 108-117.

13.   Frunzăverde, D., et al., *Failure analysis of a Francis turbine runner.* IOP Conference Series: Earth and Environmental Science, 2010. **12**.

14.   Egusquiza, E., et al., *Condition monitoring of pump-turbines. New challenges.* Measurement, 2015. **67**: p. 151-163.

15.   Yamaguchi, H., *Engineering fluid mechanics*. Vol. 85. 2008: Springer Science & Business Media.

16.   Rodriguez, C.G., et al., *Experimental investigation of added mass effects on a Francis turbine runner in still water.* Journal of Fluids and Structures, 2006. **22**(5): p. 699-712.

17.   (VSH), V.S.H., *Kaplan turbines: Heidenheim*.

18.   Tong, D., *Cavitation and wear on hydraulic machines.* International Water Power and Dam Construction, 1981. **2**: p. 30-40.

19.   Kumar, D. and P.P. Bhingole, *CFD Based Analysis of Combined Effect of Cavitation and Silt Erosion on Kaplan Turbine.* Materials Today: Proceedings, 2015. **2**(4-5): p. 2314-2322.

20.   *A review of silt erosion in hydro turbines.*

21.   *de Souza Braga D, Coelho D F, Soeiro N S, et al. Numerical simulation of fluid added mass*

effect on a Kaplan turbine runner with experimental validation[C]//22nd International Congress of Mechanical Engineering (COBEM), Ribeirão Preto, Brazil, Nov. 2013: 3-7.

22. *Rodriguez C G, Egusquiza E, Santos I F. Frequencies in the vibration induced by the rotor stator interaction in a centrifugal pump turbine[J]. Journal of Fluids Engineering, 2007, 129(11): 1428-1435.*

23. Zhou, L., et al., *Analysis of dynamic stresses in Kaplan turbine blades.* Engineering Computations, 2007. **24**(8): p. 753-762.

24. *Liu S, Li S, Wu Y. Pressure fluctuation prediction of a model Kaplan turbine by unsteady turbulent flow simulation[J]. Journal of Fluids Engineering, 2009, 131(10): 101102.*

25. Wu, Y., et al., *Numerical prediction and similarity study of pressure fluctuation in a prototype Kaplan turbine and the model turbine.* Computers & Fluids, 2012. **56**: p. 128-142.

26. Motycak, L., A. Skotak, and J. Obrovsky, *Analysis of the Kaplan turbine draft tube effect.* IOP Conference Series: Earth and Environmental Science, 2010. **12**.

27. Thiery, F., R. Gustavsson, and J.O. Aidanpää, *Dynamics of a misaligned Kaplan turbine with blade-to-stator contacts.* International Journal of Mechanical Sciences, 2015. **99**: p. 251-261.

28. Jacquet-Richardet, G., et al., *Rotor to stator contacts in turbomachines. Review and application.* Mechanical Systems and Signal Processing, 2013. **40**(2): p. 401-420.

29. (VSH), V.S.H., *Francis turbines: Heidenheim.*

30. Escaler, X., et al., *Detection of cavitation in hydraulic turbines.* Mechanical Systems and Signal Processing, 2006. **20**(4): p. 983-1007.

31. Presas, A., et al., *Sensor-Based Optimized Control of the Full Load Instability in Large Hydraulic Turbines.* Sensors (Basel), 2018. **18**(4).

32. Liang, Q.W., et al., *Numerical simulation of fluid added mass effect on a francis turbine runner.* Computers & Fluids, 2007. **36**(6): p. 1106-1118.

33. Escaler, X., et al., *Modal behavior of a reduced scale pump-turbine impeller. Part 1: Experiments.* IOP Conference Series: Earth and Environmental Science, 2010. **12**.

34. Valero, C., et al., *Modal behavior of a reduced scale pump turbine impeller. Part II: Numerical simulation.* IOP Conference Series: Earth and Environmental Science, 2010. **12**.

35. *<PhD Thesis Contribution on the Dynamic Response of Hydraulic Turbomachinery Components --Xingxing HUANG.pdf>.*

36. Tanaka, H., *Vibration Behavior and Dynamic Stress of Runners of Very High Head Reversible Pump-turbines.* International Journal of Fluid Machinery and Systems, 2011. **4**(2): p. 289-306.

37. *Liang Q. Dynamic behavior of hydraulic turbine runners[D]. Universitat Politècnica de Catalunya (UPC), 2008.*

38. Mao, Z. and Z. Wang. *Structural Characteristic in Prototype Runner of Francis Turbine Analysis.* in *Proceedings of the International Symposium on Transport Phenomena and Dynamics of Rotating Machinery, Honolulu, HI, USA.* 2016.

39. Valentín, D., et al., *Influence of the boundary conditions on the natural frequencies of a Francis turbine.* IOP Conference Series: Earth and Environmental Science, 2016. **49**.

40. Presas, A., et al., *Analysis of the dynamic response of pump-turbine runners-Part I: Experiment.* IOP Conference Series: Earth and Environmental Science, 2012. **15**(5).

41. Østby, P.T.K., et al., *Experimental investigation on the effect off near walls on the eigen frequency of a low specific speed francis runner.* Mechanical Systems and Signal Processing, 2019. **118**: p. 757-766.

42. Valentín, D., et al., *Experimental Study of a Vibrating Disk Submerged in a Fluid-Filled Tank and Confined With a Nonrigid Cover.* Journal of Vibration and Acoustics, 2017. **139**(2).

43. De La Torre, O., et al., *Experimental investigation of added mass effects on a hydrofoil under cavitation conditions.* Journal of Fluids and Structures, 2013. **39**: p. 173-187.

44. De La Torre, O., et al., *Experimental mode shape determination of a cantilevered hydrofoil under different flow conditions.* Proceedings of the Institution of Mechanical Engineers, Part C: Journal of Mechanical Engineering Science, 2016. **230**(19): p. 3408-3419.

45. Valentin, D., et al., *Feasibility of Detecting Natural Frequencies of Hydraulic Turbines While in Operation, Using Strain Gauges.* Sensors (Basel), 2018. **18**(1).

46. Luna-Ramírez, A., et al., *Failure analysis of runner blades in a Francis hydraulic turbine — Case study.* Engineering Failure Analysis, 2016. **59**: p. 314-325.

47. Saeed, R.A. and A.N. Galybin, *Simplified model of the turbine runner blade.* Engineering Failure Analysis, 2009. **16**(7): p. 2473-2484.

48. Flores, M., G. Urquiza, and J.M. Rodríguez, *A Fatigue Analysis of a Hydraulic Francis Turbine Runner.* World Journal of Mechanics, 2012. **02**(01): p. 28-34.

49. Saeed, R.A., A.N. Galybin, and V. Popov, *Modelling of flow-induced stresses in a Francis turbine runner.* Advances in Engineering Software, 2010. **41**(12): p. 1245-1255.

50. Rudolf, P. and D. Štefan, *Reduced order model of draft tube flow.* IOP Conference Series: Earth and Environmental Science, 2014. **22**(2).

51. Castanier, M.P. and C. Pierre, *Modeling and Analysis of Mistuned Bladed Disk Vibration: Current Status and Emerging Directions.* Journal of Propulsion and Power, 2006. **22**(2): p. 384-396.

52. *Wang J J, Li Q H, Zhu Z G. Vibratory Localization of mistuned bladed disk assemblies—A review[J]. Adv. Mech, 2000, 30(4): 517-528.*

53. *Wei S T, Pierre C. Localization phenomena in mistuned assemblies with cyclic symmetry part I: free vibrations[J]. Journal of Vibration, Acoustics, Stress, and Reliability in Design, 1988, 110(4): 429-438.*

54. *Wei S T, Pierre C. Localization phenomena in mistuned assemblies with cyclic symmetry part ii: Forced vibrations[J]. Journal of Vibration, Acoustics, Stress, and Reliability in Design, 1988, 110(4): 439-449.*

55. *Judge J, Pierre C, Mehmed O. Experimental investigation of mode localization and forced response amplitude magnification for a mistuned bladed disk[C]//ASME Turbo Expo 2000: Power for Land, Sea, and Air. American Society of Mechanical Engineers, 2000: V004T03A004-V004T03A004.*

56. *Kruse M J, Pierre C. An Experimental Investigation of Vibration Localization in Bladed Disks: Part II—Forced Response[C]//ASME 1997 International Gas Turbine and Aeroengine Congress and Exhibition. American Society of Mechanical Engineers, 1997: V004T14A069-V004T14A069.*

57. *Mehmed O. Experimental Investigation of Mode Localization and Forced Response Amplitude Magnification for a Mistuned Bladed Disk[J]. Ann Arbor, 1001: 48109-2125.*

58. Fang, X., et al., *Crack induced vibration localization in simplified bladed-disk structures.* Journal of Sound and Vibration, 2006. **291**(1-2): p. 395-418.

59. *Kuang J H, Huang B W. The effect of blade crack on mode localization in rotating bladed disks[J]. Journal of sound and vibration, 1999, 227(1): 85-103.* 60. Huang, B.-W., *Effect of*

number of blades and distribution of cracks on vibration localization in a cracked pre-twisted blade system. International Journal of Mechanical Sciences, 2006. **48**(1): p. 1-10.

61. *Saito A, Castanier M P, Pierre C. Effects of a cracked blade on mistuned turbine engine rotor vibration[J]. Journal of vibration and acoustics, 2009, 131(6): 061006.*

62. *Marinescu O, Epureanu B I, Banu M. Reduced order models of mistuned cracked bladed disks[J]. Journal of Vibration and Acoustics, 2011, 133(5): 051014.*

63. C., R., *Feasibility of on board measurements for Predictive Maintenance in Large Hydraulic Turbomachinery[D].* 2006.

64. Papagiannopoulos, G.A. and G.D. Hatzigeorgiou, *On the use of the half-power bandwidth method to estimate damping in building structures.* Soil Dynamics and Earthquake Engineering, 2011. **31**(7): p. 1075-1079.

65. Presas, A., et al., *Accurate Determination of the Frequency Response Function of Submerged and Confined Structures by Using PZT-Patchesdagger.* Sensors (Basel), 2017. **17**(3).

66. Valentín, D., et al., *Experimental study on the added mass and damping of a disk submerged in a partially fluid-filled tank with small radial confinement.* Journal of Fluids and Structures, 2014. **50**: p. 1-17.

67. Huang, X., et al., *Numerical and experimental analysis of the dynamic response of large submerged trash-racks.* Computers & Fluids, 2013. **71**: p. 54-64.

68. ANSYS, C., *16.2: User's Manual. ANSYS Inc., USA.* 2015.

69. Zhang, M., et al., *Failure investigation of a Kaplan turbine blade.* Engineering Failure Analysis, 2019. **97**: p. 690-700.

70. Castanier, M.P. and C. Pierre, *Using Intentional Mistuning in the Design of Turbomachinery Rotors.* AIAA Journal, 2002. **40**(10): p. 2077-2086.

71. Wang J J, L.Q.H., *Methods and Applications of reduction modeling for mistuned bladed disk vibration in aero-engine.* 2009: Nation Defense Industry Press, China.

72. D'Souza, K., A. Saito, and B.I. Epureanu, *Reduced-Order Modeling for Nonlinear Analysis of Cracked Mistuned Multistage Bladed-Disk Systems.* AIAA Journal, 2012. **50**(2): p. 304-312.

73. Wang, S., et al., *Reduced-order modeling for mistuned centrifugal impellers with crack damages.* Journal of Sound and Vibration, 2014. **333**(25): p. 6979-6995.

74. Avitabile, P., *Experimental modal analysis.* Sound and vibration, 2001. **35.1**: p. 20-31.

75. Richardson, B.J.S.M.H., *INTRODUCTION TO OPERATING DEFLECTION SHAPES.* 1999.

76. Mulu, B.G., P.P. Jonsson, and M.J. Cervantes, *Experimental investigation of a Kaplan draft tube – Part I: Best efficiency point.* Applied Energy, 2012. **93**: p. 695-706.

77. Jonsson, P.P., B.G. Mulu, and M.J. Cervantes, *Experimental investigation of a Kaplan draft tube – Part II: Off-design conditions.* Applied Energy, 2012. **94**: p. 71-83.

78. Amiri, K., et al., *Load variation effects on the pressure fluctuations exerted on a Kaplan turbine runner.* IOP Conference Series: Earth and Environmental Science, 2014. **22**(3).